



UNIVERSITAT POLITÈCNICA DE CATALUNYA  
BARCELONATECH  
Escola d'Enginyeria de Telecomunicació  
i Aeroespacial de Castelldefels



Master's degree in Applications  
and Technologies for  
Unmanned Aircraft Systems

# MASTER THESIS

**TITLE:** Contribution to the application of near ground L-band radiometry

**MASTER DEGREE:** Master's degree in Applications and Technologies for Unmanned Aircraft Systems (Master Engineering Drones, MED)

**AUTHOR:** Colin Burnham

**PROFESSIONAL ADVISOR:** Roger Jové Casulleras  
**ACADEMIC ADVISOR:** José María González-Arbesú

**DATE:** July 8<sup>th</sup> 2019





“There are days when I wish I could fly instead of spinning my wheels”

...

## Abstract

ARIEL is an L-band radiometer adapted from Earth Observation satellite technology for use in terrestrial, near to ground surveys of moisture. The key technical benefits are compact size, lightweight, mobility and high pixel density (up to 1m<sup>2</sup>).

This project demonstrates the capability of high spatial and temporal resolution L-Band radiometry to produce detailed soil moisture contour maps within a 1 km<sup>2</sup> area. The study was performed prior, during and after 12 mm of rainfall to determine the soil surface absorption and adsorption behaviour in relation to surface moisture. The radiometer was equipped with photodiodes to enable the normalised difference vegetation index (NDVI) data to be extracted concurrently. Hence this is a very near ground, high resolution and high precision study of soil moisture derived from L-band emissivity.

The project is focused on the technology application and production of useful products in the form of moisture contour maps and vegetation detection. The radiometer functioned admirably during the consecutive test campaigns and in conditions that varied from direct sun to rain and mud. Patterns of soil moisture over time and within specific sub-areas of the field are identified and quantified. The intra-field differences appear to primarily be related to soil type and soil surface characteristics which were qualitatively assessed in this study as quantified approaches are available in empirical and theoretical studies.

Average field moistures are measured daily and differentiation is made between soil types within the field. The effect of dry and moist surface emissivity on retrieved moisture is noted, as is the effect of vegetation on soil surface emissivity with the aid of the vegetation index. Comparisons are drawn to the highest resolution satellite imagery (30 m spatial, 3 day temporal) and highlight the limitations and richness of local data that is missed in relation to local soil moisture surface absorption patterns during rainfall.

The radiometer is shown to achieve very high resolution and precision that is not possible from satellite or even light aircraft. Furthermore, it is shown to be able to study ground conditions when they are occluded from satellite and hence the moisture profile maps presented are unique in their detail.

*Key Words:* high spatial resolution, high temporal resolution, L-Band, mobile radiometer, near ground radiometry, NDVI, remote sensing, soil moisture, soil moisture contour maps



# CONTENTS

<b>INTRODUCTION .....</b>	<b>1</b>
<b>CHAPTER 1: RADIOMETRY AND APPLICATIONS .....</b>	<b>4</b>
<b>1.1 Radiometry Concepts .....</b>	<b>4</b>
1.1.1 Brightness Temperature .....	4
1.1.2 Calibration .....	6
<b>1.2 Soil Moisture .....</b>	<b>7</b>
1.2.1 Dielectric Properties .....	7
1.2.2 Soil Roughness .....	8
1.2.3 Vegetation Cover.....	10
<b>1.3 From the Earth to Space .....</b>	<b>10</b>
1.3.1 Foundational Research .....	10
1.3.2 Applied Studies .....	11
1.3.3 Satellite Based Sensors (Earth Observation).....	12
<b>1.4 Near Ground Aerial Radiometry (UAV).....</b>	<b>14</b>
<b>1.5 A Study of Potential New Markets .....</b>	<b>15</b>
1.5.1 Water Resource Management and Leakage Detection .....	15
1.5.2 Agricultural Management and Leakage Detection.....	17
<b>1.6 Method Development and Data Analysis Procedures .....</b>	<b>18</b>
1.6.1 Outline of data processing.....	18
1.6.2 Results from Processing of Lleida Dataset .....	19
<b>CHAPTER 2: HIGH SPATIAL AND TEMPORAL RESOLUTION RADIOMETRIC STUDY OF A LOCAL AREA.....</b>	<b>21</b>
<b>2.1 Context and NDVI Soil &amp; Vegetation Results .....</b>	<b>21</b>
2.1.1 Location and Overview.....	21
2.1.2 Experiments and Weather Conditions.....	22
2.1.3 NDVI Introduction and Equipment Setup .....	24
2.1.4 Photodiodes and System Response to Conditions .....	26
2.1.5 Soil Adjusted Vegetation Index - SAVI.....	30
2.1.6 Vegetation Strip Trials .....	30
2.1.7 High Spatial and Temporal Resolution NDVI & Comparison to Satellite .....	33
<b>2.2 Soil Moisture Results .....</b>	<b>38</b>
2.2.1 Volumetric Soil Moisture.....	38
2.2.2 Instrument Calibration .....	42
2.2.3 High Spatial and Temporal Resolution Soil Moisture Surveys .....	43
2.2.4 Soil Types & Dry Surfaces: The Zero Factor .....	45
2.2.5 Comparison to Satellite Imagery .....	53
<b>CONCLUSIONS .....</b>	<b>58</b>
<b>APPENDIX .....</b>	<b>63</b>



## INTRODUCTION

This project aims to support the development of applications for a remote sensor, the L-band radiometer, that will generate further interest in the instrument as a remote sensor for airborne terrain surveys of top layer and surface moisture. The radiometer antennae are tuned to the L-Band frequency 1.41 GHz which is an emission band known to correlate with soil moisture.

The L-Band spectrum is a microwave frequency that spans from 1 to 2 GHz (15 to 30 cm wavelength) and incorporates GNSS, communications, aircraft surveillance radars amongst other uses. Within this space 1.4 GHz (21cm) is protected for scientific use due to its utility radio astronomy (hydrogen emissions) and Earth observation. The protection precludes the use of active sensors like Radar in near to ground applications at this frequency, hence passive radiometric sensing offers a unique window to observe the naturally emitted microwave radiation of terrestrial surfaces, both natural and man-made.

Remote sensing allows the characteristics of different materials to be measured in a rapid and non-destructive way, potentially over large areas in a short time. One of the products which becomes possible, is a continuous contour map that quantifies, visualises and even provides time lapse measurements over discrete areas. This technique provides much greater insight into distributed characteristics than is possible with point based measurements (e.g. physically located sensors). To this end, remote sensing technologies have trail blazed new applications in the last decade and underpin the success of Earth Observation and more recently the unmanned aerial vehicle (UAV) sector.

Balamis has developed lightweight, mobile L-band radiometers suitable for different vehicle mountings - aeroplane, vehicle and UAV. Of the airborne models, the aeroplane radiometer has been tested with the Cartographic and Geographic Institute of Catalunya in a light aircraft and the UAV mounted model is currently under development. The initial airborne trials will be presented, however, this study will utilise a ground vehicle mounted model that is suitable for all terrain vehicles (ATV), agricultural machinery, handcarts and sleds. In this project the ATV used is a quad-bike. The primary contribution will be to achieve repeated data collection over a series of consecutive days and different weather conditions. In this way the instrument response to changing ground moisture conditions can be ascertained. To further increase the utility of the data and open up future applications, two photodiodes are installed on the radiometer and will be used to collect visible and near-infrared wavelengths for NDVI calculations.



**Balam Ingeniería de Sistemas SL**

+34 93 131 77 88

[info@balamis.com](mailto:info@balamis.com)

Balamis dual antenna mobile L-Band radiometer with photodiode mounts (left)

In this project some background research was studied on emissivity in L-band, evolution of the technology, its relationship to top surface soil moisture (around 5cm depth) and factors that can interfere or distort good quality data retrieval.

The project was focused on achieving a high spatial and temporal resolution study of soil moisture in a nearly 1 km<sup>2</sup> field area (the Giró del Gorner vineyard, [girodegorner.com](http://girodegorner.com), access kindly granted by Gabriel Giró). The core experiment of the project was targeted to cover a 10 day period on either side of significant rainfall in order to study the soil moisture during adsorption, absorption, drainage and drying over the whole field area.

The resolution of data being sought is not currently possible from satellite, aeroplane or UAV. Native satellite radiometric resolution is up to 40 km with an absolute accuracy of 4%. An all terrain quad bike (ATV Quad) that is already used by Balamis for field trials was utilised here. The benefit is a spatial resolution up to 1 m<sup>2</sup> (direction of travel) and time resolution of 1 day. However, as a ground vehicle it was susceptible to soft soil and mud which led to one day of the experiment being dropped.

The ability to obtain high resolution data has the potential to take the global learnings achieved through satellite observation down to near Earth scenes in order to apply the knowledge at a very local level, literally to within meters or, as in this case, rows of a vineyard. The inverse is also true, detailed local data of rainfall and surface moisture interactions can feed into global predictive models on hydrology, fresh water cycles, climate change and land use.

This project was very much about the application of the new remote sensing technology with a view to future commercialisation opportunities. Hence, a real world field study and production of visual products (contour maps) formed an essential part of the project.

It is probably the first multiple day study to generate detailed moisture gradient maps at the resolutions presented here. The study was performed under weather conditions that preclude the use of satellite imagery, even if the resolution were available. Additionally the study used a radiometer with integrated photodiodes for concurrent acquisition of sensor inputs at different wavelengths: visible, near-infrared and microwave.

Chapter 1 covers the concepts, applications and evolution behind the technology. Chapter 2 contains information on preliminary experiments plus set up and location of the main high resolution experiment. Finally, section 2.2.3 contains the principal outputs achieved using radiometric technology in this new form. The moisture profile maps are presented as images in this section and are also available in short time-lapse videos. 2.2.3 can be read with the conclusion for a good overview of the effectiveness of mobile radiometry in this application.

## GLOSSARY

AOI	- Area of Interest
ATV	- All Terrain Vehicle
Absorption	- referring to the behaviour of a liquid soaking into a solid
Adsorption	- referring to the behaviour of liquid collecting or held on a surface
ECV	- Environment Critical Variable
GPR	- Ground Penetrating Radar
NDVI	- Normalised Difference Vegetation Index
NIR	- Near Infrared
NSMI	- Normalised Soil Moisture Index
NW	- North West in relation to field area
SAR	- Synthetic Aperture Radar
SE	- South East in relation to field area
SOC	- Soil Organic Carbon
SMOS	- Soil Moisture & Ocean Salinity (an ESA mission)
SVS	- Soil Vegetation Snow (used in predictive models)
SWIR	- Short Wave Infrared
TOC	- Total Organic Content
WC	- Water Content (synonymous to moisture content)
UAV	- Unmanned Aerial Vehicle (remotely piloted drone)

# CHAPTER 1: Radiometry and Applications

## 1.1 Radiometry Concepts

### 1.1.1 Brightness Temperature

Radiometry is the study of thermal and electromagnetic radiation emitted by bodies. These emissions originate from absorption of part of the energy arriving at the body or earth surface from the sun. The body initially absorbs and later radiates excess energy as heat until it is in equilibrium with its surroundings.

For thermally radiated energy the index emissivity is used and is the sum of three components: transmitted, reflected and emitted radiation. The emitted (inherent) radiation is usually the target of interest and the value will depend on the material surface being observed, the temperature of the surface, and the wavelength used for the observation.

The mathematical model is derived from Plank’s Black Body radiator which sets the ideal conditions for an emitter i.e. a body which absorbs all incident radiation and transmits and reflects none. Therefore, at equilibrium this body will be a perfect omnidirectional emitter of emissivity equal to 1. Conversely, a perfect reflector will have emissivity equal to 0.

Plank defined blackbody spectral emission as “Brightness”, the energy emitted per second (W) per unit area (m<sup>2</sup>) into a solid radian angle (sr) at a given frequency (Hz). In the microwave spectrum Plank’s law can be simplified to the Rayleigh Jeans Approximation [1], (a precursor to Plank’s law) since frequencies are low and Earth temperatures moderate:

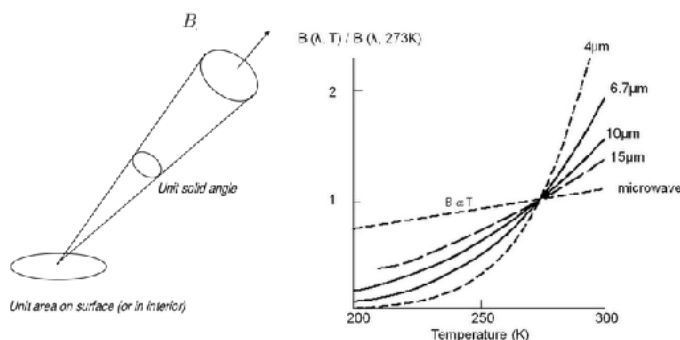
$$B = (2K_b.T) / \lambda^2 \tag{1}$$

B is the Brightness in Watts/m<sup>2</sup>/sr/Hz

T is the physical body temperature in Kelvin

K<sub>b</sub> is Boltzmann’s constant 1.38 x10<sup>23</sup> J/K

λ is the wavelength in metres for the observation frequency



Hence, Brightness can be determined with a knowledge of a body temperature and the observation wavelength (or frequency). The emissivity model and sensitivity at microwave frequencies is illustrated in FIG. 1.

**FIG. 1 a, b:** Brightness emissivity model (left) and sensitivity for typical earth scene temperatures (right)



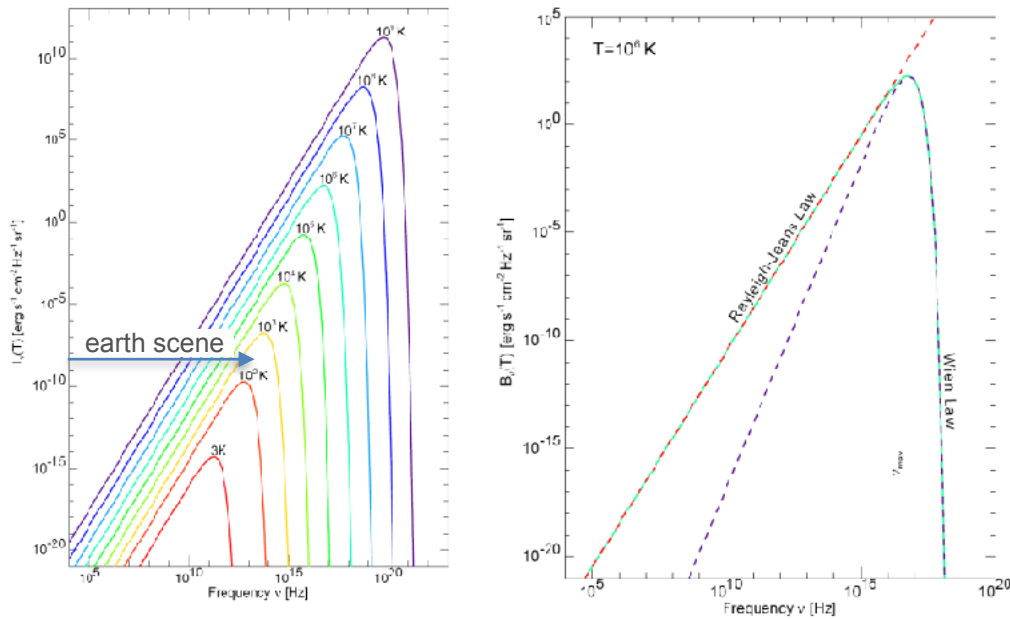


**FIG. 2: a (left) b (right):** Brightness is a linear function of frequency within a defined bandwidth for a body or scene temperature in Kelvin [1].

The Rayleigh Jeans law provides a simplified linear relationship for a given body temperature, in this case earth scene temperatures (c. 300 K, FIG 2a) and low frequencies including L band microwave (FIG.2b). If the observation wavelength is narrow enough, the Brightness will be a constant that is directly proportional to the power received by an antenna tuned to that frequency. The width of the frequency band ( $\Delta f$  in Hz) is important, the more narrow the better, then the relationship between Brightness and measured Power (P) will also be linear:

$$P = K_b.T. \Delta f \quad (2)$$

These equations are the simplified derivatives of Planks quantum theory and represent ideal “black body” conditions. Under non-ideal “grey body” conditions found in the real world we have to introduce an effective equivalent temperature and modify equation 1:

$$B_{(\text{grey})} = (2K_b / \lambda^2).T_B.\Delta f \quad (3)$$

$T_B$  in Kelvin is the brightness temperature, the effective temperature a black body would need to be at in order to produce the Brightness observed in the grey body (note,  $T_B$  is not the actual temperature). This is the definition of Brightness Temperature, the temperature at which a black body in thermal equilibrium with its surroundings would have to be in order to be equal to the observed energy intensity at the measurement frequency.

From here we can see how to introduce the concept of emissivity ( $\epsilon$ ). As mentioned, emissivity is an index, often referred to in thermal studies, which represents the relative brightness of a grey body to a black body at the same

physical temperature. Unlike a black body, a grey body will not absorb all incident radiation and therefore will not transmit or emit to the same brightness. Emissivity links the physical temperature to the Brightness Temperature:

$$e = T_B / T \quad (4)$$

To summarise, radiometric measurements are made of Brightness Temperature ( $T_B$ ) at a specified frequency. Brightness Temperature is directly and linearly related to the Power detected by the antenna at a given frequency. The narrower the frequency the more precise the linear relationship. Brightness Temperature is related to the body physical temperature via Boltzmann's constant but is not, and can vary considerably from, the actual temperature of the body or surface.

Radars (active sensors) measure the backscattering coefficient, a measure of reflectance, and are related to radiometers via Kirchhoff's law of thermal radiation that links emissivity ( $e$ ) to absorption ( $\alpha$ ) and reflectance ( $\Gamma$ ):

$$e = 1 - (\alpha + \Gamma) \quad (5)$$

### 1.1.2 Calibration

Brightness Temperature is a measure of radiance and is the fundamental parameter measured by passive microwave radiometers.

Brightness Temperature, as defined above produces a similar concept called Antenna Temperature. This is the temperature that a resistor would have to be to generate the same power density at the given observation frequency. The resistor temperature can be measured as a voltage under hot or cold load. The antenna temperature is a system measure and therefore contains contributions from all noise and interference sources whether internal or external. External noise must be minimised (close to eliminated) during calibration.

The data is collected as antenna counts from which we determine the antenna temperature and then calculate the brightness temperature in the area of interest. During operation, each antenna passes a hot and cold target in order to provide consistently calibrated raw counts. The conversion from radiometer counts to Brightness Temperature is called the calibration process and the hot and cold loads at the target antenna temperature are fundamental to successful measurements.

In the case of the Balamis radiometer, noise is minimised through design of the antenna to produce a main lobe with low magnitude side lobes and to design out and protect the electronics from electromagnetic interference. To calibrate, steady state counts are measured at a constant temperature with the radiometer facing a microwave absorber at known temperature and then at the sky, which is an extensive brightness source with a known constant (6 K in L-Band microwave, specifically at night towards the north).

## 1.2 Soil Moisture

### 1.2.1 Dielectric Properties

As expressed in equation (4), Brightness Temperature is related to emissivity and body temperature. The radiation emitted by the Earth's surface (ground or soil) is no different:

$$T_B = e \cdot T \quad (6)$$

Where  $T_B$  and  $e$  are properties of the earth's surface and account for either the horizontal or vertical polarisation of the emitted radiation. In the case of the earth, a transformation using the Fresnel reflection coefficients must be applied [2] The Fresnel coefficient unites incidence angle and the dielectric properties of soil for flat surfaces with uniform dielectric constant. Hence  $e$  can be replaced:

$$e = 1 - \Gamma \quad (7)$$

where  $\Gamma$  is the surface reflectivity for the polarisation of interest. For horizontal polarisation (the interest of this study)  $\Gamma$  is related to the incidence angle,  $\theta$  and complex dielectric constant,  $\epsilon$ , as follows:

$$\Gamma_{oh} = \left| \frac{\cos \theta - \sqrt{\epsilon_s - \sin^2 \theta}}{\cos \theta + \sqrt{\epsilon_s - \sin^2 \theta}} \right|^2 \quad (8)$$

The dielectric constant measures the “strength” of the interaction between an applied electric field and the material under study. It is a property that indicates molecular freedom in a material and for polar molecules like water the response to small electric field changes is high.

Soil emissivity at microwave frequencies is optimised at 1.4 GHz [3] and related to the soil water content by the dielectric constant [4], which is low for dry soil (c. 2 to 5) and high for water (c. 80). This provides a broad range in dielectric properties to differentiate different soil-water mixtures and the soil permittivity is highly sensitive to changes in moisture content. The permittivities of other materials that may be present are also distinct from water, for example dielectric constant of Air c. 1 and Ice c. 3. Overall, soil emissivity has become a well established proxy for determining volumetric soil moisture ( $m^3m^{-3}$ )

Volumetric soil moisture is an established measure in agriculture and land measurement where in-situ dielectric probes are used for moisture measurement. However, the dielectric constant is difficult to determine in the field and reference tables have become the established norm for different soil compositions. FIG 3. shows the almost linear increase in dielectric constant with increasing moisture. As the dielectric constant increases there is a corresponding decrease in soil emissivity.

Soil composition influences the dielectric constant due to the different capacity to bind moisture to the soil particle surfaces. Bound water is less free to rotate and therefore contributes much less to the dielectric constant. Therefore clay soils (fine particles, high bound water) show lower dielectric properties. Similarly at lower moisture contents the residual moisture is more likely to be bound to the particle surfaces and hence the linear relationship is lost at low moisture volumes (under  $0.15 \text{ m}^3\text{m}^{-3}$ , FIG 3).

As well as good linearity within soil types, the dielectric constant is independent of soil temperature for practical purposes above the freezing point where water molecules become immobile. The dielectric constant of frozen soil is much lower than dry or wet soil and this characteristic is one reason radiometry is used for Arctic ice and permafrost surveys from space and near to earth.

### 1.2.2 Soil Roughness

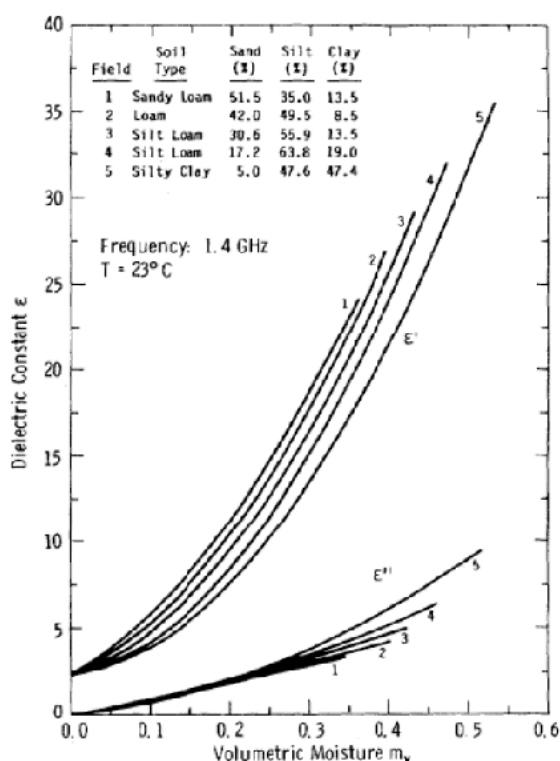


**FIG.3:** dielectric constant relationship to volumetric moisture for different soil textures and their sand, silt and clay composition. Hallikainen, 1985 [3]

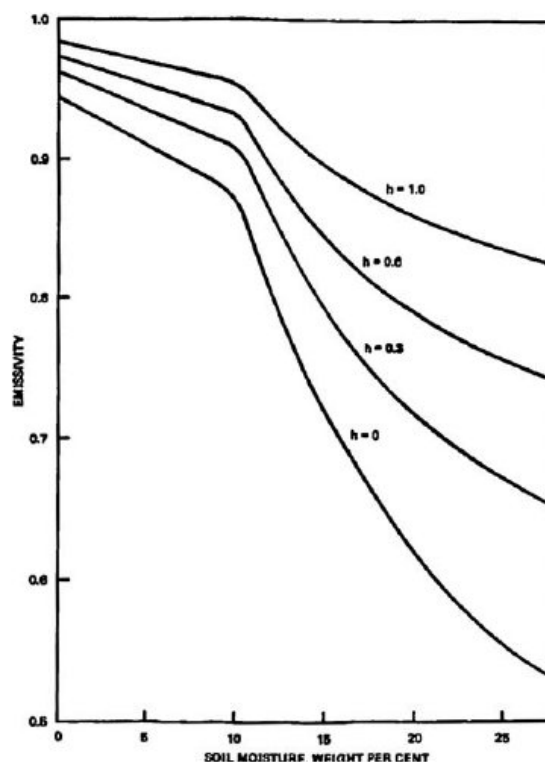


**FIG. 4:** L-Band emissivity for soil surfaces with varying degrees of the roughness parameter, h where 0 is smooth and 1 is rough. Choudhury, 1979 [5]

A parameter which is known to effect the radiometric measurements is the soil surface roughness ( $h$  or  $h_s$ ). More irregular surfaces significantly increase emissivity due to the higher surface area of the soil in contact with the atmosphere which permits increased scattering and also reduces the difference between scattering in the horizontal and vertical polarisations. Furthermore, as surface roughness increases, the relationship between soil moisture and emissivity becomes more shallow, that is to say that the sensitivity of emissivity to the underlying soil moisture decreases. As illustrated in FIG. 4 [5] the effect is significant, especially above mid to high soil moistures (>10%) where a non-linear break occurs.

In the situation where high moisture and high surface roughness exist together the emissivity is compressed to a narrower brightness band. While this does not preclude the use of radiometric measurements (the instrument is sufficiently sensitive), the change must be accounted for to maintain both accuracy (to ground truth) and differentiation between top surface moisture levels in a given area. Hence this is particularly relevant for ground vehicles measuring over soft moist soil since the vehicle can compact soil and/or increase the relative surface roughness.

A parameter must be introduced to the processing scripts to account for this relationship when inverting the brightness temperatures to soil moisture. The parameter,  $h$  proposed by Choudhury [5] modifies the Fresnel coefficient for reflectivity (*equation 8*) to account for vertical height and horizontal scale of the roughness and was quantitatively verified using both airborne and vehicle mounted radiometers in 1979.

The parameter itself is a value between 0.0 and 1.0, however soil roughness is a relatively subjective assessment. Several modified mathematical relationships have been proposed [6,7] and Wigneron et al [8] produced a semi-empirical solution in 2001 using the modified roughness parameter  $h_s$  where 0.2 represents a smooth area and 1.0 a heavily ploughed field, although these are observational values. Several other researchers and agricultural bodies have set methods to measure soil surface roughness but the parameter currently lacks a practical, quantifiable method. Perhaps the most promising solution lies with digital aerial photogrammetry which has the potential to measure low level peaks and troughs over a wide area using equipment substantially less expensive than LiDAR. Analogue versions of this technique using a line of variable height marker sticks are already in use [19] but limited in area cover.

Conversely, it should be noted that a soil surface which is smooth and dry may create a barrier to sub-surface moisture. Hard surfaces may be highly reflective and therefore high in emissivity which can result in no retrieved moisture values.

During the trials in this project the study area was not worked (tilled) during the measurement period in order to leave the soil surface as consistent as possible. However, some surface changes were still induced due to the changing weather conditions and repeated passes of the ATV, which leaves tracks on the periphery of the radiometric pixel.

### 1.2.3 Vegetation Cover

Soil emissivity is affected by vegetation canopy which can absorb and scatter the radiation emanating from the ground as well as add its own contribution. The magnitude of absorption in L-band depends on wavelength and moisture content of the vegetation. Several research teams have developed radiative models to compensate for this effect. However, during this study the soil moisture measurements were taken with no canopy cover and indeed very low to no vegetation cover. That said, in this project two photodiodes were introduced to provide NDVI data that could be used in future “above canopy” applications to identify changes in emissivity due to vegetation density. Optical depth is often used to adjust for the canopy effect and can potentially be derived from NDVI. Burke et al, 2001 [9] reported a linear relationship between vegetation optical depth ( $\tau$ , acting as a proxy for brightness temperature) and NDVI when introducing empirical parameters for vegetation water content ( $\alpha, \beta$ ).

$$\tau = \alpha + \beta(1 - \log(\text{NDVI})) \quad (9)$$

Other research into the effects of vegetation cover has verified the use of 1.4GHz as an optimal frequency to improve vegetation penetration and also the benefits of observing the horizontal polarisation to reduce canopy effects [10].

## 1.3 From the Earth to Space

### 1.3.1 Foundational Research

The brief overview in section 2 already indicates that knowing the dielectric properties is not in itself sufficient basis for remote sensing of surface moisture. The estimation of soil moisture from L-band emissions can become complicated by any factor that distorts surface emissivity. These factors are the surface texture (roughness), surface hardness, soil composition and water distribution, depth and mix within the substrate, cover from vegetation due to absorbing and scattering effects, incidence angles and the choice of the polarisation and frequency used for observation.

Research has demonstrated that passive sensors (radiometers) are less sensitive to some of these factors than active sensors (radar), which experience backscatter that can be difficult to decouple from the target measurement. Conversely, the resolution of a passive sensor is much lower than for radar, which has been a limiting feature of space based Earth observation (and one which is overcome through mobile near to earth radiometry as studied here).

Fortunately, research dating back 40 years has been published with technical insights that permitted algorithms to be developed to invert the L-Band brightness measurements to volumetric soil moisture and compensate for many variables. Balamis have implemented processing scripts that utilise parameters

elicited from the decades of research in this field, including some notable publications highlighted in table 1 that provided background to this project.

**TABLE 1:** some foundational empirical & theoretical research spanning 40 years

Concept Developed	Research Team
Radiometer sensitivity to soil surface roughness and vegetation	Choudhury, Schmugge, Chang, Newton, 1979 [5]
Predictive models for microwave emission from soil	Schmugge, Choudhury, 1981 [6]
Dielectric Mixing Models and influence on microwave emission	Hallikainen, Ulaby, Dobson, El-Rayes, Myron, Wu 1985, [3,4]
Consecutive retrieval of surface soil moisture in L-band	Jackson, Le Vine, Hsu, Oldak, Starks, Swift, Isham, Haken (1999) [25]

### 1.3.2 Applied Studies

More recently (within this decade) applied studies have put the theories into powerful practice, leveraging the advent of high resolution Earth observation to address pressing global concerns on water resources and climate change.

Initially, ground sensor networks combined with climate parameters (precipitation and evaporation) were used to demonstrate local and regional correlations to a Soil Moisture Index that can assist with drought prediction [11].

More recent local level studies explored the relationship between soil moisture, brightness temperature and fixed position moisture probes in order to build predictive models verified through a network of ground truth stations [12].

This year the predictive models have become more sophisticated through the application of satellite based SAR data and the study of soils with different textures [13].

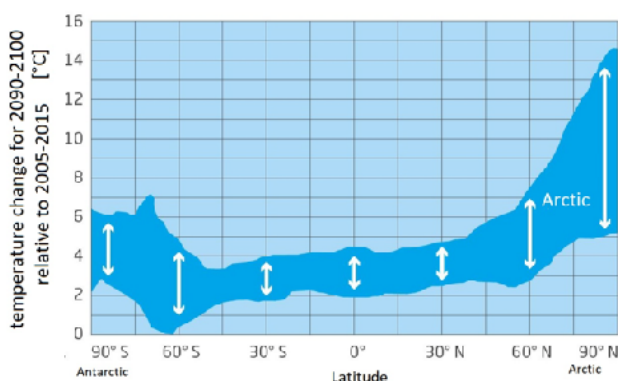


**FIG 5:** Climate change models often have a large predictive error range due to lack of detailed local process data eg. 90 year temperature change forecast of Arctic sea ice (left) and a mobile, sled mounted radiometer for ice thickness (photo: Lars Kaleschke).

Soil moisture is an Environmental Critical Variable (ECV), a fundamental driver of the global climate system and hydrological cycle due to evapotranspiration, these studies look set to continue and have expanded to include phenomena such as permafrost. The Balamis radiometer entered ice sheet thickness

studies in March 2019 to support MOSAiC (Multidisciplinary drifting Observatory for the Study of Arctic Climate, FIG. 5), a year long scientific ice drift expedition, which is planned from September this year. The radiometric near ground observation data can be used to verify and refine satellite observation data. In turn this can improve the climatic input variable needed for predictive climate models. High resolution studies of local processes provide a temporal and spatial resolution which is out of reach of satellites and can serve global needs as well as local needs.

### 1.3.3 Satellite Based Sensors (Earth Observation)

Satellite based L-Band sensing of soil moisture started in the 1970's with SkyLab, however the most recent launches achieved the highest resolution to date through compact, innovative antenna design and interferometry. The ESA SMOS (Soil Moisture and Ocean Salinity) mission launched in 2009 carries an L-Band radiometer with a maximum 5 day revisit time at the equator. The instrument is known as MIRAS (Microwave Imaging Radiometer using Aperture Synthesis) and the mission collects soil moisture at a volumetric accuracy of

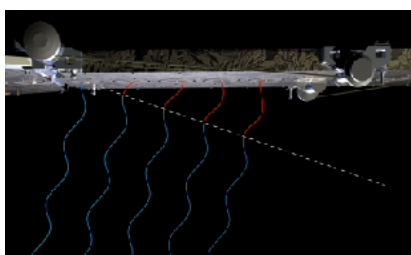
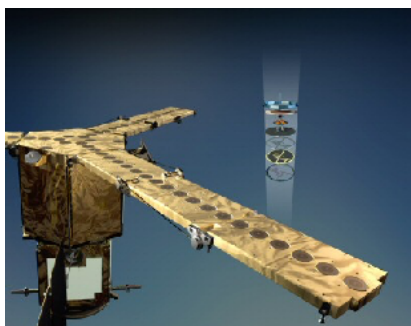


**FIG 6:** satellite L-band antennae and interferometry principle (courtesy ESA)

0.04 m<sup>3</sup>/m<sup>3</sup> (4% absolute or the equivalent of one teaspoon of water in a handful of soil) at a spatial resolution of 35 km for the radiometer at its centre field of view. To achieve this resolution an array of 69 "LICEF" antenna elements are distributed over 3 arms in a "Y" shape (FIG. 6). Each element passes its L-Band signal to a central processor that cross correlates the observations from all possible element pairs in the array at different viewing angles as the satellite orbits. In this way the phase difference of the incident radiation can be measured and interferometry calculations applied. Techniques and algorithms were advanced to achieve an interpolated resolution (downsampled) for soil moisture up to 8 km from around 2010 [2]. The results depend on certain assumptions that may compromise the accuracy of results retrieved compared to the native radiometric resolution.

NASA launched the SMAP (Soil Moisture Active Passive) mission in 2015 with combined L-Band radiometer and L-Band SAR (Synthetic Aperture Radar), also designed to measure moisture content in the top 5 cm soil layer and through moderate vegetation cover. Algorithms to combine the passive and active measurements into a spatial resolution of 10 km were developed and validated in near earth studies. However, this mission is only returning data via the radiometer due to an early technical failure of the radar amplifier.



Since the SMOS mission space borne L-Band measurements have delivered the spatial and temporal resolution necessary for global monitoring of meteorological, hydrological and agronomical phenomena. However, the native spatial resolution remained large at around 35 to 40 km . The need for greater, more precise and more connected understanding of the Earths systems in relation to hydrology and climate change continued to demand higher resolution. To improve further, ESA launched complimentary land monitoring satellites in 2015 and 2017 operating in visible and infrared with up to 10 m



**FIG 7:** Sentinel image distinguishing maize and sunflower crops, France 2015 (Copernicus Sentinel data/ESA/ University of Louvain)

resolution. This Sentinel 2 pair are now in orbit with a 13 band multi-spectral imager ranging from optical to SWIR and including four red edge bands at up to 20 m resolution. The Sentinel pair revisit time is under 3 days at 41° latitude, which for the first time is sufficient to monitor and respond to plant health conditions even during the rapid summer growth months. The multispectral imager permits various indices to be calculated automatically and for moisture and vegetation indices to be mapped at 30 m<sup>2</sup> resolution by interpolating between sensor wavelengths (see appendix).

These Earth observation investments indicate the importance of remote sensing data and its value to decision making from economic use of resources (water, fertiliser) to climate change and land usage strategies. As the sophistication of experimental studies increases and the availability of processed data improves, the benefit of remote sensing versus traditional sensor networks and point data will become more mainstream for industry and service providers.

The trend towards instrument integration - acquiring multiple data sets from one observational pass is also important. In the case of the Balamis radiometer photocells have been incorporated to provide NDVI information from thermal emissivity in NIR (near infrared) as well as emissivity in L-Band and this thesis will assess the combined application of both the photocell sensors and microwave antennae.

Hence, the Balamis radiometer used in this study has a role to play in increasing the resolution of L-band measurements for a closer study of local environments and changes. Additionally the instrument can be invaluable in verifying the algorithms being developed to interpolate satellite data to higher resolutions. The addition of NDVI data will further improve utility and support the approach to integrate multiple data sources which is happening in other areas of land monitoring.

## 1.4 Near Ground Aerial Radiometry (UAV)



FIG 8a : Nadir and Oblique Mounts

Early in this study proof of principle trials were performed to demonstrate the UAV mounting of a Balamis radiometer in both nadir and oblique (40°) angles of incidence to the ground (FIGs 8a and 8b). A small co-axial quad copter was modified to support a ring mount and to minimise interference from the onboard receivers, navigation and motor speed control through a Faraday cage. The UAV was intended to fly a standard grid pattern at very low altitude, between 15 m and 25 m using a FPV camera to permit flight distances up to 200 m.

The test flight proved successful and the radiometric data has been processed outside of this study. This trial was limited to a small UAV for proof of principle. The largest drawback in this situation was the limited battery power and low aerodynamics of the payload, which placed a disproportionate demand on the power drive system. In the event of light wind gusts a, controlled descent was forced outside the target landing area. Similar small UAV experiments have also been performed with radiometers and SAR [14].



FIG 8b: UAV Radiometry

	Plane	UAV	Ground
Central Frequency	1.413 GHz (radiometric accuracy 0.7K at 1Hz)		
RF Band Width	20 MHz		
GNSS	GPS, Glonass, Beidou accurate to 2.5m (0.025m in RTK) WGS82 EPSG:4326 format		
Beamwidth (FoV)	22° & 36°	36°	36°
Weight	15 kg	3 kg	6 kg
Dimensions	to fit plane	410mm diameter	400mm x 260mm
Voltage	12V to 35V	12V	12V
Circuit Current	0.7A		
Heat Current	4A	1A	1A

Table 2 provides some physical characteristics of the different Balamis radiometers according to their vehicular platform.

## **1.5 A Study of Potential New Markets**

### **1.5.1 Water Resource Management and Leakage Detection**

Potential applications beyond soil moisture and land monitoring were investigated, considering i) the lightweight portable form factor of the Balamis instrument ii) its radiometric sensitivity to changes in surface emissivity caused by the dielectric activity of moisture under ambient radiant conditions iii) ability to distinguish surface and sub-surface characteristics iv) market growth and industry need.

A new potential application exists within environmental management and the water distribution industry. This market segment is made up from national government, private operators and government standards agencies (“watch-dogs”) for compliance. The user side of the market consists of private individuals and industrial users. Perhaps more importantly there is a growing body of NGO advocates [15] for protection of fresh water resources and wet wildlife areas.

Operating standards are evolving rapidly at European and National levels due to the dual pressures of increasing demand through population growth and reduced availability due to climate change. This has led to the development of the “blue economy” in Europe and national level strategies to improve or better prepare fresh water management and distribution.

In Britain, the supply and demand lines for fresh water are forecast to cross in about 25 years, leading Sir James Bevan (chief executive of the Environment Agency, UK) to set ambitious targets to cut people’s water use by a third and to cut leakage from water company pipes by 50%. Many of these pipes form part of a long distance underground supply network of ageing infrastructure. Sometimes the only sign of a major water leak is a pressure drop between pumping stations that may be separated over considerable distances. Radiometric surveys could potentially assist with leak detection and support the infrastructure projects for large new reservoirs, desalination plants and water transfer systems that will be needed across the country.

Economic incentives to invest in leak reduction are set through consumer price rise limitations and substantial fines. This is intended to balance private sector returns to shareholders with the need for long term investment. For example, Britain has a leak reduction target of 15% by 2020 and it is public record that the largest water company, Thames Water, was fined £120 million for failure to tackle leakages in 2018. Subsequently, Thames Water froze payouts to investors, in contrast to the previous year when it returned £100 million of its £638 million operating profit to shareholders in dividends (this was during a period where corporation tax had been deferred ten years to assist with the capital investment in infrastructure).

Water network and leak strategy companies design leak resistant networks, monitoring and detection solutions. Hydrosave (UK) is a good example that

works with manufacturers and universities to develop new technology over the established acoustic, camera, thermal and GPR (ground penetrating radar) techniques. Alliances with this type of business, experts in the sector, could facilitate the introduction of radiometric solutions.

Spain has also declared a strategic plan to prepare the nation for future fresh water scenarios. Governments will need to impose continuously improving service standards on water distribution and infrastructure and will expect investment in leak mitigation where near earth radiometry may assist.

The issues do not pertain to only hot, drought prone countries or to cooler, high precipitation countries. Across Europe, improvements in water conveyance systems have resulted in an estimated decrease of water use for households by 18%, whereas Europe's population has increased by around 10% in the last two decades. Substantial water savings have been achieved in western Europe, with the water supply to households declining from 230 litres per capita in 1990 to 134 litres per capita in 2015 [15]. However, European metropolises and dry regions are still the most vulnerable to water stress.

A mobile and airborne radiometer has the potential to form part of fresh water security planning with its capability to be both a detector, locator and a predictive device. The Balamis radiometer can be a complimentary sensor to satellite based Earth observation and provide local or region insights at a much higher resolution monitoring service than is possible today over flood plains, cross country transfers and river basins.

It is widely appreciated that the frequency of major floods is rising and set to continue due to the relentless progress of climate change in the face of insufficient corrective actions and loose international political policy. One statistic from the UK's National Ecosystem Assessment in 2011 [15] states that 42% of floodplains in England and Wales are separated from their rivers largely by engineering. These economic, infrastructure and housing assets are vulnerable to floods and an industry has grown up around flood recovery as well as flood prevention. In recovery, close monitoring of structural humidity and asset humidity (for example paper, furniture) is required to optimise drying times and resume to normal operation. A radiometer could be ideal for monitoring progress and targeting more humid areas for faster drying.

Polygon, a Swedish company, is one of the property damage specialist companies working in assessment, prevention, recovery and restoration (including monitoring of drying) following due to water and flood incidents. Polygon's own case studies achieved cost reductions of 30% to 70% due to monitored drying processes that can speed up recovery and reported saving expensive structural elements avoiding the need to strip out and replace building materials, sheet rock and utilities.

Other businesses perform comprehensive inspections of civil assets, patrimonial or industrial buildings. Typically it is necessary to assess value, quality and insurance cost, as well as to document issues or design a

maintenance plan at key points in the buildings life. Common timings for these inspections are prior to purchase, at the start or end of a commercial lease agreement, prior to or after construction work and modification. The data assists owners and tenants in assessing damp and moisture that may cause or already have caused structural damage and therefore assign corrective actions and ownership, reducing the risk of future disputes and prolonging the life and safe usage of the asset.

The potential of the Balamis radiometer to assist in patrimonial building and civil engineering moisture detection has been demonstrated through internal company case studies of asphalt, concrete and ceramic composite characteristics and water infiltrations through roofs.

Currently, the radiometer is likely to be limited in the value it can contribute to “last mile” water services. There is a demand for efficient solutions to issues that arise in urban distribution, however the urban environment tends towards high electromagnetic noise. Early proof-of-principle tests of water infiltration have shown that pattern detection is possible in walls, roofs and other constructions.

### **1.5.2 Agricultural Management and Leakage Detection**

Minimisation of leakage to preserve resources is one important strategic element of water distribution, however public supply only accounts for 14% of water usage across Europe. A strategy is also needed for the *usage* of fresh water. Understanding the relationship between field surface, rainfall and irrigation through near ground radiometry could supplement satellite data to optimise water usage in agriculture. The start point would be to study the highest demand areas to produce detailed maps similar to FIGs 30, 35, 36.

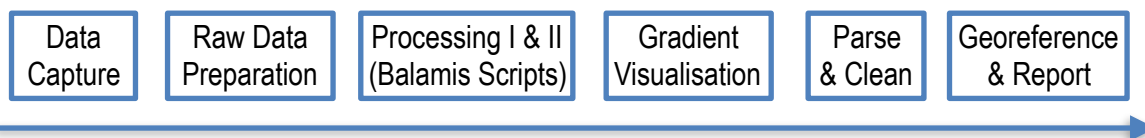
In Europe only 7-8% of agricultural areas are irrigated with Southern Europe reaching 15%. However, this portion of arable crop land represents around 40-45% of total annual water use in Europe with the most intensive periods being April to August in Southern Europe when the consumption can reach 80% according to the EEA [15]. During this period crops grow, precipitation decreases and actual evapotranspiration increases too. Southern Europe uses around 90% of the total volume of irrigation water in Europe, half of which is used solely in seven river basin districts: Ebro, Po, Southern Apennines, Guadiana, Tagus and Western, Jucar and Douro. All of these river basins experience water scarcity conditions throughout the entire year.

The EEA estimates that around one third of the EU territory is exposed to water stress conditions. Agricultural areas with intensive irrigation, islands in southern Europe popular with tourists and large urban agglomerations are deemed to be the biggest water stress hotspots. Thus the areas which can most benefit from higher resolution data (both temporal and spatial) through radiometric wide area monitoring are already known.

## 1.6 Method Development and Data Analysis Procedures

### 1.6.1 Outline of data processing

A basic workflow was developed and tested on recently collected data from farmland in the Lleida area of Catalunya:



Data capture may be through any of the radiometer versions or vehicle mounts (terrestrial and aerial). The principle difference in processing data from airborne radiometers is the introduction of pitch, roll and yaw to the raw data. This IMU data can serve to estimate the radiometric observation angle which is typically nadir or 40° from the horizon. This project used a front mounted radiometer on an ATV Quadbike.

Raw Data Preparation is classic big data handling to remove erroneous points. These may occur due to interference, unintended static location (e.g. ground truth data collection), read-write and translate errors, loss of GNSS location etc.

Processing I permits the adjustment of radiometer and substrate characteristics. For the instrument this includes the introduction of temperature specific calibration, contribution of sky brightness and polarity. This project used the sky brightness of 6 K in microwave and the horizontal polarity [10]. The soil composition can be modified to reflect sand and clay contents as referred to in FIG. 3. In this case Sand 35%, Clay 24%. Finally, close attention needs to be paid to the surface roughness and the Hs parameter adjusted (see FIG. 4). To this end it is helpful to have geolocated photographs of the sample area.

Processing II runs the scripts to invert the raw data to brightness temperatures to volumetric moisture. The converted data is output to a comma separated values file suitable for further processing in a spreadsheet, python / panda data frame or geolocation software. In this project QGIS from ArcSoft was used for geolocation and to generate gradient maps of the different attributes. Gradient (contour) visualisation is achieved by processing a .csv data frame into a shape file (ESRI's .shp format) then exporting as a rasterised vector data set with specified intervals that can be used to write a GeoTIFF image (FIG 9). A full step by step method was developed and documented to assist future users or to semi-automate the tasks in QGIS.

Parse & Clean refers to optimising the data set for specific analysis once the base .csv file has been visualised. This may include segmenting areas by time and location where ground truth samples were taken or eliminating tracks that do not form part of the core data set. Georeference is the final step and permits data to be overlaid onto a map with real world locations eg. agricultural fields, river valleys or civil buildings.

In this project topographic and orthophoto maps at 1:2500 and 1:25000 were used from the wms server ([http://geoserveis.icgc.cat/icc\\_mapesbase/wms/service?](http://geoserveis.icgc.cat/icc_mapesbase/wms/service?)) provided by the Cartographic Institute of Catalunya (<http://www.icgc.cat>). Note that satellite map images are correct for location, *not time*.

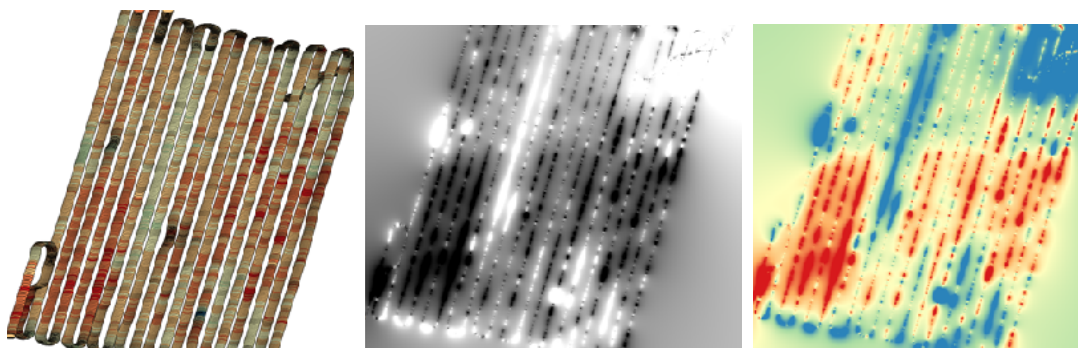


**FIG 9:** showing field volumetric moisture data using (left to right) a) discrete data points b) grayscale brightness c) continuous spectral image of moisture

### 1.6.2 Results from Processing of Lleida Dataset

The data set covering the field comprised 6092 data points which produced the image in FIG 9a. Approximately half the total data was discarded as extraneous non-field areas. A further 2% of values were removed due to a low skew with variable results. This accounted for moisture values under approximately 8% but had no significant effect on the mean. Neither high nor low values above 3 Standard Deviations significantly changed the mean results. That said, the total data set mean (16.4%) is not a useful measure given the non-uniform distribution of moisture over the area as seen in FIG 9c. It is one reason why point based sensor networks may not provide an accurate reflection of actual moisture distribution - each point result will depend on the sensor location and can vary within the space of a few metres. Eliminating the 2% of low moisture values improved visualisation and reduced the probability of reporting interference. The field was known to be very wet to saturated (puddles) and covered in strewn vegetation (stems and stalks). This led to the question of the correct soil roughness factor to apply and after some iterations 0.5 was chosen (Table 3.1). This is centre range and also the lowest value to achieve coincidence with the reference ground sample. It can also be seen that the Maximum moisture value recorded was over 50% (Table 3.0) which indicates a fully saturated area of field (no porosity). FIG 10 visualises the data distribution, showing a normal profile with high end skew (as expected for a saturated field) and the spatial distribution over the field based on the sampling pattern.

The results were converted to a contour map (FIG 11a) and the soil moisture content of a set of ground samples was calculated and geo-located. The ground samples coincide extremely well with radiometric data (FIG 11b) both showing tight standard deviations, possibly due to the very wet nature of the soil. Finally, geolocated photos were added to the topographic map to describe the nature of the field (FIG 11c).

Table 3.0 - macro results, whole field (retrieved horizontal polarised moisture)						
n=6092	mean	Std. Dev	Max	Min	+3SD Max	- 3SD Min
Hs = 0.5	16.4 %	0.05	53 %	8 %	32 %	3 %

Table 3.1 - Effect of Hs on Ground Sample Area				
Hs	0.5	0.6	0.7	0.8
Radiometric n = 600	26.7 %	28.0 %	29.9 %	31.8 %
Ground Sample n=3	27.0 %			

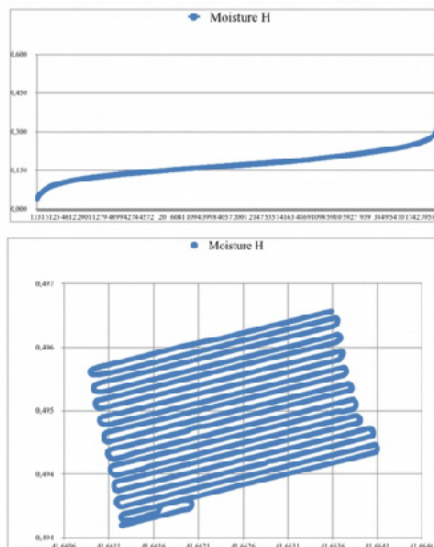
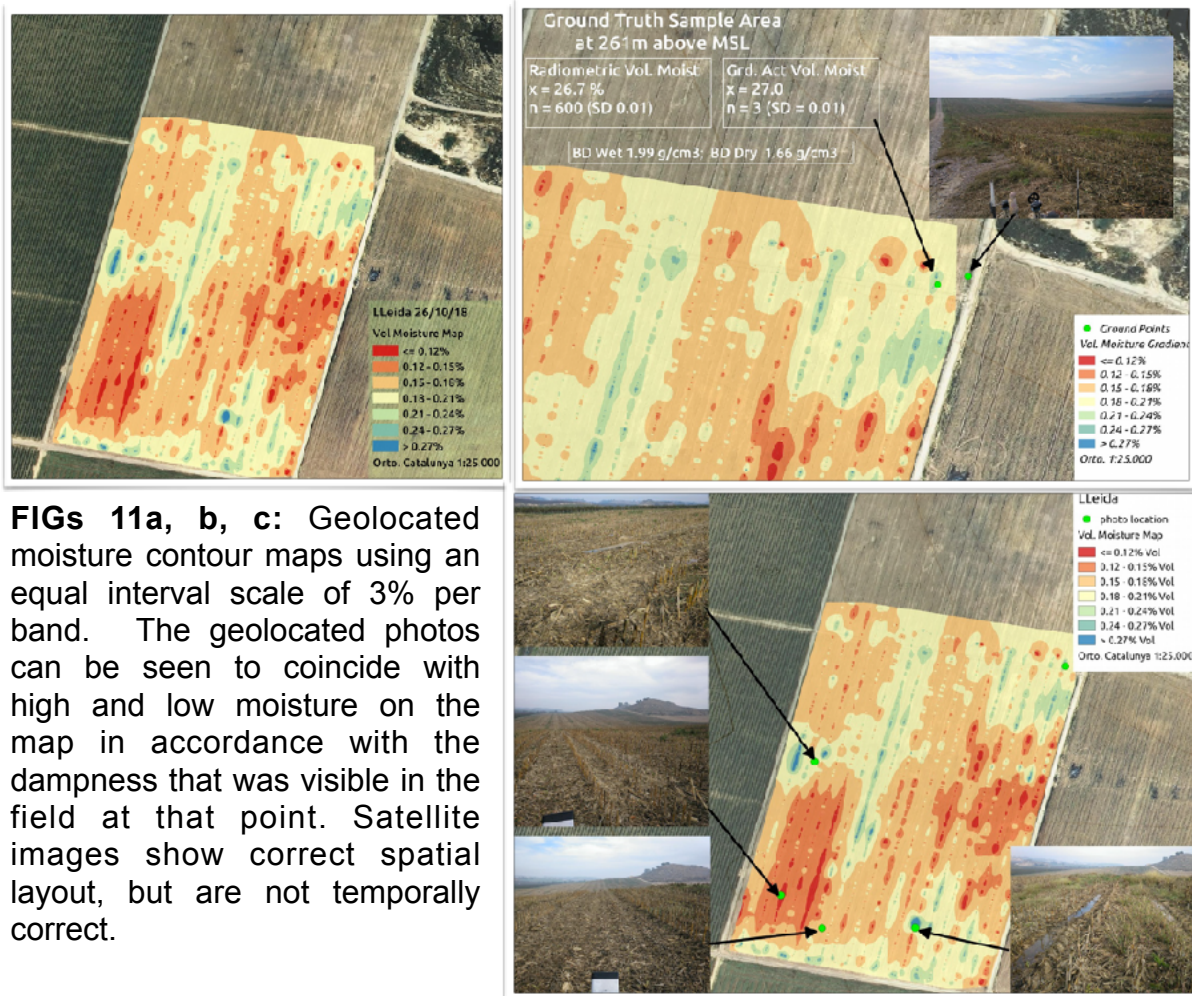


FIG 10 Data Distributions: top is time sequenced normal with high end skew and bottom is spatial distribution the acquisition pattern.



FIGS 11a, b, c: Geolocated moisture contour maps using an equal interval scale of 3% per band. The geolocated photos can be seen to coincide with high and low moisture on the map in accordance with the dampness that was visible in the field at that point. Satellite images show correct spatial layout, but are not temporally correct.



## CHAPTER 2: High Spatial and Temporal Resolution Radiometric Study of a Local Area

### 2.1 Context and NDVI Soil & Vegetation Results

#### 2.1.1 Location and Overview

A vineyard (Giró del Gorner, [girodegorner.com](http://girodegorner.com), FIG 12) in the wine growing region Penedés, Catalunya, Spain was used for this field study during early May when the vines are in their initial leafing stage. The upper left corner of the field (NW) falls to the lower right corner (SE) with a drop of 12 m to 13 m over a diagonal about 470 m (around 2.6 m fall per 100 m although it is not an even gradient over the whole area). The altitude is approximately 200m above sea level (ASL).



FIG 12 a, b: Vineyard field location shown by yellow markers (Google Maps)  
The area in Penedés contains 5 fields separated by roads, tracks or drainage ditches. The longest edge is 543 m with a circumference of 1.4 km. Total area 93,522 m<sup>2</sup> (approx 9,325 Hectares). The area slopes from its highest point in the upper left corner to the lower right corner of the field which is orientated NW to SE.

The objective was to study soil moisture changes from a dry condition to a wet condition and returning to dry during a consecutive 10 day period. In actuality 9 measurement runs were made during the 10 day period. One day, 5th May, in the middle of experiment was dropped due to wet ground conditions which made passage with the ATV Quad extremely difficult and was causing compaction of the soil in the quad tracks as well as increasing the risk of collision with vines due to mud-encased tires. Recorded rainfall for the day was 12.1 mm per m<sup>2</sup>, equal to 1.13 million litres over the whole field area (table 4.1).

The measurements were performed once per day in the morning, except for two days in the first half of the experiment: day 1 due to logistical issues and day 4 due to rain conditions. On these days measurements started at 13:30. Additionally, during the first few days a small part of the field was not accessible due to difficulty crossing a steep water runoff ditch, which was later resolved.

The field area was worked by tractor (tilled) prior to commencing the measurement runs and was not worked again until after the trial period. This helps to minimise contribution to emissivity due to changing surface area exposure (soil roughness). It also avoids artificially increasing surface evapotranspiration by turning a moist sublayer up to the sun exposed surface.

However, some tractor passes were necessary for spraying and weed control. Additionally, multiple passes of the ATV Quad did cause some light compression under dry conditions and relatively heavy compaction under wet conditions. The tracks fall under the peripheral observational area of the antenna, which from the ATV mount is  $0.9 \text{ m}^2$  in the horizontal polarisation that and  $36^\circ$  beam width that has been used in this study (FIG. 13e).



**FIG.13:** a,b,c,d,e (left to right). The field area contained visually different soil areas from brown to sandy to red. The main area appeared to alternate between a dark and light brown (13 a, b). This is likely to be due to tilling every other row at different points in time prior to the trial. Dark brown (13a) appears to have been tilled more recently while light brown (13b) appears to have had a longer surface drying period. The higher level rows (NW) were observed to be relatively sandy (13c). A small area (13d) contained red soil which is likely to have a different mineral content. One row (13e) was very compacted and studied separately.

In the data analysis section the soil surface roughness parameter,  $h_s$  has been kept constant at 0.2, a commonly used value, in order to facilitate comparisons between days. Hence, the moisture contour maps for each day are produced with this value. The radiometer sample rate was set to 1 Hz, which provides the best brightness temperature sensitivity and resulted in an acceptable calibration.

## 2.1.2 Experiments and Weather Conditions

- Photodiode NDVI Surveys
  - NDVI surveyed concurrently to Soil Moisture
    - a. consecutive days, different time and different light (days 01; 02)
    - b. effect of soil character / colour (days 07, 08)
    - c. effect of wet soil conditions. (day 05)
  - Vegetation strip study of NDVI and brightness temperature data
  - Comparison to Sentinel Satellite data for coincidental days
- Radiometric Soil Moisture Surveys:
  - 9 daily surveys at 1.41 GHz over approximately 9,300 Ha
  - Survey of soil type based on visual differences (day 02)
  - Survey of soil type in alternate rows of lower field (days 06; 07; 08)
  - Sparse data survey to simulate UAV ground speeds (day 09)
  - Ground sample collection and drying to compare to radiometric (day 09)
  - Time of day difference under constant dry conditions (days 01; 02)

The tables 4.0 and 4.1 summarise the survey dates and local meteorological conditions respectively.











**Table 4.0: record of the study dates and times**

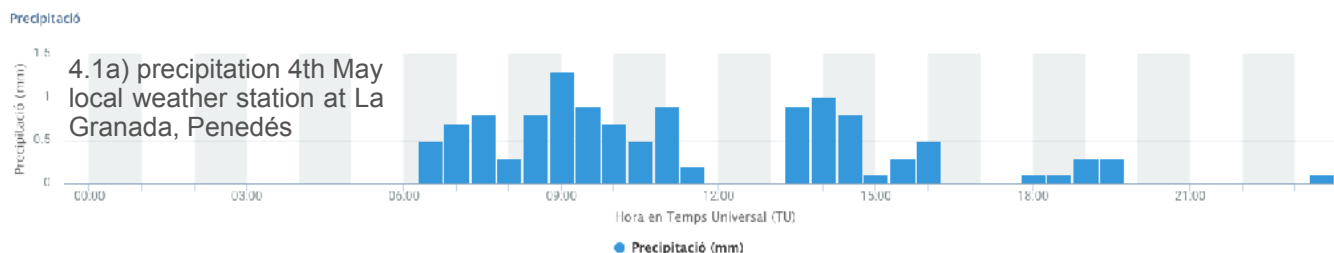
Day	1	2	3	4	5	6	7	8	9
Date	30/4	1/5	2/5	3/5	4/5	6/5	7/5	8/5	9/5
Start Time	13:30	11:30	10:55	13:25 <sup>1</sup>	10:05	10:30 <sup>3</sup>	10:40 <sup>4</sup>	10:30 <sup>5</sup>	10:30
Finish Time	14:25	12:30	11:40	14:15	11:45 <sup>6</sup>	11:20	11:40	11:30	10:55 <sup>2</sup>
Soil Surf. <sup>7</sup> Temp °C	—	32	32	13	—	19	16	18	24
Condition	part cloudy	part cloudy	sunny	light rain (wet terrain)	sunny (soft terrain)	part cloudy	part cloudy	cloudy	sunny

Table 4 footnote

- <sup>1</sup> delayed start to allow heavy rain to pass; some interruptions to wipe face of radiometer
- <sup>2</sup> 1 row in 3 sparse sample (higher speed to represent typical ground speed of UAV)
- <sup>3</sup> 1 row in 3 starting 1st upper row
- <sup>4</sup> 1 row in 3 starting 2nd upper row; lower half bottom field every 2nd row, brown soil.
- <sup>5</sup> 1 row in 3 starting 3rd upper row; lower half bottom field every 2nd row, white soil
- <sup>6</sup> difficult terrain conditions led to some interruptions and resampling

**Table 4.1: record of the weather conditions and meteorological parameters from the local weather station at La Granada, Penedés**

Day	1	2	3	4	5	6	7	8	9
Date	30/4	1/5	2/5	3/5	4/5	6/5	7/5	8/5	9/5
									
obs.	part cloudy	part cloudy	sunny	light rain & wet terrain	sunny & very soft muddy terrain	part cloudy	part cloudy	cloudy	sunny
Solar MJ/m <sup>2</sup>	19.1	24.7	20.9	4.6	30.9	27.0	5.9	16.8	28.5
Tmin °C	11.8	8.8	8.7	6.9	4.7	6.8	7.0	13.9	12.5
Tmax °C	20.1	21.4	21.4	12.5	20.6	17.5	15.9	22.1	22.3
Rain mm/m <sup>2</sup>	0.1	0.0	0.0	12.1	0.0	0.0	0.0	0.0	0.0
%RH avg	82	76	77	92	46	67	85	78	46



### 2.1.3 NDVI Introduction and Equipment Setup

The vegetation in the aisles of the vineyard was very well controlled with few plants or weeds and no vegetation cover. However, in preparation for future applications where airborne sensing or sensing over different terrains and substrates is envisioned, the NDVI capability was tested.

NDVI (Normalised Difference Vegetation Index) has been derived to determine plant health over a terrain, usually agricultural, grassland or forestal. The formula provides a normalised index between two electromagnetic wavelengths - visible red (Red) and Near Infra-Red (NIR):

$$NDVI = [NIR-Red] / [NIR+Red] \tag{11}$$

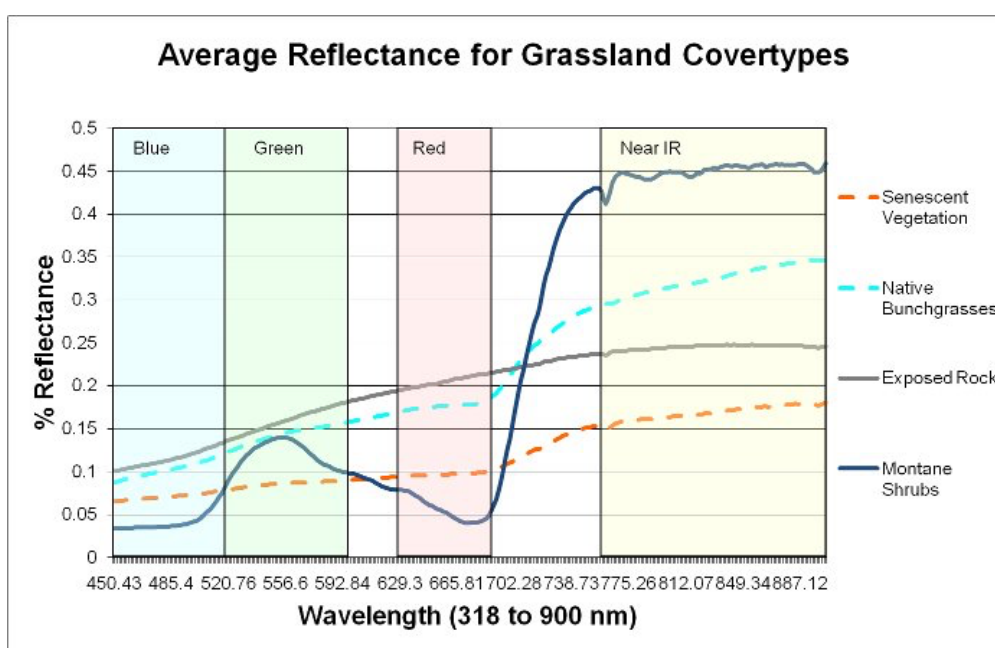


**FIG.14** reflectance values by wavelength for different plants and terrain. Montane shrubs show high greenness with low red edge reflectance and high NIR reflectance. (public domain image from a USDA joint project, [landscapetoolbox.org](http://landscapetoolbox.org))

NDVI may be referred to as Red Edge when specific wavelengths are used to indicate the maximum difference between absorbed photosynthetically active radiation (at the red edge) and reflected NIR. As shown in FIG 14 this absorption difference occurs at a peak green reflection (“greenness”) when there is active photosynthesis in healthy plants.

NDVI and related indices are typically derived from earth observation satellites (eg. Landsat or Sentinel 2) and have become a common indicator in precision agriculture and land management where airborne remote sensing is used. As shown in FIG 14, it is a measure of vegetation “greenness” and studies have developed correlations for different types of vegetation and grasslands.

Although the index is based on plant greenness, it is worth noting that interpolated satellite images will often replace RGB (Red-Green-Blue) with NRG (NIR-Red-Green), which creates images where the *red* colour brightness correlates positively to NDVI. The Sentinel 2 satellite constellation is equipped with a Multispectral Imager covering 13 bands, including Red and NIR at 10 m resolution and four vegetation Red Edge bands at 20 m resolution.

NDVI is potentially a valuable accompaniment to radiometric soil moisture data, especially when collected via aerial remote sensing. NDVI can also be used to determine vegetation coverage over soil or differentiate between terrains of interest that may have different emissivity properties. For example, roads and fields, buildings and water or ice cover. Therefore this index has the potential to assist in the expansion of mobile radiometric applications such as those discussed in section 1.5 where coverage of different terrains may be required.

Mathematically the NDVI index can range from -1.0 to 1.0, however the negative half of the index has few ecological correlations. It simply implies very low or no near infrared reflectance, which for example occurs with water. The relevant range for this study is 0 to +1.0 and may be divided into representative bands depending on the type of area being monitored:

- 0.0 to 0.1 barren areas (rocks, soil, sand, snow),
- 0.2 to 0.3 shrub, grassland or stressed, unhealthy plants, sparse cover
- 0.3 to 0.6 moderately healthy plants, green areas with light vegetation
- 0.6 to 0.8 healthy plants, good ground coverage and healthy canopy
- 0.8 to 1.0 healthy plants, dense coverage, full canopy, temperate forests

Note that the index will be less sensitive to changes in “greenness” density at the high end of the scale i.e. a small change in NDVI may represent a large change in plant health or, more likely, canopy density. The upper range may be combined as 0.6 to 1.0 and considered the “healthy” range in typical usage.

As an index, NDVI partially moderates external effects that influence recorded values, especially under different illumination (sun irradiance) and surface reflectivity conditions (the common challenge for remote sensing in the electromagnetic spectrum). It is possible to compare images over time but radiometric effects should be accounted for to be truly accurate as they can be influenced by the inherent characteristics of the subjects being monitored: vegetation moisture, vegetation coverage, photosynthesis activity peaks, soil moisture, soil roughness, reflected light from the ground (that in turn may be influenced by the local terrain activities, irrigation, pruning, tilling). Some standard operating procedures help to mitigate these variables for example by measuring over the same area at specific times of day where sun irradiance is constant [16] and technical solutions to measure incident sun radiation can help.

In the current application NDVI will be measured over large areas of bare soil (in between emerging vine canopies). It has been reported that soil surface has a large impact on NDVI values when the vegetation cover is low, between 45% and 70% [17]. In this application the main consideration is the near absence of vegetation hence some trials were performed over field edge vegetation strips.

These and other limitations have led to the development of several modified indices including Enhanced Vegetation Index, Wide Dynamic Vegetation Index, Soil-adjusted Total Vegetation Index, Soil-adjusted and Modified Soil-adjusted Vegetation Index. In the context of the current trial the Soil Adjusted Vegetation Index (SAVI) was evaluated as it introduces a weighting factor (L) for partial and low vegetation cover (see FIG 18). However, little value was gained over the standard NDVI. The L factor did drive differentiation in results but also increased sample noise (standard deviation) and NDVI was sufficiently precise and differentiated with the photocell sensors that were used, even over barren soil.

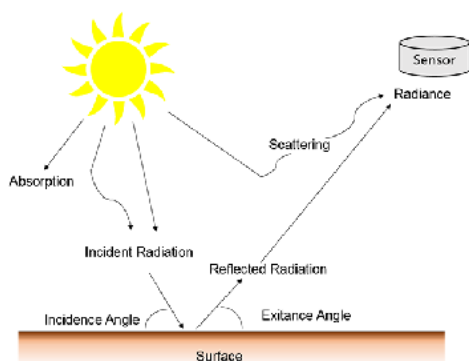


**FIG. 15:** Radiometric calibration is applied to digital cameras and multi spectral sensors data in remote sensing applications in order to compensate for differences across the reflected spectrum. This is especially important as scattering is related to wavelength. In the current application for NDVI only two wavelengths relatively close to each other are used and the instrument is close to the ground. Both of which minimise reflectance effects. However, variation in incident radiation (sun luminosity) still needs to be accounted for (image: Humboldt State University).

#### 2.1.4 Photodiodes and System Response to Conditions

NDVI is derived from measurements at two specific wavelengths. Ideally, as discussed, the reflectance from the body or surface under study will be equal at these wavelengths, at least for given light conditions. It is also essential to ensure that the sensor response to the different wavelengths is also equal otherwise a correction factor will be required when processing the raw data.

In this case, the Balamis radiometer was equipped with two Vishay silicon photodiodes (model BPW20RF) providing a linear photocurrent across a very wide illumination range (seven decades) [FIG 16a]. Each photocell was covered with a filter from Edmund optics with the first centred on 660 nm (visible Red) and the second on 780 nm (NIR). The photodiode is sensitive across a range from blue to near infrared and particularly sensitive in the area of interest (index 0.75 to 0.9) [FIG 16b]. The lowest sensitivity is in blue.

Hence, the inherent properties of the photodiode indicate linearity should not present an issue and sensitivity may be considered comparable at the wavelengths of interest. Therefore, the challenge with collecting reproducible NDVI data is centred on the external radiometric factors discussed above.

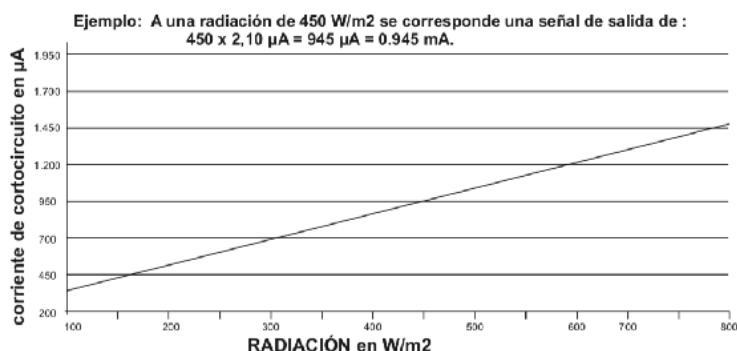


FIG 16a Photodiode with linear response to incident radiation

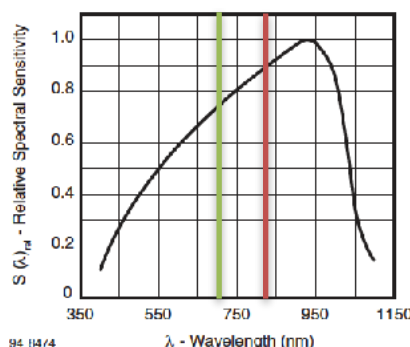


FIG 16b Photodiode spectral sensitivity vs. wavelengths of interest

To verify the system response to different conditions and determine the degree of influence external factors may have, a series of tests were made (Tables 5.0 to 5.3). The results may provide direction for development of operating procedures or a future calibration algorithm. For calibration, a standard laboratory procedure would use a calibrated reflectance target which ensures equal reflectance across the spectrum (visible and NIR) under different, quantified illumination conditions. A calibrated target is a substantial investment (up to \$2,500) and requires known illumination sources or a luminosity measurement instrument. In this application the photodiode is validated by the manufacturer and we are interested in just two discrete wavelengths. This led the tests to be performed with non-calibrated, coloured test cards under field conditions taking into account time of day (1 hour pre and post midday), between day (1 hour before midday), direction of travel and soil characteristics.

Three test cards, green, red and white were chosen and held in front of the photodiodes for approximately two minutes at 1 Hz sample rate. The photodiodes are mounted in the lower frame area of the radiometer facing the direction and at the 40° angle of the L-band antennae. The cards were held parallel to the photodiodes at 15 cm distance and avoiding direct sunlight. These cards reflect a relatively wide portion of the spectrum of visible light to some degree and have an intensity spike in their colour transmission range. For reference, the transmission wavelength band was measured using an Eisco handheld spectroscope for visible light with 500 lines/mm diffraction grating under daylight. Under monosource illumination this simple instrument can achieve a maximum resolution of 5 nm. In this case, there is a spread spectrum as can be seen in Table 5 where green is biased toward blue and red is biased toward yellow.

**Table 5:** spectroscopically measured transmission band for the test cards confirms discrete visible bands for Green and Red while White encompasses both.

wavelengths /nm	Visible Green 495 - 570	Visible Red 620 - 750	Visible White 380 - 750	NIR Spectrum 760 - 900
Transmission Green Card	510 - 540			
Transmission Red Card		590 - 630		
Transmission White Card			410 - 650	
NIR				—

As expected, the green card shows a higher NDVI response (less visible red reflection) than either red or white. Additionally, no significant difference was found for the green channel between days at the same time and under similar illumination (cloudy, no direct sun).

However, all other differences between mean values were significant at 95% confidence interval. The data sets were found to be normally distributed hence this verification uses the standard confidence interval t-test:

$$\text{Mean } \pm (\text{Standard Deviation} / \sqrt{n}) \cdot (1.96) \tag{12}$$

**Table 5.1:** NDVI using test cards on 1st May at 1 hour before midday and 1 hour after midday with a repeat of 1 hour before midday on 2nd May. Constant diffuse light through cloud layer.

NDVI	01 May			02 May		
	Green	Red	White	Green	Red	White
AVG 11:00	0.17	0.03	0.01	0.18	0.08	0.06
Std Dev	0.01	0.006	0.005	0.008	0.019	0.018
n	107	104	100	109	108	113
95% CE	0.168-0.172	0.029-0.031	0.009-0.0011	0.0165-0.0195	0.076-0.0835	0.057-0.063
AVG 13:00	0.20	0.13	0.11	—	—	—
Std Dev	0.06	0.006	0.005			
n	107	73	102			
95% CE	0.19-0.21	0.129-0.131	0.10-0.111			

Despite the statistical difference, which may be attributable to the precision and sensitivity of the photodiodes, the NDVI difference observed between days may still be considered *not meaningful*. Essentially, the interpretation of the index does not change, it remains less than 0.1 which is considered barren. However, time of day had a more significant influence and seems to have widened the reflectance differences disproportionately at one wavelength over the other. Nonetheless, the shift is only marginally meaningful at best considering it remains in the “barren” level of the index.

One additional test was performed with the green card due to a change in light conditions from cloudy to sunny. This data set (disregarded above) found the mean NDVI under cloudy conditions was 0.156 and sunny conditions 0.173, again, a small but significant difference at 95% confidence.

In line with existing radiometric evidence, this test indicates that obtaining values for NDVI that can be read directly over time will require a calibration with a standardised luminosity or lux-meter. Values should be measured for each test and can then be incorporated into processing algorithms. Potentially an upward facing photodiode could generate the necessary luminance reference. This technique features in parrot sequoia airborne NDVI sensors. Alternative solutions may be portable spectrometers for solar irradiance like the portable JAZ 350-1000 nm spectrometer from Ocean Optics that can be ground or



vehicle mounted. These instruments represent an investment and a full radiometric calibration to permit sampling under different light conditions would be time consuming and may be limited to the time of year it is performed.

However, it is also true that the relative difference between green and red or broad spectrum reflectance remains very distinct and sequential day results did not show a meaningful change. Hence, for this study NDVI to NDVI comparisons will use results from sequential days i) with different time of day and different light (days 01 and 02) ii) at the same time of day and similar light (days 06 and 07) iii) under wet conditions (day 05). In this way the effect of the differences in reflection can be assessed in the real world application.

Another potential variable was briefly tested, the direction of travel. The field orientation is NW to SE and the trial was performed at oblique sun angles where NW is away from the sun and SE is towards the sun. The radiometer is mounted very low at 40° to the horizontal, which could lead to a greater change in reflectance according to direction of travel compared to airborne nadir instruments. In this case the most consistent (compact) row as selected and no meaningful difference was measured (Table 5.2).

**Table 5.2: brief test over travel direction**

NDVI	02 May	
	Compact NW	Compact SE
Mean 12:00 HRS	0.039	0.034
Std Dev	0.007	0.005
n	47	54
95% CE	0.037-0.041	0.033-0.035
%Vol Moist	2.64 %	2.78 %

**Table 5.3: Travelling over different soil types (visually different colour and surface texture)**

NDVI	01 May			02 May	
	White (Sandy)	Brown	Red*	White (Sandy)	Brown
Mean	0.026	0.033	0.039	0.037	0.040
Std Dev	0.012	0.023	0.031	0.018	0.007
n	786	621	256	300	89

Direction of travel over a compact soil row towards sun (SE) and away from sun (NW) revealed a statistically significant difference but *not* a meaningful difference. For this run the radiometric moisture values were also consistent in both directions.

Additionally, given the initial observations, data was collected over specific soil types with visual differences (Table 5.3). NDVI uses a visible wavelength so a visible difference may be expected to change results. While statistically true (the instrument and index are sensitive), *no* meaningful differences were found in the context of NDVI's (Table 5.3)

Examination of the data within any one set shows discrete changes but no meaningful differences over soil (example in FIG. 17).

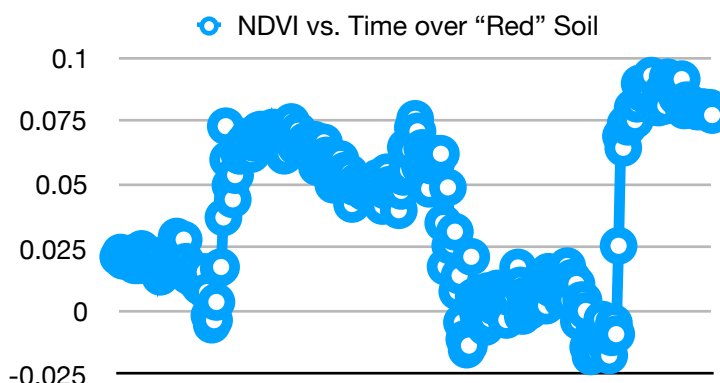
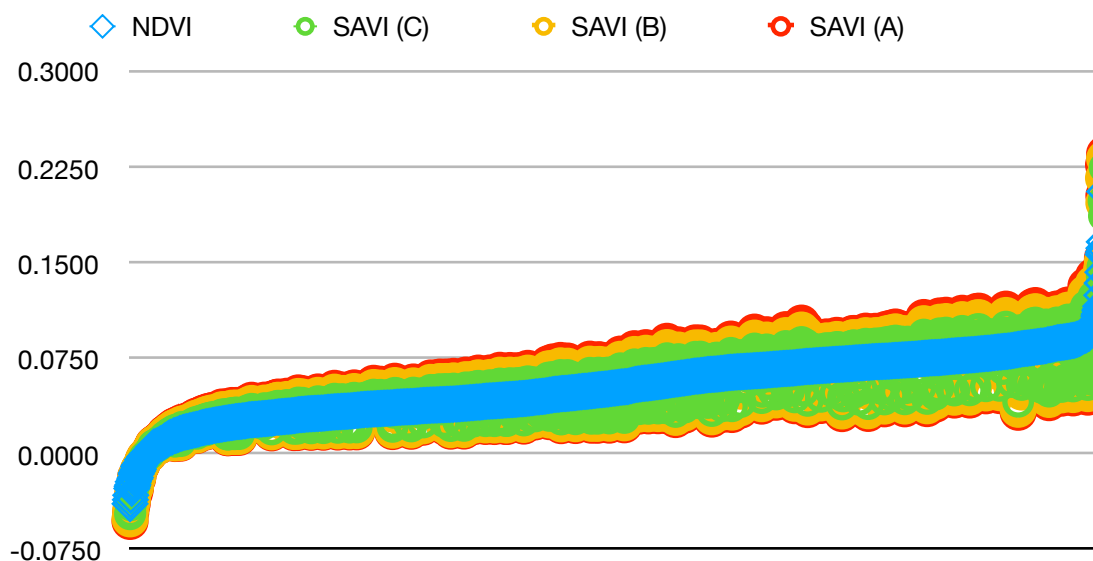


FIG 17: NDVI vs. Time

### 2.1.5 Soil Adjusted Vegetation Index - SAVI

SAVI modifies the NDVI to improve sensitivity over partially covered terrain, typically 45% to 70% [17]. In this case of low to no vegetation cover the adjustment tends to drive slightly increased noise as well as higher differentiation due to the mathematical factor ( $L = 0$  to 1). It can be a useful adjustment when processing for visual map overlays, however this was not strictly necessary for QGIS at the resolution intervals achieved with the photodiode even in the range of 0 to 0.1. Hence, basic NDVI was used.

$$\text{SAVI} = (\text{NIR} - \text{Red}) / (\text{NIR} + \text{Red} + L) \cdot (1 + L) \quad (12)$$



**FIG 18:** Effect of SAVI for different L values: Data sorted for ascending NDVI to show effect of driving increased differentiation in the basic index (06May Set). At  $L = 0$ , SAVI = NDVI. At higher L, greater differentiation in the index is observed by extending the range and standard deviation (slightly). Given the precision of the photodiode this was modification was not considered necessary.

### 2.1.6 Vegetation Strip Trials

To verify the response to vegetation, field edges were chosen where vegetation density (cover and greenness) was variable from none to above 80% along the strip. Some strip data was analysed using NDVI and SAVI before confirming the use of NDVI for the production of the geo-located contour maps. During the strip trials both radiometric emissivity and photodiode data were collected in order to compare the concurrently collected results as moisture and vegetation indices.

FIGs 19 a, b, c verify the vegetation response for different strips. FIG 19c from 6th May corresponds the the geolocated data in FIGs 20 a, b, which show that NDVI coincides with emissivity. The emissivity increases (retrieved soil moisture decreases) due to low level vegetation cover on the ground at this distance. The correlation fit (Brightness Temp to NDVI) is  $R^2=0.67$  however the mathematical relationship is undetermined between linear, log or polynomial (see appendix).

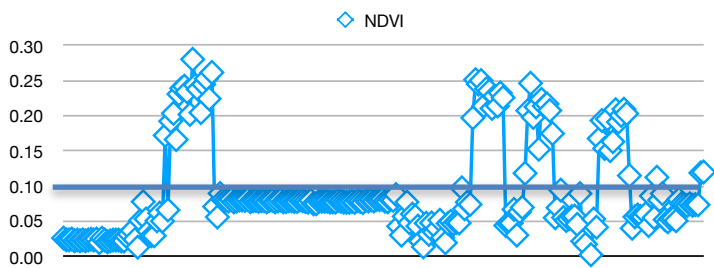


**FIG 19a:** 30April data showing NDVI response between soil and vegetation patches (vegetation >0.1 NDVI)

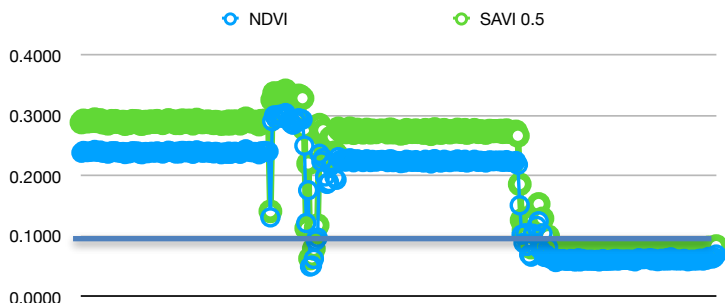


**FIG 19b:** 01 May sample. NDVI vs. SAVI for L = 0.5 over a strip of vegetation interrupted by soil and finishing in a strip of soil. Both indices show a clear change between vegetation and soil

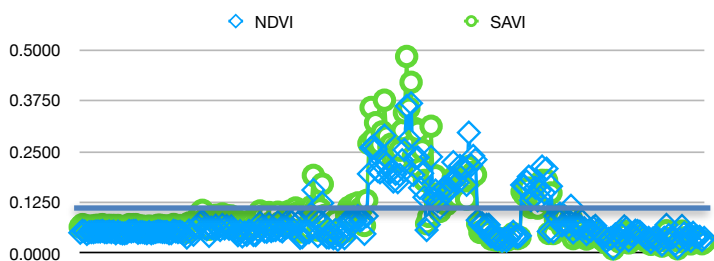


**FIG 19c:** 06May sample. NDVI vs. SAVI for L = 0.8 over a strip of soil - vegetation - soil - partial vegetation - soil.



**FIG 20a:** Emissivity (06 May)  
A seven level equal interval classification using inverse distance to power in QGIS. Note that samples were taken in a single row and the interpolated width is exaggerated.

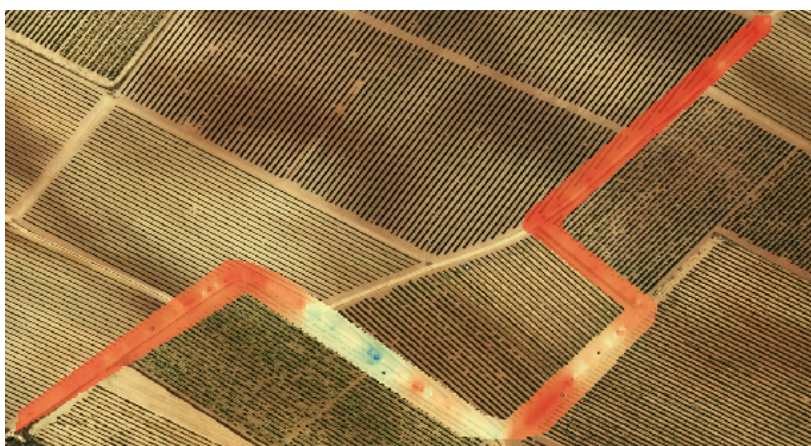
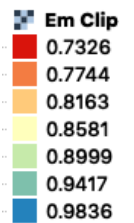
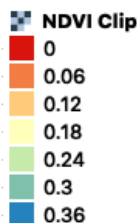


**FIG 20b:** NDVI (06 May)  
A seven level equal interval classification using inverse distance to power in QGIS. Note that samples were taken in a single row and the interpolated width is exaggerated.



**FIGs 19 & 20:** Vegetation Strip Trials showing NDVI response over barren, sparse and vegetation areas

Geolocated photos of the actual vegetation cover are presented in FIGs 21. The data is expanded to the whole field area in FIG 21b to illustrate barren and sparse measurement points. Differentiation of barren from green at the soil level (below canopy) may be useful for the targeted application of herbicides. More sophisticated correlations may exist to soil organic content [24,25,29,30].

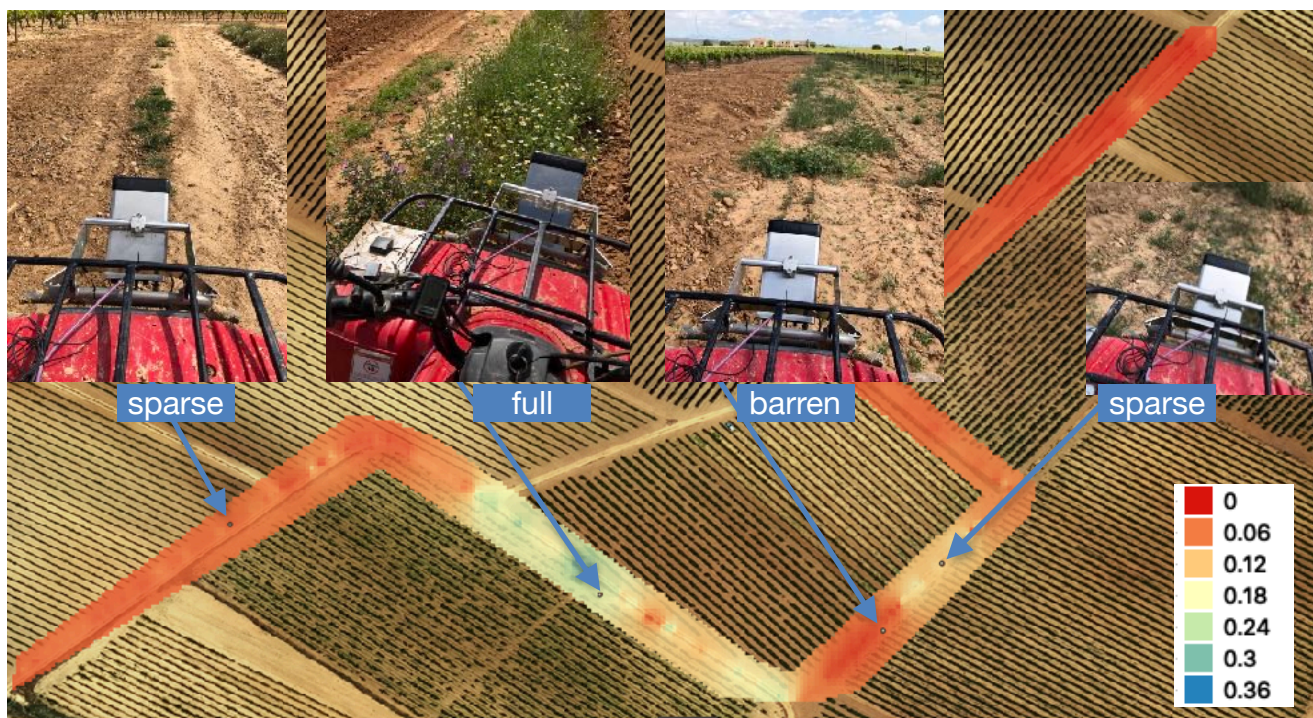


**FIG 21a:** NDVI (06 May). Photo locations for Vegetation Strip Trials over field borders show the vegetation cover at different points with the corresponding NDVI. The photocells provided very good sensitivity to vegetation cover.

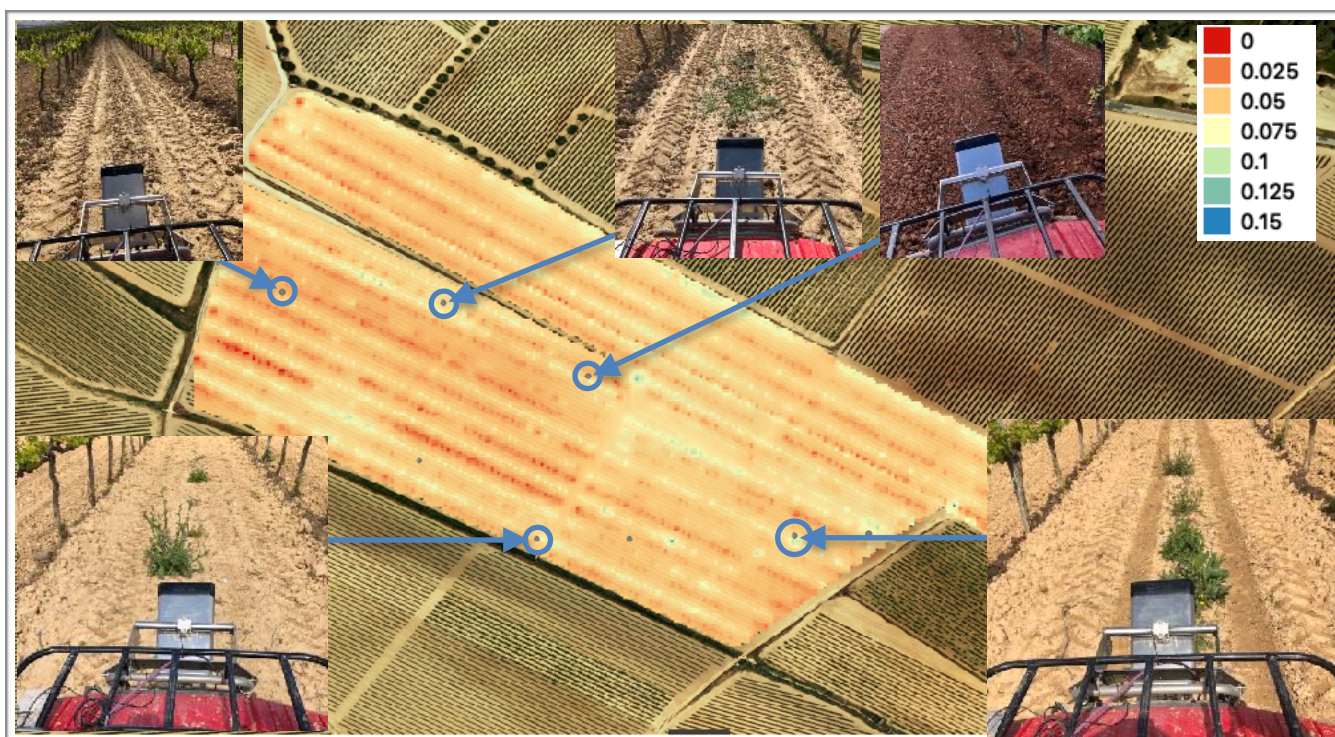


**FIG 21b:** NDVI (06 May) Photo locations to show some sparse vegetation locations. NDVI permits sparse vegetation to be detected on barren surfaces. Light green and above (>0.1) indicates presence of light vegetation on this finely interval scale.

### 2.1.7 High Spatial and Temporal Resolution NDVI & Comparison to Satellite

The contour colour scheme and number of levels is consistent between the images above to aid comparison between NDVI, soil moisture and emissivity data, although these are very different attributes. The following FIG 23 continues the comparison showing the data captured over the same field surface at the same time (06 May). NDVI intervals are very narrow at 0.025, which creates 4 levels under the first meaningful breakpoint of 0.1, above which sparse vegetation may be registered. The potential for high resolution capability is evident, however empirical work is needed to relate the contours to meaningful differences in the soil surface characteristics. The statistical differences do not yield meaningful differences in the conventional use of this vegetation index but could be explored in relation to soil organic content [29,30].

For the next tests, the scale was modified to 5 levels with a break point from light to colour at >0.1. Satellite data was then downloaded from the earth observation service *Sentinel Hub* for the same geolocations as the trial area. Sentinel L2A data for NDVI is available at a maximum 30m resolution (more information on Sentinel capabilities and L2A data is given in the appendix). Only two Sentinel 2 visit dates (01 and 06 May) coincided with the trial and had no cloud or shadow interference (clouds generate low NDVI). 06 May was chosen to present (FIG 22) due to its higher contrast, probably resulting from the recent rainfall.

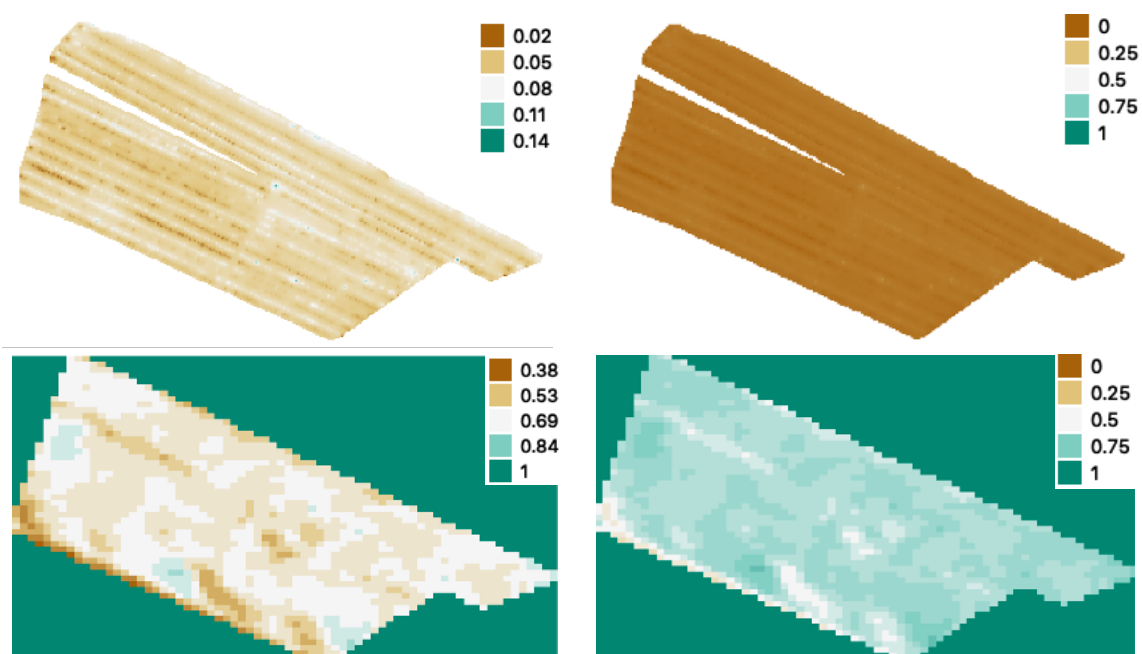


**FIG 22 a, b:** 06 May NDVI. The top row images show NDVI near earth (soil, 1m) and lower images show NDVI satellite (canopy, 30m). Left hand side (22a) is optimised scale, right (22b) is normalised scale and forces a colour difference between the near ground NDVI at 1m and above canopy satellite NDVI at 30m.

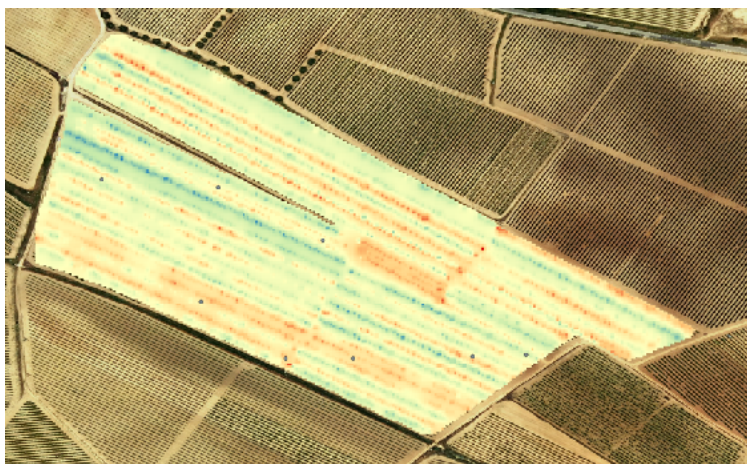


**FIG 23a: Emissivity (06 May)**  
Seven level equal interval classification using inverse distance to power in QGIS.

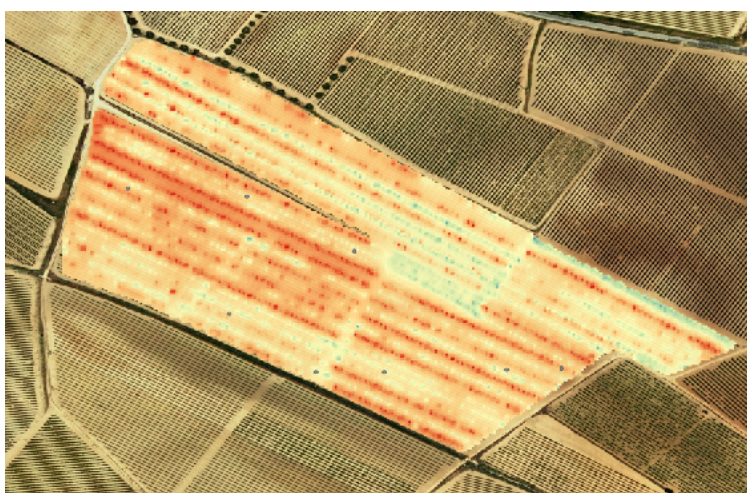
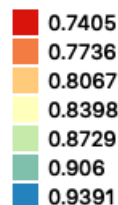


**FIG 23b: Moisture (06 May)**  
Seven level equal interval classification using inverse distance to power in QGIS.

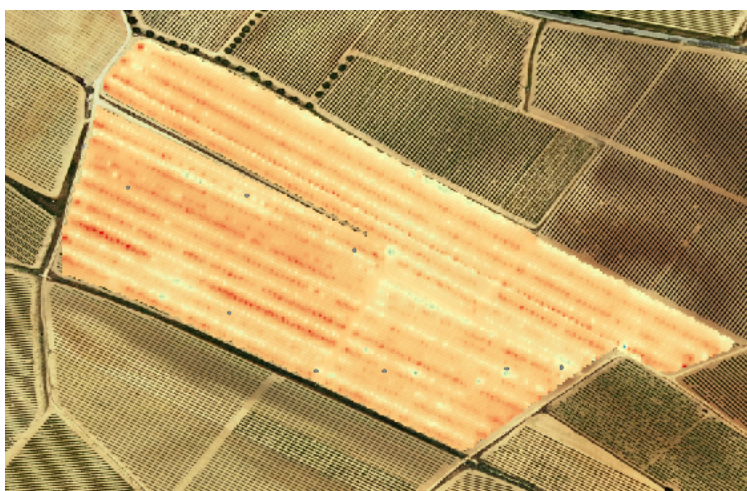
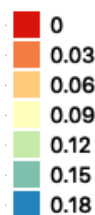
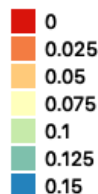


**FIG 23c: NDVI (06 May)**  
Seven level equal interval classification using inverse distance to power in QGIS.

Note, this is a very finely intervallic scale for NDVI in order to be consistent with the schemes presented above.



**FIGs 23:** Soil emissivity (22a, top), inverted to soil moisture (22b, centre) and the NDVI captured simultaneously (22c, bottom). Grey dots in each image indicate geolocated photo features used in FIG 21.

In the optimised scale (using the max-min range in FIG 22a), the extra precision of the ground level photosensors is evident, including picking out individual ground level plants (green dots). When switching to a normalised scale (FIG 22b), detail is lost and the contrast between ground based observation and above canopy observation is stark. Putting aside that at 30 m the satellite cannot distinguish between rows, it does register the emerging vineyard canopy at 0.5 to 0.75 index. At this scale the ground level radiometric data simply and correctly shows as barren or sparse ( $<0.25$ ).

### **To summarise the NDVI study:**

NDVI met expectations for accuracy during strip tests over variable vegetation and coincides with Emissivity (FIGs 20b, 21a). It also appeared to be far less sensitive to radiometric effects than either vegetation, moist soil or soil colour in this near to ground application. Hence, detailed NDVI maps were generated over the whole field: FIG 24 presents the high temporal and spatial results for NDVI over soil. It compares daily runs to a normalised scale of 0.02 to 0.14. Under 0.1 index, patterning is evident on the dry days and appears to relate to soil colour differences between rows (discussed later). Also, occasional sparse vegetation clumps are encountered and appear as green dots in the rows. However, the most meaningful change in the index occurs i) when encountering vegetation and ii) during the rain and subsequent wet ground. Under wet conditions the NDVI is pushed up over 0.1 in large parts of the field. These areas did not show a relationship to the retrieved moisture data which is visualised in the contour maps of FIG 25.

Although these maps are mostly at the “barren” level ( $<0.1$ ) of the index that currently has little ecological meaning, research has been published using the visible and near infrared in a multivariate model to predict relative soil moisture under laboratory conditions [30]. Additionally, the near infra-red frequencies used for NDVI may serve to determine SOC (soil organic carbon) or SOM (soil organic matter) using field [28] or remote [29] spectroscopic methods. Once established these algorithms may significantly enhance the utility of L-Band moisture retrieval by incorporating multispectral sensors that provide information on soil type, structure or surface conditions.

NDVI did distinguish different surface areas (tarmac, field, vegetation, water...) which can be useful when measuring emissivity in areas of mixed manmade and natural surfaces. Vegetation was found to increase the L-band emissivity in this experiment, hence retrieved moisture dropped as NDVI increased. The index may provide a complementary parameter that can inform the necessary parametric adjustments to account for emissivity changes due to vegetation cover or indeed other surfaces. Incorporating L-Band and NDVI capability to the low level operations of UAV's will be a step towards concurrent acquisition of soil moisture and canopy health.

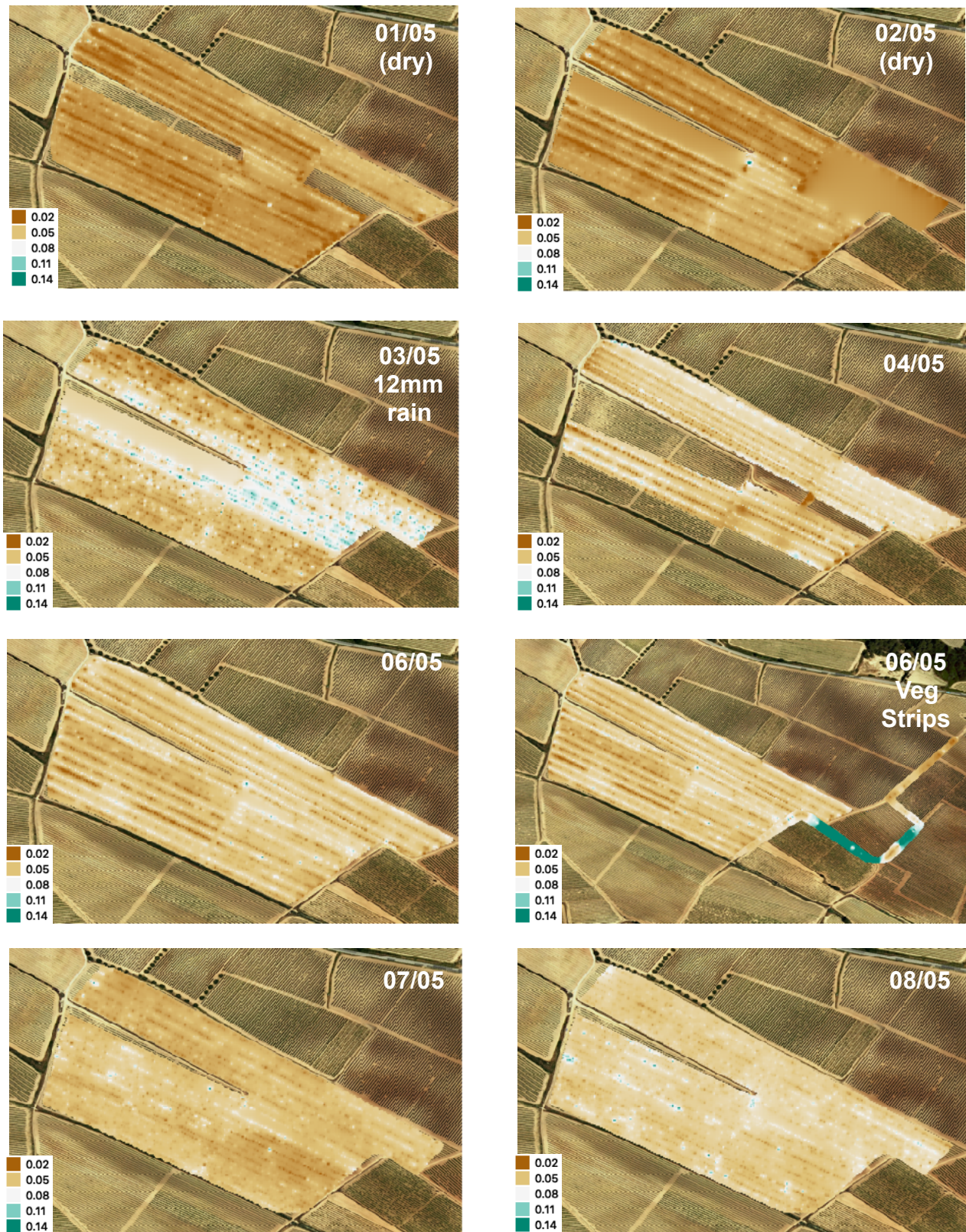


**FIG 24:** NDVI (01 to 08 May, normalised scale). The most significant effect over barren soil is caused by rainfall and vegetation. 01 to 02 May were produced at different times of day and light conditions but the results are very similar. 07 and 08 May perhaps indicate the difference in predominant soil type measured (07 Dark Brown; 08, Light Sandy). However, only two instances index over 0.1: during rainfall (03 May) and over puntual or strip vegetation.



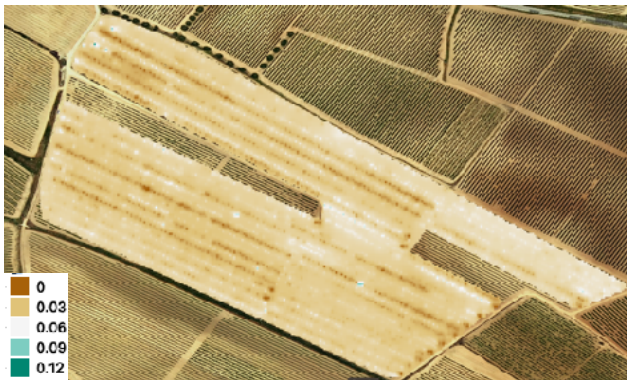
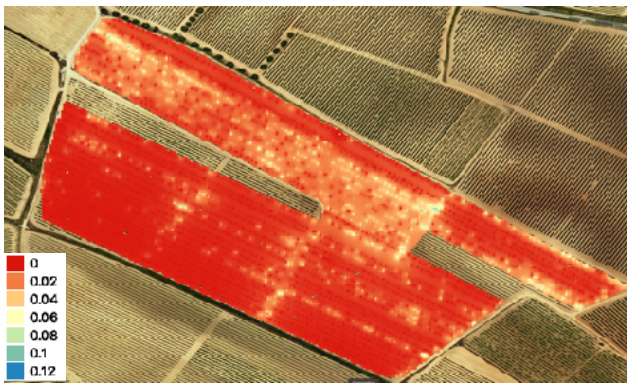


FIG 25a: 01 May (moisture top, NDVI bottom)

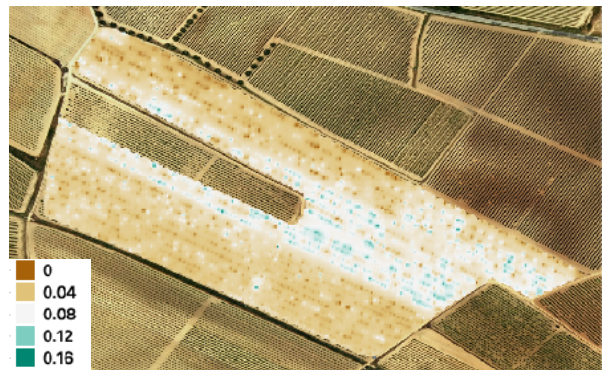
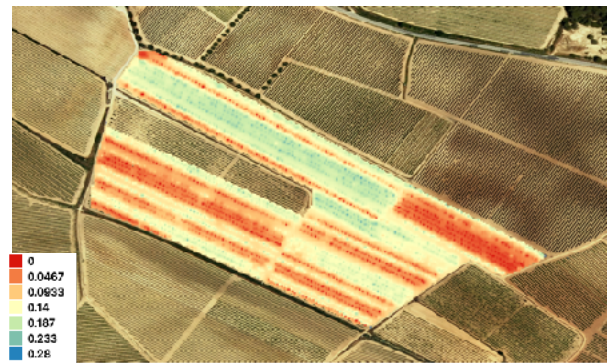


FIG 25b: 03 May (moisture top, NDVI bottom)

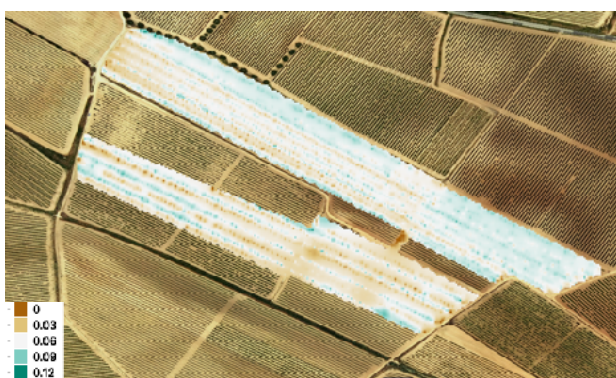
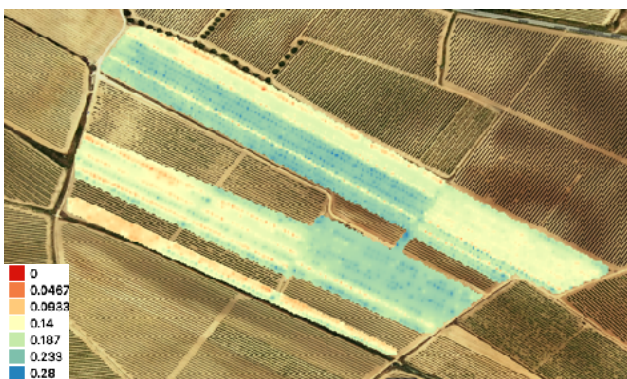


FIG 25c: 04 May (moisture top, NDVI bottom)

**FIGS 25:** A comparison of soil moisture and ground NDVI simultaneously captured with the radiometer and photodiodes. Note, individual scales are optimised to maximise data differentiation here. Photos below show the radiometer operating successfully during the adverse field conditions on 04 May after rainfall.



FIG 25d: 04 May ATV Quad and radiometer operating near to ground during wet field conditions.

## 2.2 Soil Moisture Results

### 2.2.1 Volumetric Soil Moisture

The relationship between soil emissivity in L-band and soil moisture content is well established as discussed in 1.1 and 1.2 and the objective of this project is to evaluate the practical application of mobile radiometry. Even so, the opportunity was taken to collect soil ground samples in order to assess the sampling method and provide recommendations on its effective application for future correlation and ground truth exercises. The volumetric moisture obtained via the bulk density method was compared to values obtained radiometrically at the same spot. Remote sensing offers the enormous advantage of interpolating a high density of measurements from a very wide space to map the area of interest. It is also advantaged in the sense that it is immune to individual techniques once the processing parameters are set. The alternative method for measuring soil moisture content in real time requires a network of in-situ soil moisture sensors or lysimeters. Both methods require careful calibration to provide accurate measures of soil moisture content [11, 18] and both devices can be used to provide a relative measure in a fixed area without calibration.

Single point ground samples generate one or a small cluster of data points and require diligence to correctly perform the field sampling. Soil scientists apply strict protocols to the collection of soil samples and use their experience to assess the suitability of the samples collected. The location and time of collection are both factors since the soil moisture will redistribute after rainfall in accordance with soil characteristics e.g. permeability, gradient, vegetation coverage. In conjunction with soil moisture, soil scientists may collect data on other key attributes - soil composition, soil surface texture for which difference methods have been developed [19].

In this exercise several issues were noted with the collection of ground samples. The difference between surface and sub-surface textures (hard and soft respectively), the degree of compaction and the stone, clump and particle content. As a density method, it is essential to ensure samples are not compacted during collection. However soil surfaces were very hard in some cases due to sun drying and compaction was an issue due to the preceding wet weather and number of repeat ATV Quad runs along the vineyard. Gravel (stone particles over 2 mm) and clumps appeared in some samples but were not accounted for during this sampling exercise.

The soil quality organisation of Australia places limits on coarse fragments for this type of method: gravel >2 mm at 10% content or stones and particles of 2cm. Above these limits the accuracy of the conventional method employed is significantly reduced [20]. The main concern noted here arose from particles (soil clumps) >2 cm which will influence the pore space and therefore bulk density measurement. In fact, coarse fragments are reported to have twice the typical soil density, reaching 2.2 to 3.0 g/cm<sup>3</sup>. For this reason the ground sample method is known to work best for soils without gravel or soil clumps.

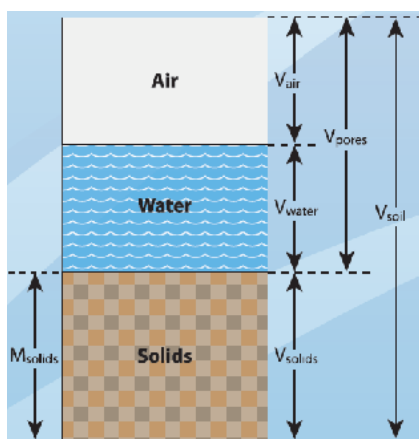


**FIG 26a:** Structural composition of soil showing the soil fraction ( $V_{solids}$ ), pore space of air ( $V_{air}$ ) and water content ( $V_{water}$ ). Image: Soil Quality of Australia ([soilquality.org.au](http://soilquality.org.au))

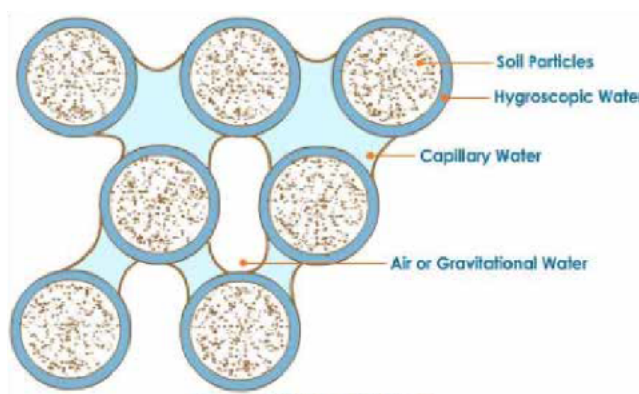


**FIG 26b:** Three types of soil moisture. Hygroscopically bound to soil particles, partially bound capillary moisture between particles and free moisture in gravitational pockets (courtesy ESA Earth Observation Summer School, 2012).

Before proceeding further, it is helpful to look at the nature of water in soil and be familiar with bulk density in this context. Soil is considered to be a composite of solids, air and water. The water is distributed through a given volume as a water phase, which may be continuous or discontinuous and vary in the degree of free or bound moisture and therefore lability (dipole lability is related to the dielectric constant as covered in Chapter 1). Air pockets and distributed solid components form the rest of the structure (FIG 26 a, b). The volumetric water content must be derived from a gravimetric measurement within a known volume that permits an estimate of the soil bulk density. Importantly, soil bulk density is also known as dry bulk density ie. it is the *dry* soil mass divided by the total soil volume including all material phases. This approach allows porosity to be estimated based on the volume of air (difference between total volume and water plus solids), which is a useful soil structure attribute that can be related to permeability and ease of root growth. Soil bulk density is classified in Table 6.

Table 6: Classification of soil bulk density		
	Bulk Density ( $g/cm^3$ )	
<b>Upper Limit</b>	1.6	generally accepted upper limit before root growth become restricted. Varies with soil type
<b>Coarse Sandy Soils</b>	1.3 to 1.7	The higher bulk density comes from larger but fewer pore spaces which are also less likely to hold water for long periods, leading to a soil with greater permeability and water movement under the surface
<b>Fine Silt or Clay</b>	1.1 to 1.6	In finer soils the particles are also smaller and permit more small pore spaces. The finer particles also provide a greater surface area and higher electrostatic forces which reduce water mobility (larger forces required to move or remove water compared to coarse soils)
<b>Peat / Rich Organic</b>	<0.5	High organic matter content can lead to low densities

The soil properties will influence moisture retention and emissivity. At any one spot, independent variables of the local soil attributes (e.g. surface roughness, porosity) may cause divergence of results when sampling.

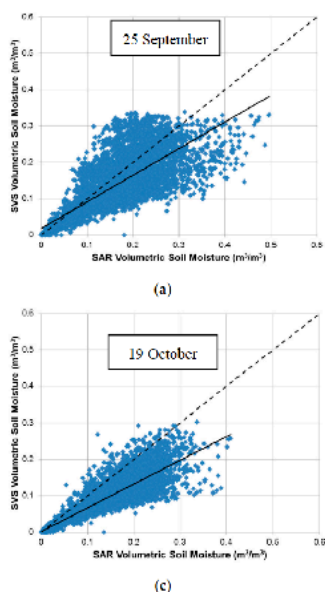


**FIG 27a:** Scatterplots of SVS Model and SAR estimated soil moistures. The dashed line is 1:1 relationship and the solid line is actual point to point regression between the techniques [21].

*In-situ* soil measurements were made during the same study (red line FIG 27b) and show moisture change every 2 days, recording a range from 0.25 to 0.45 m<sup>3</sup>m<sup>-3</sup> over two weeks. This is higher average moisture than we expect to find in Catalunya but it shows the large changes that occur.

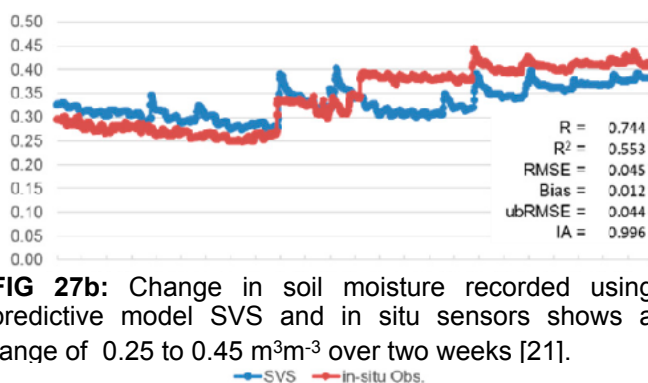




**FIG 27b:** Change in soil moisture recorded using predictive model SVS and in situ sensors shows a range of 0.25 to 0.45 m<sup>3</sup>m<sup>-3</sup> over two weeks [21].

The scale of data shown in FIG 27b requires the infrastructure of a ground station and sensor network not available for this exercise. Ground samples were taken using individual stainless steel soil collection containers (5 cm high x 5 cm diameter giving a volume of 98.17 cm<sup>3</sup>) at 4 different 1 m<sup>2</sup> points. 3 Samples were taken in a triangular pattern around the centre of the row. The 3 samples from each location were later weighed and combined for drying. This reduces the inherent sampling error (the error between samples was not of interest). The locations represented three edges and a centre point, which also covered three distinct soil types. A radiometric reading was taken adjacent to the sample area for approximately 2 minutes at 1 Hertz. Unfortunately 2 of the 4 samples were discarded. One produced over 50% of zero-value radiometric readings (possibly due to the very hard surface) and one due to a high stone and grit content. The two remaining results are shown in Table 7 (green box).

With this background, the variability of soil moisture and state of the art modelling techniques are worth taking into account. For perspective, a large scale study by a Canadian research team [21] reported this year on the use of the RADARSAT-2 SAR (Synthetic Aperture Radar providing spatial resolution of 100 m) to assess Soil, Vegetation and Snow (SVS) surface moisture contents in order to refine a sophisticated hydrological model that includes moisture transport through soil.

Soil type was noted to be influential with the model achieving higher correlation over coarse textured sandy soils than fine textured clay. This may be a model issue but it does point to the importance soil type. The sample distribution for the model prediction versus SAR is in FIG 27. The team established an impressively high Index of Agreement (IA over 0.9) with correlation values around 0.68 to 0.86 over large data sets.

Table 7 : Soil Ground Samples and Volumetric Moisture Calculation		
Location	1	4
Sample Pots	01-03	13-15
Soil Wet Weight /g	352	413
Soil Dry Weight /g	323	386
Moisture /g	29	27
Gravimetric Moist %	9.0 %	7.0 %
Sample Volume /cm <sup>3</sup>	294.5	294.5
θ <sub>g</sub> Grav. Moist / g	0.090	0.070
ρ <sub>soil</sub> Bulk Density Dry g/cm <sup>3</sup>	1.097	1.311
θ <sub>v</sub> . Volumetric Measured Moisture (ground sample) cm <sup>3</sup> cm <sup>-3</sup>	0.098	0.092
Radiometric Retrieved Moisture (h <sub>s</sub> = 0.2) cm <sup>3</sup> cm <sup>-3</sup>	0.083	0.073
Radiometric Retrieved Moisture (h <sub>s</sub> for rougher surface) cm <sup>3</sup> cm <sup>-3</sup>	0.098 (h <sub>s</sub> =0.5)	0.092 (h <sub>s</sub> = 0.6)
Porosity ε	0.58	0.50
location	upper SE corner	upper NW corner
observation	hard, firm	soft & sandy
soil surf. temp (IR)	24°C	29-31°C
Visual of sample locations. Soil Mix (theoretical model): Sand 35%, Clay 24%		

For retrieved emissivity and a theoretical soil composition (sand 35%, clay 24%), the radiometric results are 1.5% to 2% (absolute) lower than the ground samples using h<sub>s</sub> 0.2. Adjusting h<sub>s</sub> for greater soil surface roughness (0.5 to 0.6) brought the ground and radiometric moistures into exact agreement at 9.8% and 9.2% volumetric moisture for sample 1 and 4 respectively.

**For the calculation:**

Gravimetric moisture, θ<sub>g</sub>, is the mass of water per mass of dry soil:

$$\theta_g = (\text{mass wet} - \text{mass dry}) / \text{mass dry} \tag{13}$$

Volumetric moisture, θ<sub>v</sub>, is the volume of water per volume of soil, which is the mass of water/density of water all divided by the mass of dry soil /density of dry soil. Assuming the mass of water is equal to the volume of water i.e. density = 1, this simplifies to:

$$\theta_v = \theta_g \times \rho_{\text{soil}} \tag{14}$$

ρ<sub>soil</sub> is the bulk density of the soil, which has been noted refers to the dry soil mass per volume i.e. *dry* soil bulk density.

Soil porosity,  $\varepsilon$  is related to soil bulk density by:

$$\varepsilon = 1 - (\rho_{\text{soil}} / \rho_{\text{solid}}) \quad (15)$$

where  $\rho_{\text{solid}}$  is approximated by a constant  $2.6 \text{ g/cm}^3$  to represent the maximum soil particle density [22]. Hence, porosity indicates the maximum unoccupied volume in the sample and the value  $\theta_v$  indicates how much of this space is occupied by water, which is a useful reference for irrigation planning to reach an even distribution of water volume over a field area. A porosity around 0.5 is considered saturated.

An objective measure of soil surface roughness over an area would assist the accuracy of high resolution radiometry and potentially reduce uncertainty arising from the bulk density based ground sampling method. Digital photogrammetric methods could be considered to statistically determine surface height differences.

## 2.2.2 Instrument Calibration

Instrument calibration was performed on 29th April just ahead of the trial. The calibration consisted of raising the instrument temperature to  $40^\circ\text{C}$  (via an internal hot load circuit) and then sampling for two minutes facing a microwave absorber (295 K) and two minutes facing the sky (6 K). The temperature and passive L-band readings were logged and the variables were entered into the calibration file referenced by Balamis scripts for conversion of the L-band voltage readings into soil brightness and moisture. The calibration method requires an average of hot and cold load voltages during a stable time and temperature period for the instrument. This is best performed in an area free from potential electromagnetic interference including passing traffic, laptops and mobile phones. The effect of a received mobile phone connection can be seen in FIG 28c where a small but significant increase in detected power can be noticed at the lower right after the test time was complete.

All field measurements began once the radiometer temperature had self-stabilised at  $40^\circ\text{C}$  as verified via the instrument web interface. A temperature log is recorded for each sample period.

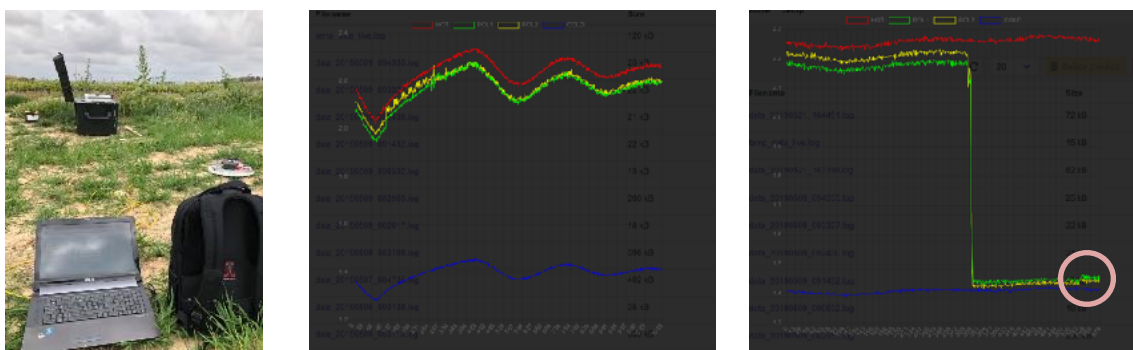


**FIG 28 a, b, c:** (a) Calibration set up (b) and screenshots showing temperature stabilisation and effect on antenna power sensed in both polarisations (c) inversion from absorber to sky at stable conditions. The circle marks an incoming phone call that registered with the antennas.

### 2.2.3 High Spatial and Temporal Resolution Soil Moisture Surveys



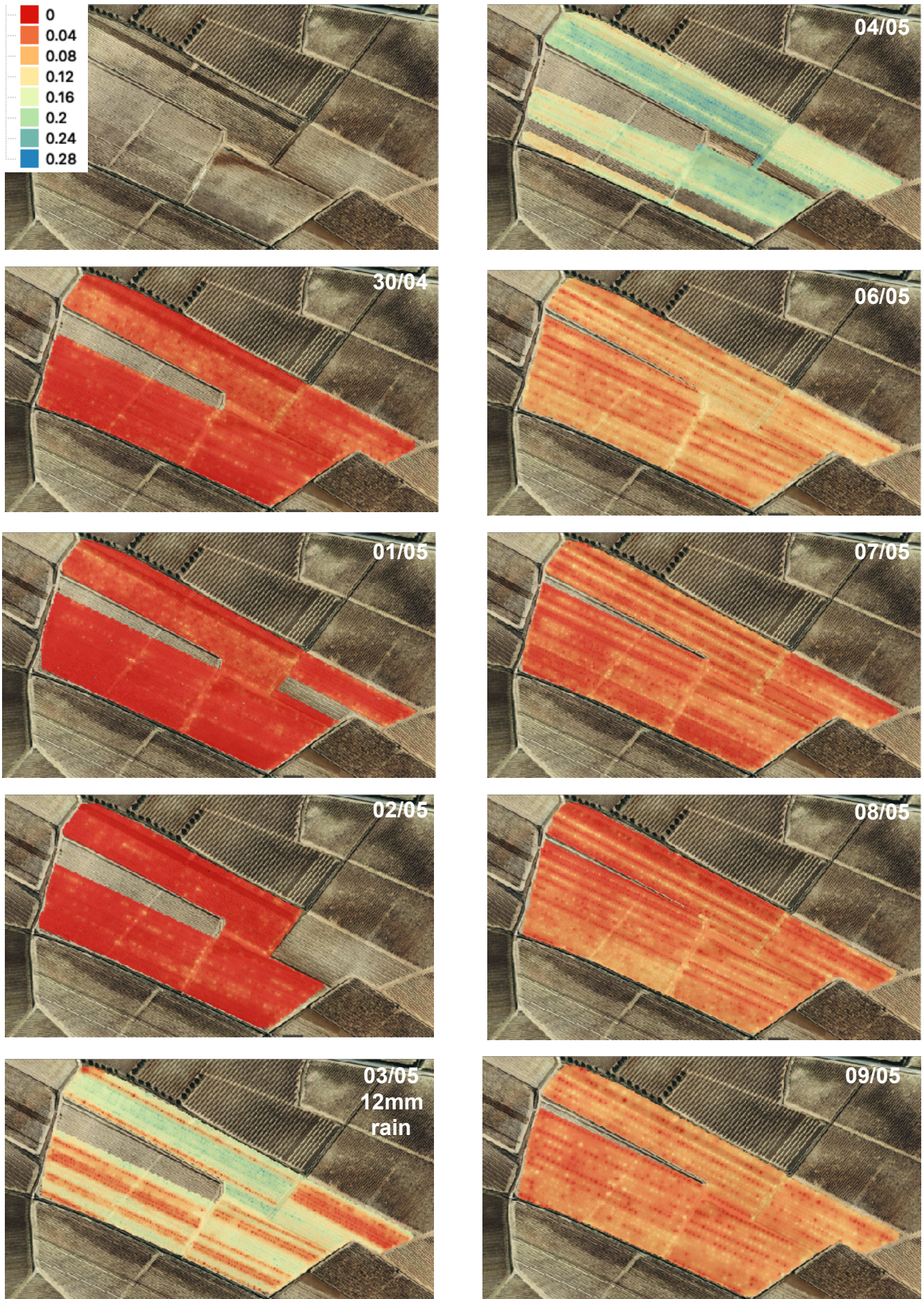
**FIG 29:** 9th May. Geolocated field moisture map over orthophoto. Volumetric moisture optimised to retrieved value range - 0 to 16%

Figure 29 above introduces the results which can be achieved using the technology in this study. However, the first figure to appreciate in this final section is the daily temporal resolution measured at approximately 0.9 m<sup>2</sup> spatial resolution at 1 sample per second frequency (FIG 30).

There is an evident pattern of stable emissivity being disrupted by rainfall. The measurements on 3rd May were taken during a short remission in the rainfall and appear to show the effects of different absorption rates of moisture into the soil. The following day, 4th May, the moisture settles into the subsurface and a similar pattern is observed where two large areas (upper north west edge and centre south-east) are visibly more wet than the rest of the field. All areas of the field have become more wet and indeed this presented difficulty in traversing the area using the ATV Quad.

Based on observation of the soil types (presented earlier), it was hypothesised that the higher soil moisture absorption related to softer, more sandy and less dense areas of field. The analysis of this hypothesis follows shortly. In FIG 30, the upper north west area appears more moist than the field average, then there is evident striation can also be seen from 3rd May forward. This striation is due in part to the linear sampling method and the distance that needs to be interpolated between rows to create a continuous contour map (sampling is 1 Hz in direction of travel and every 2 to 3 rows laterally in the field).

However, the underlying vector (FIG 31) data also shows groups of rows where moisture is similar and groups where there is notable disparity. One of the features of high resolution radiometry is the differentiation which is possible between very small sample areas of a few metres.



**FIG 30:** Sequential survey data **normalised to 0% to 28%** volumetric moisture, measured radiometrically in L-band at a resolution of 0.9 m<sup>2</sup> and 1Hz. The results show the daily change in soil moisture over a 0.09 km<sup>2</sup> area from a stable dry period through rainfall into a slow drainage period. Data processed in QGIS 3.6 for Mac and rasterised with eight equal interval contours after applying inverse distance interpolation to the vector data.



Hence, the sampling pattern was adjusted on 7th and 8th May to deliberately target rows of darker brown soil (07 May) and lighter, sandier soil (08 May). Both soil appearances occurred in the lower third of the field in approximately alternating rows. The day prior (06 May), a random row pattern was followed and the day following (09 May) a random pattern was followed at a higher velocity. The principal aim of this final trial was to compare a “sparse” or coarse data collection to the standard, dense pattern from the 6th May. The aim was to evaluate whether the higher velocities of a UAV (c. 25 to 30 km/hr) would produce equally robust results to the slower ground vehicle speeds (c. 15 to 20 km/hr) at the same 1 Hz sample frequency.

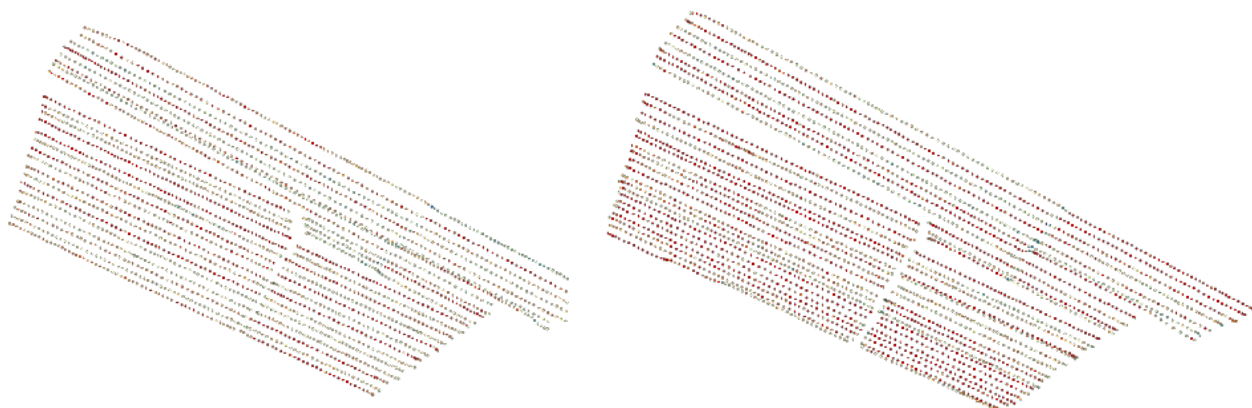


**FIG.31:** Vector data for 6th and 7th May shows examples of patterns in alternate and clustered rows. Note that adjacent rows are opposite travel directions and no pattern was detected linked to travel direction. Indeed moisture swings were likely to occur across internal field boundaries while staying consistent in row.

These data were analysed to determine whether the retrieved moisture data was showing a statistical difference versus the average in the field, the average over days and the average between the apparent soil types. The results are summarised in Table 8.

The analysis in Table 8 considers the entire field and the area of interest (AOI) defined by the *type of soil*. Firstly, with all data samples and then with values under 1% retrieved moisture removed. The vast majority of this data is zero and relates to emissivities  $> 0.89$ . The difference in data set size is indicated by  $\Delta n$ .

#### 2.2.4 Soil Types & Dry Surfaces: The Zero Factor

In table 8,  $\Delta n$  is the number of zero-value records retrieved (actually moisture  $< 1\%$  the vast majority of which were zero). Clearly the distributions cannot be normal in situations with a high number of “zeros”. The corrected mean values are in bold after zero-values are removed to approximate a normal distribution. The 06 May values are significantly different to each other and all other values at 95% confidence interval. This is expected based on the contour map which shows the recent rainfall is still penetrating the surface layers. On 06 May the AOI (area of interest) also shows a lower average than the total field with a similar percentage of zero values. This indicates that random sampling was

equally effective in all areas of the field and improved immunity to zero values. Notably, removing zeros does statistically increase the average retrieved moisture content. Reading from the datasets with less than 15% of zero values the change can be +5% to +20% of the mean. This signifies that zeros need to be managed to improve the radiometric accuracy.

**Table 8: Statistical comparison of field and AOI between days with similar weather and mid-moisture contents to see influence of soil type**

	Total Field Area				Area of Interest (lower SW field)			
	Mean	n	Std Dev	$\Delta n$	Mean	n	Std Dev	$\Delta n$
<b>06 May Random</b>	0.071	2720	0.044	416	0.068	1110	0.040	159
<b>&gt;0.01</b>	<b>0.085</b>	2304	0.036	15 %	<b>0.078</b>	951	0.031	14 %
<b>07 May (AOI Dark)</b>	0.041	3217	0.041	1264	0.030	652	0.035	304
<b>&gt;0.01</b>	<b>0.068</b>	1953	0.031	39 %	<b>0.056</b>	348	0.030	47 %
<b>08 May (AOI Light)</b>	0.047	3176	0.041	1046	0.068	659	0.029	27
<b>&gt;0.01</b>	<b>0.070</b>	2130	0.030	33 %	<b>0.071</b>	632	0.026	4 %
<b>09 May Sparse</b>	0.061	1602	0.038	244	0.062	522	0.036	67
<b>&gt;0.01</b>	<b>0.072</b>	1358	0.031	15 %	<b>0.071</b>	455	0.029	13 %

Comparing 09 May to 06 May the profiles are very similar. The field is drier after the extra 3 days and the sample count is lower (more sparse) due to the higher velocity, which results in approximately 60% of the sample count obtained at slower speeds. However, the field moisture is identical to the previous day average and importantly there is no loss of precision and no change in lost data due to zeros, which indicates the same quality of data could be collected at UAV flight speeds of 25 to 30 km/hr.

The data set of particular interest is 07 May with the focus on dark soil rows. In this case the field moisture as retrieved is markedly lower at 3% to 4% than the other data sets at 6% to 8%. The percentage of zeros found in the data set is very high, approaching 50%, which in itself could be a justification to discard the sample. However, observationally the dark areas were harder on the surface and may have different emissivity properties or heat more quickly in the direct sunlight to further promote surface drying. After cleaning the 07 May data set the mean values come closer to the field average but a significant difference remains between the soil moistures of the dark rows versus the lighter, sandier rows. It is likely that the cleaned data set is providing a more accurate value.

Retrieving a zero moisture can be a genuine result for a dry top surface. However, it can also be caused by a hard and reflective surface layer or by

interference causing emissivity to spike. Hence, it is prudent to rule out a device effect caused by local interferences. A look at emissivity to retrieved moisture correlation (FIG 32) shows excellent agreement for 06 May and  $R^2$  only drops slightly from 0.80 to 0.73 when the zero values are removed. There is no indication of spikes caused by external interference. 07 May shows a lower  $R^2$  correlation fit and this drops notably when zeros are removed from 0.75 to 0.56. This is a smaller data set but there appear to be more outliers although not so extreme as to indicate interferences.

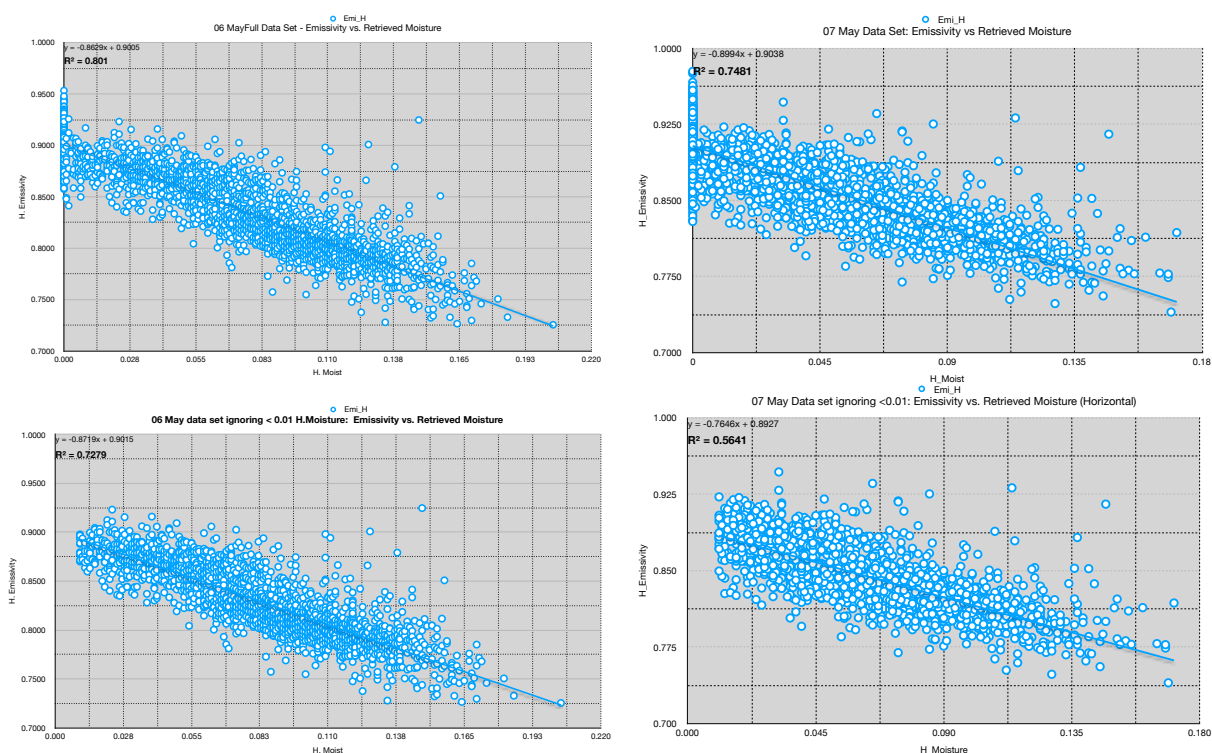


**FIG 32:** Retrieved moisture vs. emissivity for 06 May (left) and 07 May (right). Top charts include zeros and lower charts exclude zeros and moisture < 0.01. 07 May which targeted dark soil rows shows a substantially lower correlation fit ( $R^2 = 0.56$  versus  $R^2 = 0.73$  for 06 May random sampling pattern).

Combined with analysis of moving averages and the lack of any consistent pattern between soil moisture and direction of travel (moisture may be high or low in either direction and swings occur both up and down crossing field boundaries), it is very likely to be a surface effect of the soil. Most probably a hard surface layer, which was noted while attempting ground sampling in the dark brown soil areas.

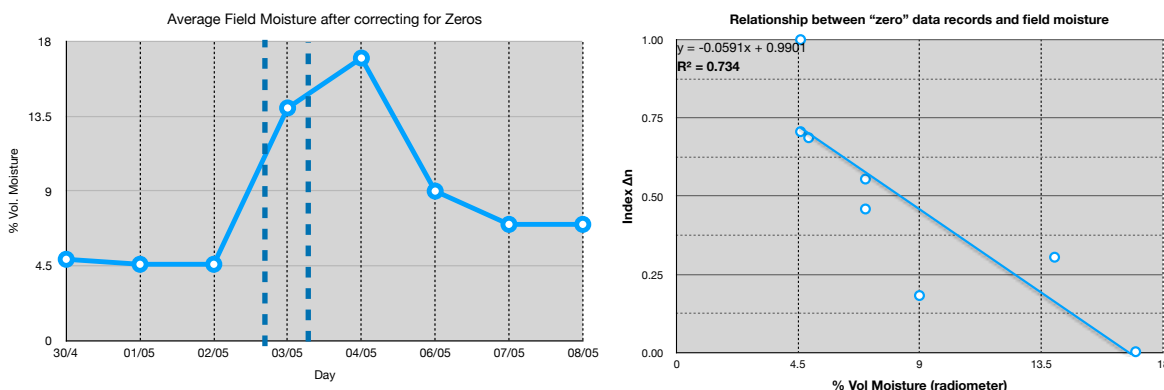
Considering this indicator, it is possible that working at high resolution means the radiometer will be sensitive to very local soil surface characteristics beyond roughness. Hard surface layers may drive emissivity to zero when dry and those same hard surface areas may induce surface water to remain longer during rain (adsorption). Potentially this would account for the contour map on 03 May where different field areas showed distinct emissivity (and moisture) differences despite receiving the same 12 mm of rainfall per  $m^2$ .

Table 9 extends Table 8 to include the initial dry and very wet days. FIG 33a then shows the profile of moisture over time derived from Table 9. The standard

error of the mean around each data point is low at +/-0.2 percentage points.

FIG 33b shows a correlation at  $R^2 = 0.73$  between the number of zero-values removed and the retrieved moisture. The zero values are distributed throughout the data sets and removing zeros brings the data distribution close to normally distributed. In this case zeros or zero values refers to records  $\leq 0.01$ .

Table 9: Total field - average volumetric moistures (with and without values under 0.01 vol moisture, "zeros")									
Date	30/4	01/05	02/05	03/05	04/05	06/05	07/05	08/05	09/05
Mean	0.020	0.016	0.012	0.11	0.17	0.07	0.04	0.05	0.06
Mean >0.01	<b>0.049</b>	<b>0.046</b>	<b>0.046</b>	<b>0.14</b>	<b>0.17</b>	<b>0.09</b>	<b>0.07</b>	<b>0.07</b>	<b>0.07</b>
$\Delta n$	1565	2279	1609	695	7	416	1264	1046	244
% $\Delta n$	53 %	67 %	72 %	24 %	0 %	15 %	39 %	33 %	15 %



**FIG 33:** Left chart (a) shows field moisture profile over time with major 12hr rainfall period marked, standard error of means +/- 0.2pp at 95% confidence interval. Right chart (b) inverse correlation between index  $\Delta n$  (number of zero value retrieved moisture records) and average volumetric field moisture. Consecutive sample days from 30/4 to 08/05 (excludes 09/05 due to sparse data set).

The conclusion from the relationships shown in Table 9 and FIGs 33 must be that low soil moistures are more difficult to measure accurately with high resolution radiometry. However, applying this simple data correction to normalise the distribution by removing "zeros" appears to result in greater accuracy. At higher soil moisture contents the data is already close to normally distributed and almost no "zeros" occur (exactly 7 out of 3237 in 04 May data) indicating that emissivity is more constant when the soil surface has been moistened considerably and that moisture is being absorbed into its structure.

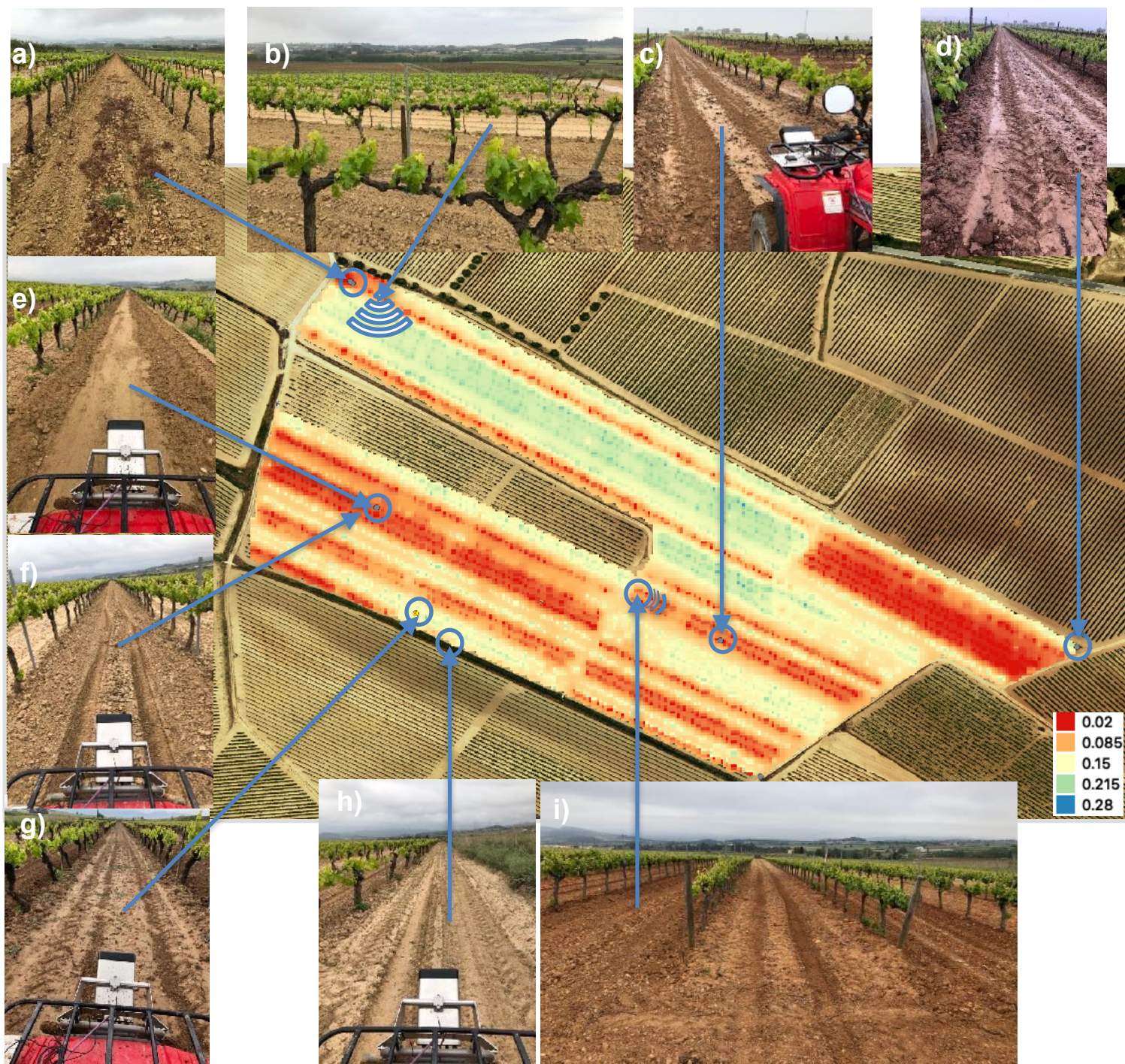
There are risks with this assumption as it is also possible the emissivity will be influenced by adsorption effects. That is to say surface moisture before it is absorbed into the soil, which is probably occurring in the data from 03 May and can be seen in the contour maps from that day.

A search for studies on emissivity influences beyond surface texture revealed satellite based research from 2014 by H.Manns et al [23] confirming soil texture as the primary physical process controlling soil water content between fields. However, crop residue was also an important factor, accounting for 37% of variation in soil water. Specific effects related to tillage were also identified “that could contribute significant improvements to interpretation of remotely sensed soil WC” (water content). Furthermore, H.Manns and A.Berg differentiate the principal correlating factors between moist and dry field conditions [24] by introducing soil organic carbon (SOC) alongside soil texture class. Together these optimally predict soil water content across all moisture levels: the sand content or soil carbon content alone could account for 82% of the variability in moisture content across three of the textural classes. Additionally, in dry conditions soil organic carbon accounted for greater variance, while in wet conditions soil texture accounted for greater variance. H.Manns concluded in 2015 that soil organic carbon is more highly correlated to soil moisture than either soil texture or bulk density, although all factors are significantly intercorrelated [25]. This presents an interesting opportunity to assist L-Band radiometric measurements

The visible soil surface differences in this project are shown via geolocated photographs in FIG 34. These are geolocated to the 03 May trial which showed distinct dry and wet areas in the field before all of the moisture was absorbed into the top layer following day. These are observational points but it is notable that the sandy soil in the upper NW length of the field was quick to absorb moisture during the rainfall (FIG 34b) and high moisture values over 20% were retrieved. Soil that was observed to be dense but not hard shows intermediate moisture levels from 9% to 15% (FIG 34 g, h, i). These are occasionally interspersed with low values of 2% where the surface texture changes to be more smooth (FIG 34c). At the same time, in areas with notably dense and compact soil (FIG 34 e, f, h) or with dead vegetation cover that had become soaked, less than 2% soil moisture was retrieved radiometrically.

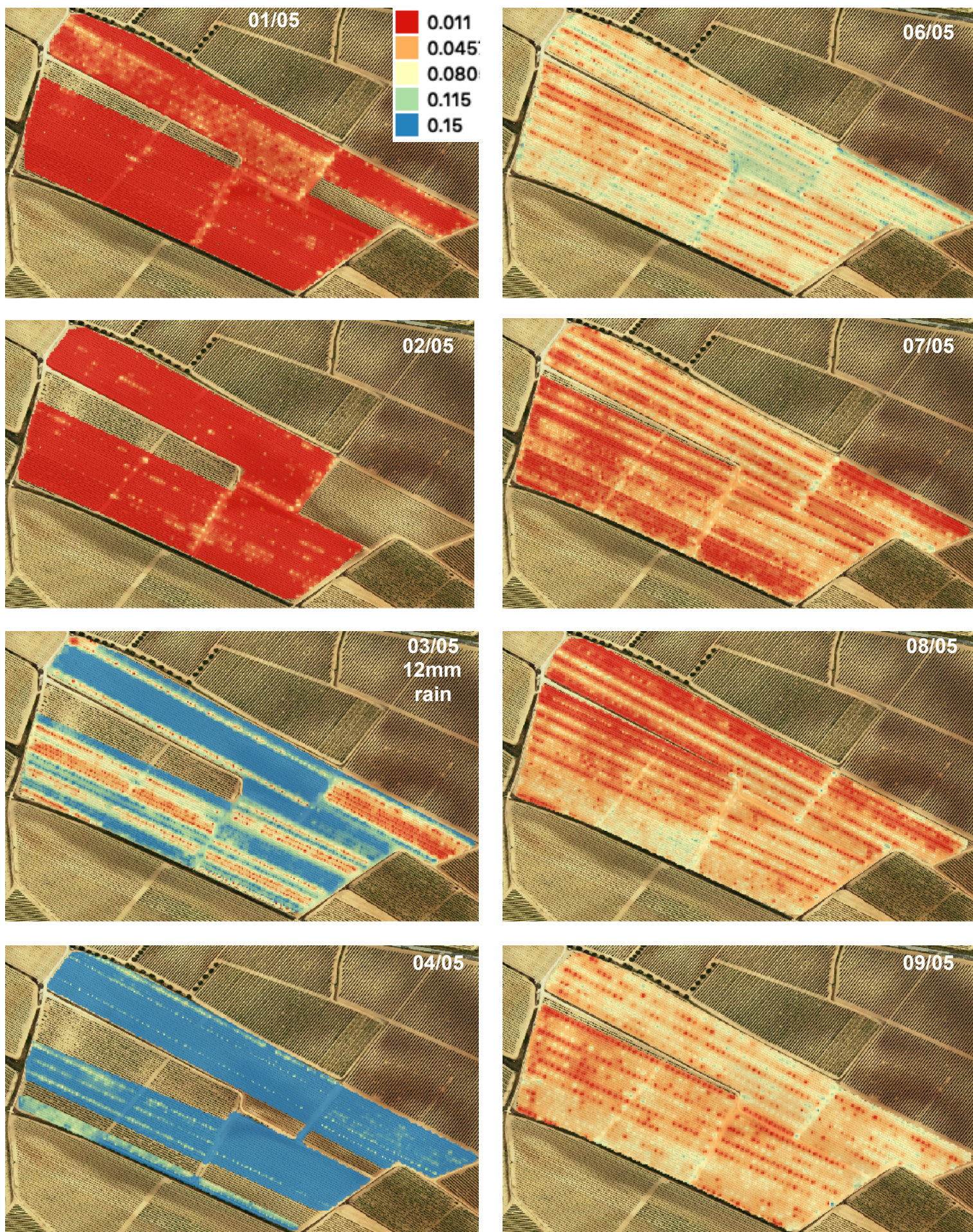
FIG 35 represents the consecutive days temporal resolution taking into account the patterns observed. Values under 1% are removed and an upper limit of 15% moisture is applied to the contour scale. The effect is to emphasise the very wet areas of field in contrast to the very dry areas. The moisture migration pattern and the speed of moisture absorption into the soil become more apparent, especially between 03, 04 and 06 May. The resolution is sufficiently high to determine clear differences in the rate of moisture absorption between rows (03 and 06 May, pre and post the peak saturation).

FIG 36 takes this a step further and optimises the scale for 06 May to a range of 1% to 10% moisture, which allows the final stages of drainage under the sub-surface to be observed in more detail.



**FIG 34:** 03 May (12mm rain) optimised to range of 2% to 28% volumetric moisture.

- a) strewn dead and wet vegetation, likely to increase emissivity (lower retrieved moisture)
- b) view south from upper rows showing the area of sandy-soil rows in background (high retrieved moisture)
- c) hard surfaces in rows possibly driving surface adsorption (high emissivity and low retrieved moisture)
- d) start point where surfaces are broken, wet and rough (high retrieved moisture)
- e) very hard, compact row showing very low moisture absorption even during wet days (low retrieved moisture)
- f) hard with large clumps of dried surface soil pieces (mid to low retrieved moisture)
- g) broken, worked surface showing high retrieved moisture (mid retrieved moisture)
- h) soft, sand lower rows showing high and quick moisture absorption (mid to high retrieved moisture)
- i) view SE down rows of dense red/brown soil (mid to low retrieved moisture)



**FIG 35:** Sequential survey data **normalised to >0.01% to 15%** volumetric moisture, measured radiometrically. This scale provides a good visualisation day to day from the very dry to very wet to moderate moisture conditions. Values under 0.01% (“zeros”) are excluded. Selecting an upper limit that defines the target moisture level for a crop / area of field can be a useful feature of contour maps.

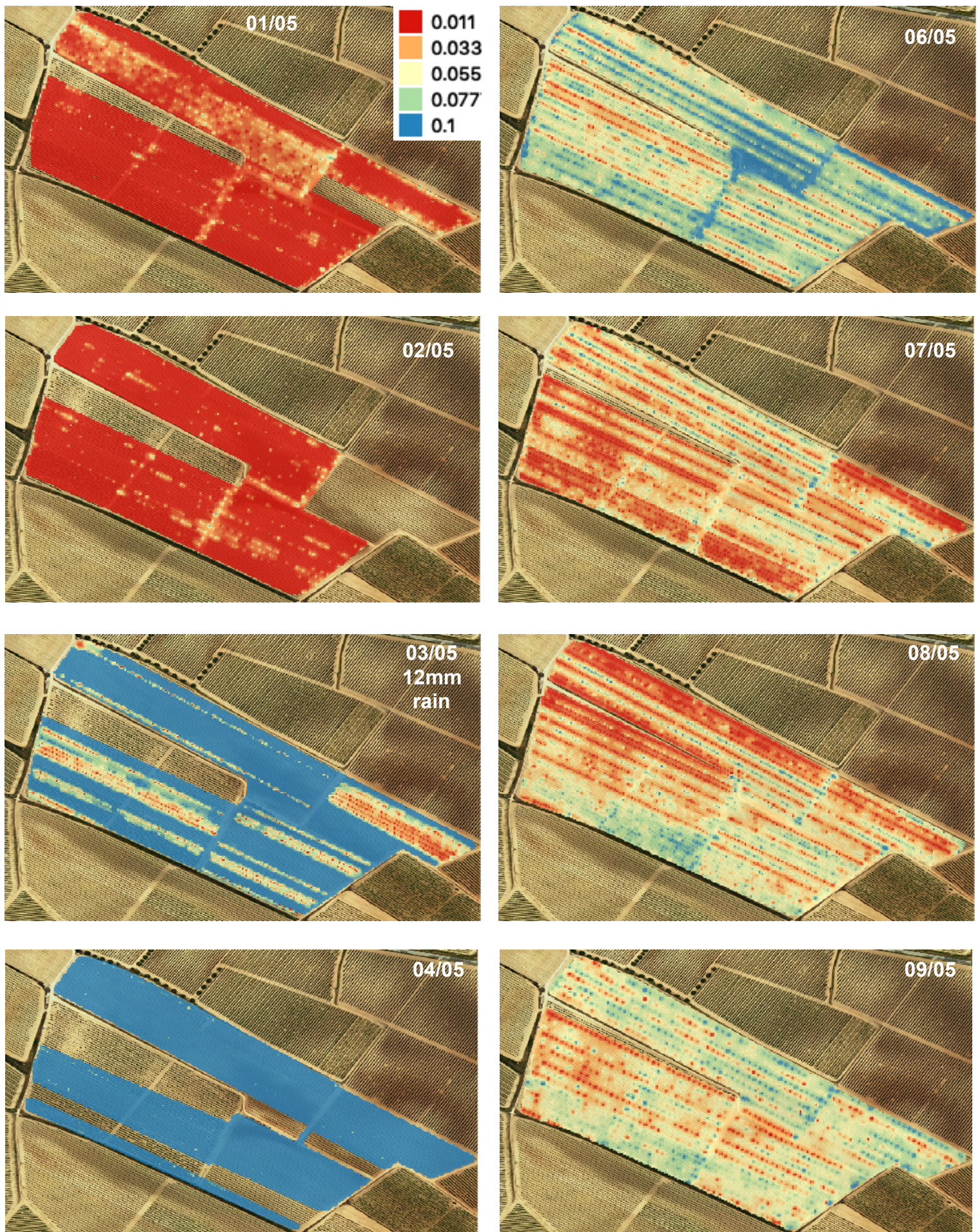


**FIG 36:** Sequential survey data normalised to > 0.01% to 10% Moisture volumetric moisture. Compressing the scale to a 10% upper limit helps to differentiate the “wet” areas from the “dry” areas. Portions of the field where moisture absorption is slower become very evident. This is true even down to the individual row (03/05) where a compact soil row is visible and later becomes saturated (04/05). Additionally, the final stages of drainage under the sub-surface can be observed in more detail (06/05).



## 2.2.5 Comparison to Satellite Imagery

Images from the Sentinel constellation were studied for comparison to the high resolution radiometric data. Sentinel Hub web service was used to obtain processed images. Images at 100 m resolution are available free of charge and higher resolutions (up to 30 m for the bandwidths studied here) are available via subscription (trial basis or from 20€ per month non-commercial). The service generates several indices, raw data statistics and permits area selection and scripting to incorporate preferred correction algorithms and processing parameters. In this case the standard L2A data (corrected, bottom of atmosphere refraction) was used. Two non-cloud and no ground shadow days coincided with the trial (01 May and 06 May). Cloud cover drives low NDVI and high moisture index. More technical information on the Sentinel multispectral image sensor is provided in the appendix along with further temporal comparisons at 100 m.

At 100 m (FIG 37) the field forms part of a wide region pattern using various indices. Changes over time are apparent provided the data is not occluded on the days of interest (e.g. moisture index FIGs 37 a, b).

The temporal resolution was notably hindered due to cloud cover and shadow incidences. This occurs despite the relatively frequent 3 day visit time for 41° latitude. It was not possible to cover the period of the trial with equally spaced “dry” and “wet” days. A later window was identified from 23rd to 26th May, one day either side of 25 mm continuous rainfall. Comparisons either side of this rainfall are provided for the field area of interest in FIG 38 using the maximum 30 m resolution.

At 30 m it becomes possible to extract broad patterns for inside the field area (in this case 0.09 km<sup>2</sup>). In FIG 38 the lower field boundary (a verdant green drainage ditch) is clearly evident in NDVI. It is also evident in moisture index but requires prior knowledge of the features in the local area as the interpolated data reduces resolution. It is also true that NDVI benefits from knowledge of local features in order to distinguish between farm tracks with vegetation (western field boundary) and ditches (southern boundary). This same local knowledge may lead to conclusions similar to the ones drawn regarding moisture absorption over sandy soil in the upper NW corner of the field.

However, the satellite maps do not provide a detailed image of the field moisture pattern in sufficient spatial resolution. Nor is the temporal resolution sufficient to study drainage patterns. The 30 m spatial resolution covers about 10 rows in a field per pixel, which is a large footprint considering the farm is worked row by row. The near ground radiometer was able to provide daily images with alternating row to row precision. The near to ground temporal resolution allowed the study of rainfall absorption during cloud cover and revealed clear patterns related to soil characteristics within the field that are not possible to diagnose from satellite.

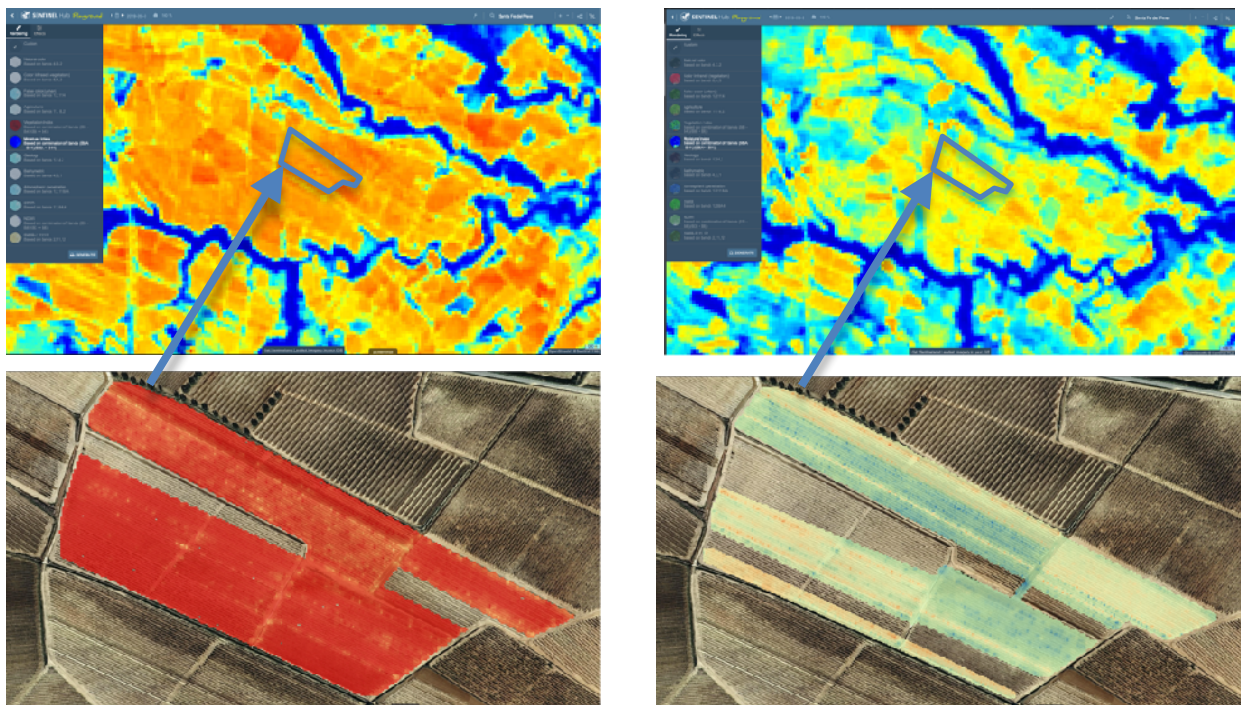


**FIG 37 a, b:** A perspective of ground moisture to illustrate the difference between standard, (processed free of charge) satellite images at 100m and near to ground radiometric images at 1 m (line of travel). Satellite images from Sentinel Hub are top and near ground radiometric images are bottom. Both have a clear response to changes induced by rainfall. Red to orange indicates low moisture and yellow to blue indicates higher moisture with dark blue the highest moisture (note the indices are not scaled to be directly comparable)

The left pair of images (FIG 37a) show a dry situation on 4th May after a long period with no rainfall. The right pair of images (FIG 37b) show a wet situation, however the dates do not coincide for this pair: 4th May for near ground radiometer following 12 mm rainfall and 26th May for satellite following 25 mm rainfall. Satellite data not available for 4th May (no visit and subsequent occlusion).

The Sentinel Hub provides a Normalised Difference Water Index (NDWI) using the NIR and SWIR difference ratios and also a multi-band Moisture Index as used here and derived as follows (see appendix):  $\text{Band } 8a - (\text{Band } 4 / (\text{Band } 4 + \text{Band } 8))$ .

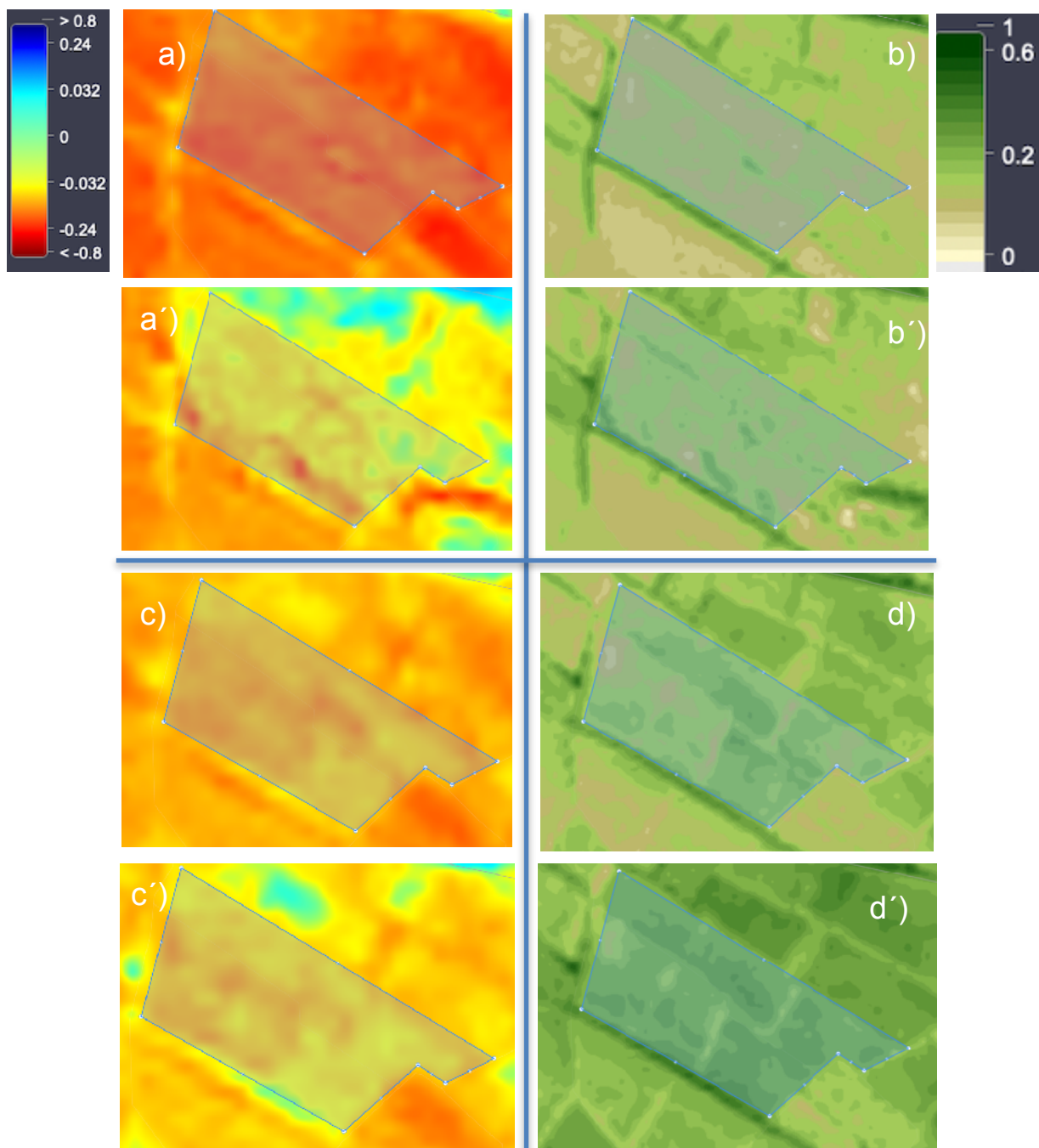


**FIG 38:**  
Sentinel L2A images at 30 m resolution for Moisture Index (left) and NDVI Vegetation Index (right), pre and post two rainfall events:

- |                                |   |
|--------------------------------|---|
| a) Moisture Index: 01 May Dry  | a') 06 May, 2 days after 12 mm rainfall |
| b) Vegetation Index 01 May Dry | b') 06 May, 2 days after 12 mm rainfall |
| c) Moisture Index 23 May Dry   | c') 26 May, 1 day after 25 mm rainfall  |
| d) Vegetation Index 23 May Dry | d') 26 May, 1 day after 25 mm rainfall  |

The area of interest represents the 0.09 km<sup>2</sup> field. Source: Sentinel Hub

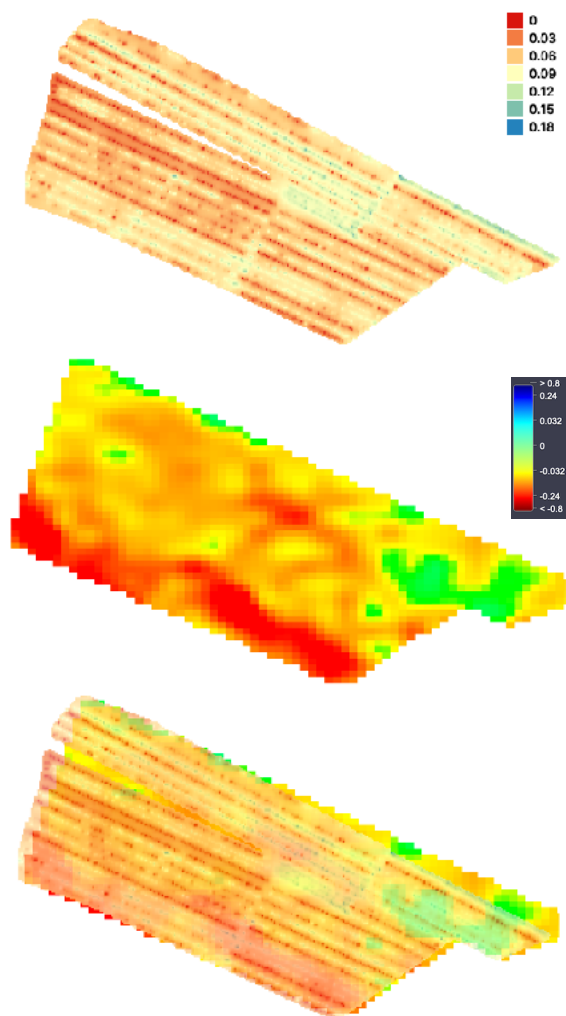


**FIG 39 a, b, c:** 06 May, from top to bottom - Radiometric moisture results c. 1 m then Sentinel moisture index at 30 m then radiometer overlaid to Sentinel. The images demonstrate the difference in resolution that is achieved with near ground radiometry. Although it is possible to visually interpret patterns within the field with the satellite data, the greater interpolation distance means these cannot be associated to local areas in the field and only a loose correspondence between more moist and more dry in the data sets is possible.

The field moisture index at 30 m was extracted for 6th May and compared to radiometer data with an optimised max-min interval scale (FIG 39). The canopy coverage is low at this time of year. The satellite resolves higher moisture areas, for example the upper row NW corner is typically more moist (sandy), however the satellite appears to be influenced by the adjacent tree line on the field boundary, extending the interpolated moist area on this edge. There is also some directional fit with the drier SE lower corner and moister NE upper corner. However, the satellite interpolation distance also leads to poor correspondence in other field areas. Overall the diagnostic utility at this scale is very limited if the interest is to understand the local field conditions.

FIG 40 makes a final comparison between satellite and near ground radiometry data to illustrate the difference in resolution. We previously saw in the NDVI discussion that vegetation close to the ground influences the emissivity and therefore the retrieved moisture results. It would make sense therefore that satellite NDVI would report a higher “greenness” index compared to near to ground which is below and between the canopy. Even, as in this case, if the canopy is less than 40% of the surface area. In practice the large interpolation distance (50 m and 30 m in FIG 40) causes a blending effect between soil and vine canopy, complicating the interpretation of canopy health from satellite (nor via the near to ground radiometer on the ATV). A low level aerial operation is required to extract canopy health detail, one reason UAV’s are popular for this type of data collection.

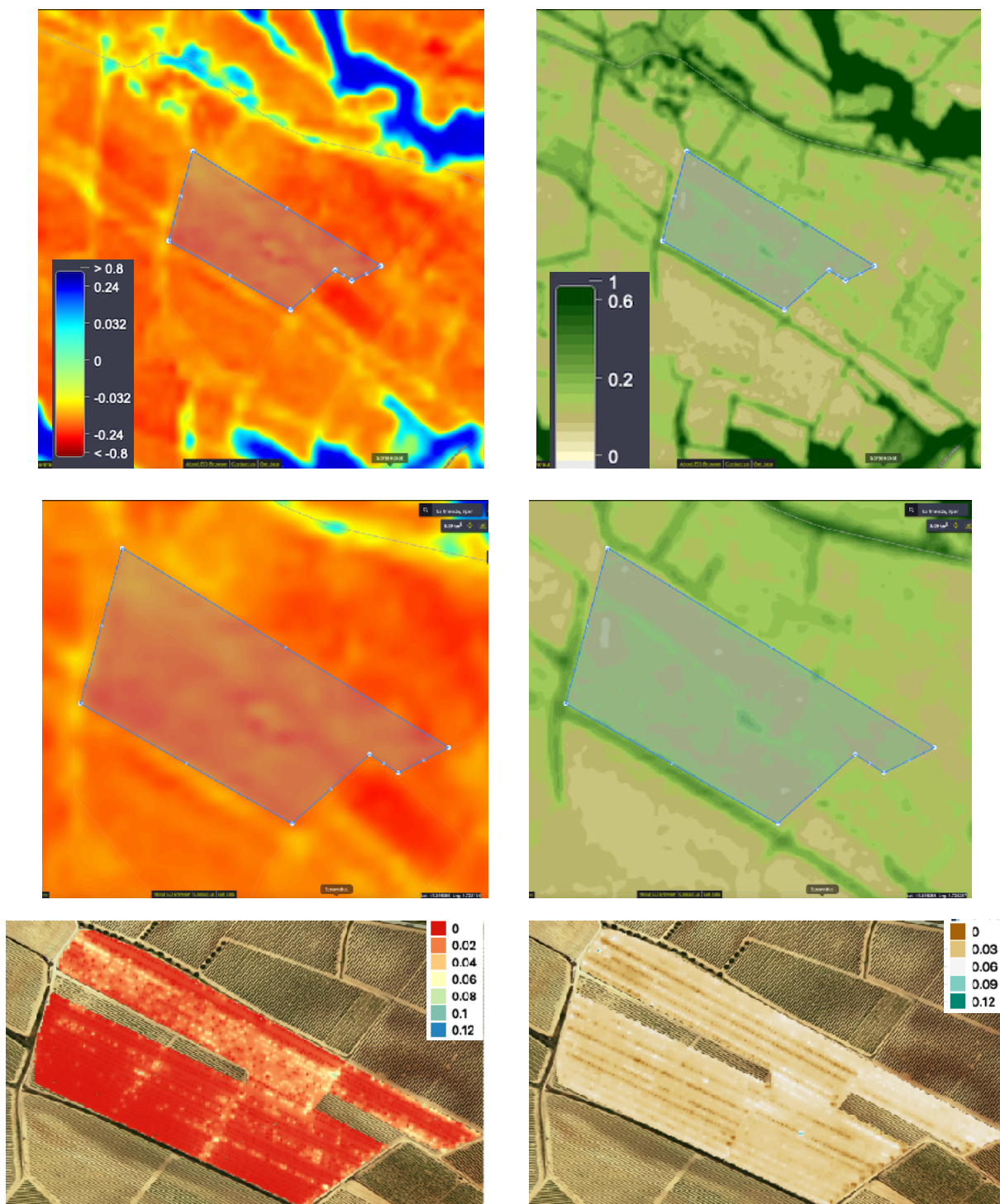


**FIG 40** Sentinel 2 (L2A) 01 May Moisture Index (left) and NDVI (right) from Sentinel Hub EO Browser. Top images at 50 m and centre images at the maximum 30 m resolution. Geolocated field area of interest is marked for reference. Satellite provides wide area patterns but intra-field information is limited. Bottom images show the radiometer results at ground level and up to 1 m resolution (direction of travel) for the same area on 01 May. Moisture Patterns can be associated to individual rows and individual plants can be detected as blue dots in NDVI.

## CONCLUSIONS

The Balamis L-band radiometer is an instrument which enables very high temporal and spatial resolution of soil moisture using passive microwave as the proven proxy. It works near to ground and can be combined with other spectral sensors, in this case optical and near infra-red, to acquire concurrent and complimentary data. It proved to be very precise in both soil moisture percentage and vegetation index, permitting contour maps to be produced based on statistically significant differences, up to a standard error +/- 0.2 percentage points for retrieved moisture over a local soil area (0.09 km<sup>2</sup>).

The spatial resolution of the radiometer in L-band is up to 0.9 m<sup>2</sup> in the direction of travel, working with a 36° beam width from a low ground vehicle mount. The temporal resolution is only limited by human resources and the vehicle's capability to traverse the area of interest. These resolutions are significantly ahead of the high resolution approaches that already exist:

- The original pioneering studies of Jackson et al in 1999 [26] used airborne radiometry to achieve around 1 km<sup>2</sup> resolution over a 10,000 km<sup>2</sup> area on a daily frequency during one month. This approach remains valid but requires skilled personnel and use of an aircraft dedicated to the study area, which increases cost, reduces frequency and negatively impacts sustainability today.
- The development of downscaling algorithms at the Technical University of Catalunya [2] allows soil moisture data to be interpolated up to 1 km<sup>2</sup> resolution by utilising land temperature and NDVI from different satellite sources. Dependence on infra-red and the co-ordination of multiple satellite visit times reduced temporal resolution and spatial is still bigger than the size of the field in this study.
- LICEF interferometry on the Sentinel 2 satellites achieves up to 30 m<sup>2</sup> resolution for moisture and NDVI indices. This also uses infra-red wavelengths to improve spatial resolution which compromises temporal resolution due to the effect that cloud cover and shadow have on infrared frequencies. The Sentinels could not achieve +/- 1 day around the central day of interest in this trial due to cloud cover.

The Balamis radiometer can operate without these impediments. It continues to operate even under adverse weather conditions and can utilise existing land vehicles and the established daily trajectories on a farm for measurement purposes. There is a convenience factor to add to this capability due to the relative immediacy and ease of processing the emissivity data into useful geolocated products like the moisture maps. Alternatives include the free Sentinel satellite data from ESA, which requires pre and post processing within a python or java environment in order to extract raw data, merge image tiles and remove non-data areas (cloud cover) [27]. Subscription services can assist but are still limited to a 30 m spatial resolution (Sentinel Hub).

At very high resolution, local factors should be considered if the objective is to determine accurate moisture values rather than a relative index. A knowledge of soil type and surface roughness is needed for accuracy and should be obtained empirically or through verified models that produce algorithms consistent with local ground truth. With that caveat, this study still measured significant differences within the field area that were not obtainable by other means.

***To Summarise the Key Findings:***

- Flexible high resolution soil moisture and NDVI contour maps:
  - 1 day temporal and c.1 m<sup>2</sup> x c. 6 m<sup>2</sup> spatial (direction of travel x lateral)
- Moisture absorption rates during and immediately after rainfall
  - Associated to field areas and soil type / condition
  - Achieved under rain conditions and cloud cover that preclude satellites
- Average moisture contents over time (daily)
  - Including average difference between intra-field soil types
  - Drainage patterns across the field and intra-field soil types

It was possible to observe the changing moisture patterns day to day from dry fields (under 5% moisture) to wet fields (up to 30% moisture) with high precision (standard error +/- 0.2 percentage points moisture). The resolution was sufficient to detect significant differences between rows, along rows and at field boundaries. The final products can be visualised as time-lapse geolocated contour maps.

The temporal resolution (1 day in this study) allowed the changes in top layer moisture profile, absorption and adsorption patterns to be clearly distinguished. The average moisture content ranged from 4.5% after a dry period to 17% after 12 mm rainfall and returned to a stable 7% during the subsequent dry days. Additionally, a very clear pattern emerged of the moisture interaction with the soil during the wet period that appears to be related to the soil type and characteristics in the different areas of the field. Soft, sandy soil showed higher moisture absorption than areas observed to be more dense or have hard surfaces. A comparison under similar weather and average field conditions revealed sandy, white soil with an average of 7.1% moisture and harder, dense dark soil with an average of 5.6% moisture.

During the wet period radiometric errors (zero values) were at their lowest with no errors detected at peak moisture absorption. In contrast under dry soil conditions a high number (around 15% to 30%) of zero-values occurred in retrieved moisture. Under dry conditions over the dark soil areas this value approached 50%, probably due to the combination of dry conditions and hard surfaces. It proved necessary to eliminate the zero data to approach a normal distribution of retrieved field moisture. It is very likely that accuracy improves once zero values are removed and a knowledge of soil surface roughness allows further adjustment of retrieved data to ground truth. High resolution radiometry will benefit from a more objective measure of soil surface roughness.

NDVI coincided with emissivity during strip tests over variable vegetation. Higher NDVI was associated to higher Brightness Temperature at this distance, at  $R^2=0.66$ . However, the mathematical relationship (linear or logarithmic) was not clear and the data set was insufficient to differentiate or determine a relationship at  $NDVI > 0.1$  (above barren only).

### **Future Work - SOC (Soil Organic Carbon)**

The ground sampling method was time consuming and prone to errors. It relies on bulk density which is known to work best for certain soil types, notably without clumps or gravel. Given the variability of soil appearance inside the 0.9 km<sup>2</sup> field area of this study, it is likely that ground truth will always be challenging to establish without a sensor network and ground station. Developing a cross correlation to related, remotely sensed soil attributes may be a more robust approach to assure accuracy when working with L-Band radiometry.

Correlations using soil organic carbon (SOC) and soil organic matter have not previously been considered for remote sensing algorithms according to Hida Manns [25], who concludes “Soil organic carbon was more highly correlated to the average SWC (soil water content)... than soil texture or bulk density although all soil variables were significantly correlated with each other” [25]. Manns also notes that soil texture was the most dominant variable in moist conditions but in dry conditions “SOC alone explained the highest percentage of variability in SWC” (soil water content). Incorporating soil organic carbon or similar soil properties into processing algorithms could further refine the retrieved moisture and assure accuracy, including over hard, dry surfaces.

Field ready spectroscopic methods have been proposed to determine SOC [28]. Research into the remote sensing of SOC is also an active area due to its relevance as a carbon sink in global climate management. A 2017 study of SOC in Spain [29] used both airborne and satellite based hyperspectral sensors to achieve similar results with correlations around  $R^2 = 0.6$  between remotely sensed and ground samples. Interestingly, the relevant wavelengths for Total Organic Carbon (TOC) predictions were the red region of the spectrum (600–700 nm), and the short wave infrared region (SWIR) between ~2000–2250 nm. The Balamis radiometer provides options to include photodiodes sensitive to different wavelengths. Future development work should consider a collaboration with research teams developing SOC models and engineering a near to ground remote sensing solution to detect SOC concurrently with L-band emissivity.

### **Future Work - NDVI**

Vegetation was found to increase the L-band emissivity in this experiment, hence retrieved moisture dropped as NDVI increased. The index may provide a complementary parameter that can inform the need for parametric adjustments that compensate for emissivity changes due to vegetation cover or indeed other surfaces. Based on the observations in this project NDVI can differentiate ground conditions beyond vegetation cover, including man-made or artificial substrates and surface moisture.



Additionally, the visible and near infra-red frequencies used for NDVI may serve to determine SOC (soil organic carbon) or SOM (soil organic matter). Research is appearing that combines the NDVI data with multivariate models to determine relative soil moisture and organic matter contents [30]. The benefit is to use the basic spectral data popular for NDVI to generate NSMI (normalised soil moisture index). Under lab conditions this moisture index achieved a correlation  $R^2 = 0.88$  to actual soil moisture. However, the real interest must be to use these spectral frequencies to assess soil organic matter alongside the long established soil emissivity in L-Band in order to improve accuracy over different soil types. Due to the sensitivity sought, a real time radiometric calibration will probably be needed for this application.

The benefits of low level NDVI operations using UAV's are widely reported. In this case a high resolution view of the canopy and ground could be achieved with the Balamis radiometer mounted on a drone. Proof of principle trials demonstrated a lightweight radiometer can be carried in nadir or oblique on a small UAV. Ground vehicle data collection at 1 Hz and aerial travel velocities (25 to 30 km/hr) indicated that robust data collection will be possible. With further development the opportunity exists to simultaneously measure canopy health and L-Band soil moisture while compensating for vegetation emissivity effects.

#### ***To summarise future technical opportunities:***

- Determine NDVI to Brightness Temperature relationship in order to compensate soil moisture retrieval under sparse vegetation or canopy.
- Development of the UAV mounted radiometer with concurrent sensors and exploration of the relationship between NDVI and Brightness Temperature.
- Develop a quantifiable metric for soil surface roughness over c. 100 m<sup>2</sup> areas.
- Remote determination of soil properties through the concurrent spectral acquisition of soil organic carbon to improve intra-field accuracy of L-Band soil moisture. This work will need to include a radiometric calibration solution.

#### **Sustainability**

Hardware and algorithm development is needed in order to satisfy the demand for earth observation and satellite based information products. These products support essential human and planetary policies on climate change, fresh water hydrology and the sustainable use of land and resources. Near earth technology can contribute to the development of more precise models and long term forecasts that improve policy decision making.

The series of technologies and mathematical techniques behind remote sensing are essential to humankind's ability to manage its own planetary habitat. The advent of lightweight and mobile near earth radiometry is set to improve the accuracy of predictive models at region and global scales through high temporal resolution observation of local ECV's (environmental critical variables), which include both soil moisture and ice-sheet thickness. The need to understand ECV's at a near to ground level is well articulated within the MOSAiC arctic drift expedition planned for later this year (<https://www.mosaic-expedition.org>)

There may also be simple short term benefits. For example, precise knowledge of the drainage characteristics within a field could assist in optimising the interaction between natural rainfall and the soil surface. That is to say, selectively tilling more resistant soil areas to improve water absorption and reduce irrigation. These insights may benefit crops and conserve fresh water resources in the industrial and geographical areas that consume by far the most fresh water. Importantly, the insights can be gained without introducing additional kilometres in aeroplanes or petrol driven vehicles simply by mounting a radiometer to existing farm vehicles.

### Ethical Considerations

As discussed, there are opportunities for collaboration between different research groups with the diversity of skills and knowledge needed to take advantage of this new measurement technology. The collaboration would need to span the lean global community engaged in this research and development area. As with any similar venture, ethical funding needs to consider how to ensure fair prioritisation amongst competing technologies in order to drive the forward the scientific insights that can most urgently assist to mitigate the pending global crises.

The future commercialisation of these technologies should be considered in the context of the user groups who will need (and expect) plug and play operation. User groups outside of the academic and scientific community can greatly accelerate the generation of precision data around the globe. Since this technology will be outside of the normal expertise of these users it will require ease of use and “mistake proofing” to assure the data quality and allied decision making is well informed. Finally, the commercialisation should take into account how to reach communities in areas of the globe that can most benefit from the insights that near ground radiometry generates. Countries like India with high population densities and extreme weather events may be able to benefit early.

=====



**Colin Burnham** runs a collider consultancy, Animar Tech, to commercialise new technologies that contribute to improved sustainability. He holds a BSc Hons. Chemistry (1991, Birmingham University UK) and produced this thesis for a Masters Engineering in UAV Technologies at the Technical University of Catalunya, Spain (2019). Colin is a science and technology leader with a prestigious career in FMCG innovation. During his career he has been at the forefront of industry change, consumer innovation and breakthrough manufacturing technology. In the last six years he was the R&D executive on the management board for a large operating company, business category leadership team and global innovation leadership function. He is accustomed to influence and pursue technology-enabled business transformation across Europe and Sub-Sahara Africa within tight regulatory, environmental and human sustainability frameworks. He is also accustomed to building lean, multidisciplinary STEM teams who partner with design, marketing, supply chain and manufacturing to define and commercialise innovative technologies, products and services.  
[www.linkedin.com/in/colinburnham](http://www.linkedin.com/in/colinburnham)



email: [animar101@icloud.com](mailto:animar101@icloud.com)  
skype: Animar101



# APPENDIX

## SENTINEL MSI SENSING FREQUENCIES AND ASSOCIATED RESOLUTION

Source:

<https://earth.esa.int/web/sentinel/user-guides/sentinel-2-msi/resolutions/radiometric>

Sentinel Level 2A (L2A) images used in this document. L2A are atmospherically corrected based on the Level 1C (L1C) brightness temperature. L1C provides top of atmosphere reflectances while L2A, which became available in March 2017, provides bottom of atmosphere reflections in cartographic geometry of 100 km pixels. L2A compensates for atmospheric interference and reflectances.

Bands and Indices Calculations:

- a) Terrain (RGB optical)
- b) Infra Red
- c) Agriculture (bands 11,8,2)
- d) Veg Index (B8-B4 / B8+B4)
- e) Moist Index (B8a - B4/(B4+B8))
- f) NDWI (B3-B8/B3+B8)

Table 1: 10 m Spatial Resolution Bands and associated Signal to Noise ratio (SNR)

Band number	S2A		S2B		L <sub>ref</sub> (reference radiance) (W m <sup>-2</sup> sr <sup>-1</sup> μm <sup>-1</sup> )	SNR @ Lref
	Central wavelength (nm)	Bandwidth (nm)	Central wavelength (nm)	Bandwidth (nm)		
2	492.4	96	492.1	96	128	154
3	560.8	15	550.0	16	128	163
4	664.6	38	664.9	39	108	142
8	832.8	145	832.9	133	103	174

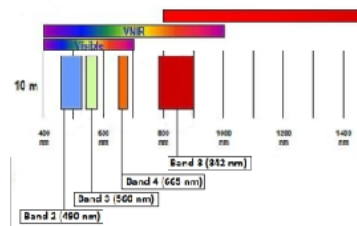


Table 2: 20 metre Spatial Resolution Bands and associated Signal to Noise ratio (SNR)

Band number	S2A		S2B		L <sub>ref</sub> (reference radiance) (W m <sup>-2</sup> sr <sup>-1</sup> μm <sup>-1</sup> )	SNR @ Lref
	Central wavelength (nm)	Bandwidth (nm)	Central wavelength (nm)	Bandwidth (nm)		
5	704.1	19	703.8	20	74.5	117
6	740.3	18	739.1	18	68	89
7	782.8	28	779.7	28	57	106
8a	864.7	33	864.0	32	62.5	72
11	1613.7	143	1610.4	141	4	100
12	2202.4	242	2189.7	238	1.5	100

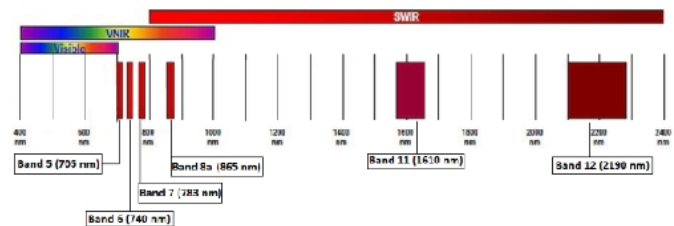
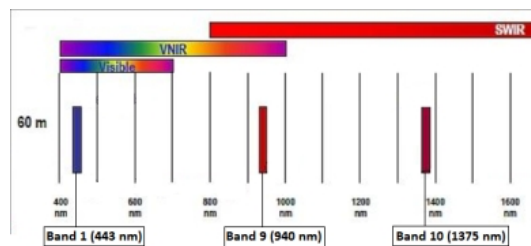
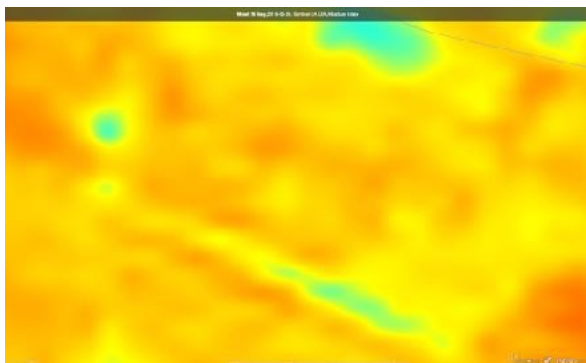
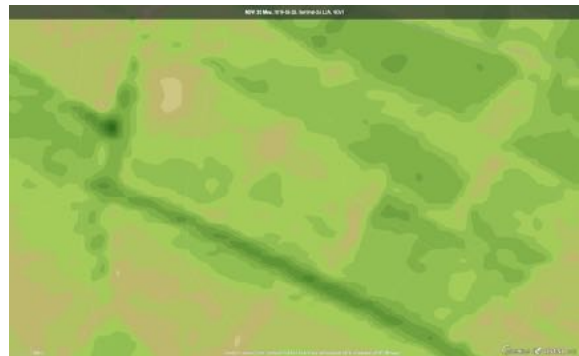
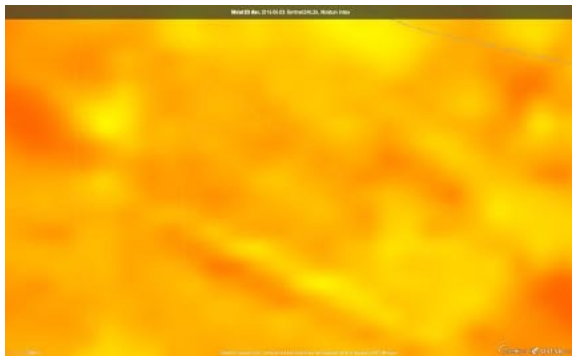
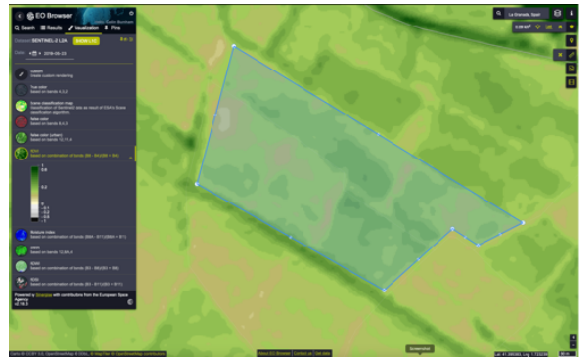
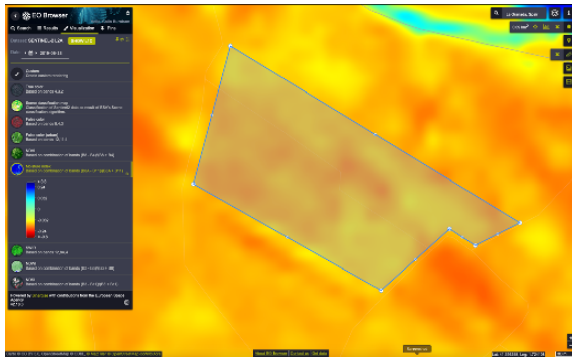


Table 3: 60 metre Spatial Resolution Bands and associated Signal to Noise ratio (SNR)

Band number	S2A		S2B		L <sub>ref</sub> (reference radiance) (W m <sup>-2</sup> sr <sup>-1</sup> μm <sup>-1</sup> )	SNR @ Lref
	Central wavelength (nm)	Bandwidth (nm)	Central wavelength (nm)	Bandwidth (nm)		
1	442.7	27	442.2	45	129	129
9	945.1	26	943.2	27	9	114
10	1373.5	75	1376.9	76	6	50





**FIG App I)** May 23 and May 26 L2A Sentinel 2 Images at 30 m with field mask removed (text reference FIG 38, Sentinel Hub EO Browser)

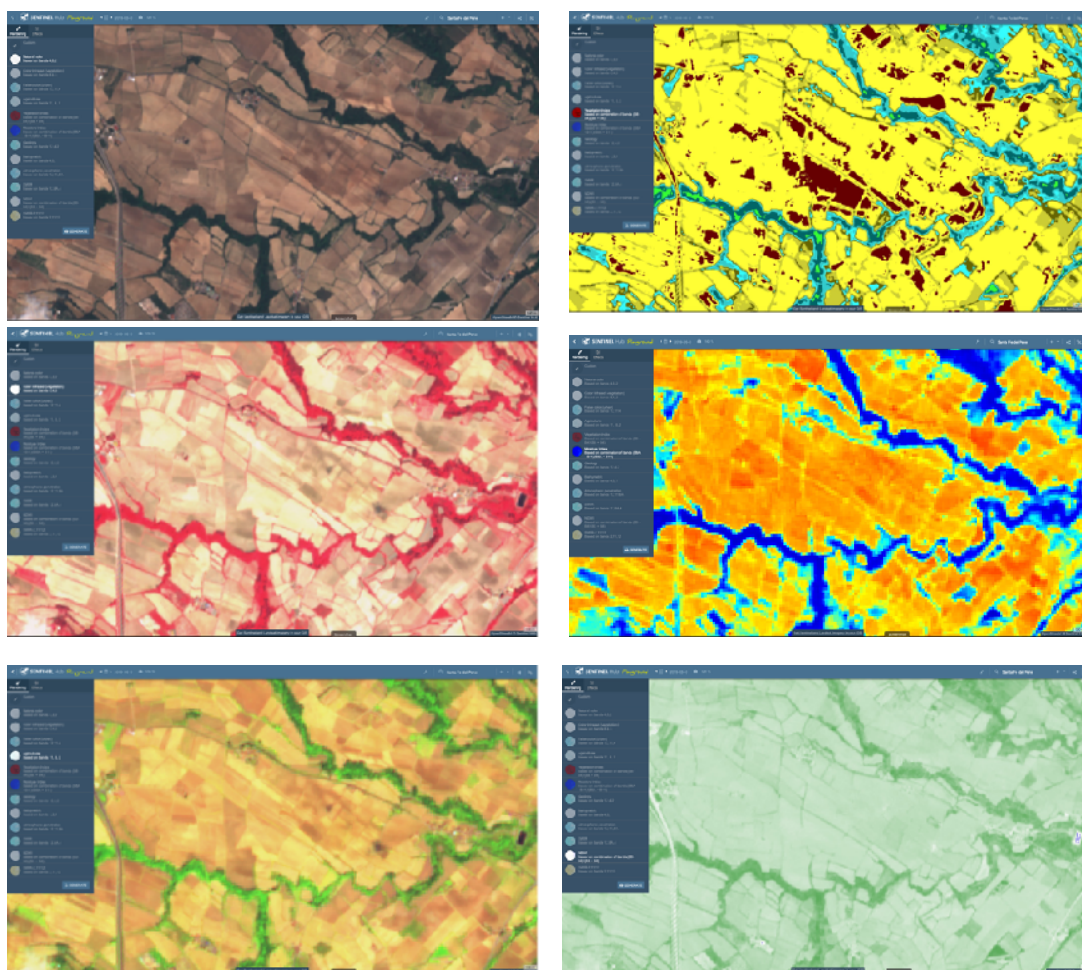


**FIG App II):** 01 May. Sentinel 2 Images (clear sky). Images 2 days prior to 12 mm rainfall. Images available at 100 m Resolution from Sentinel Hub EO Browser

- |                               |  |
|-------------------------------|--|
| a) Terrain (RGB optical)      | d) Veg Index ( $B8 - B4 / B8 + B4$ )   |
| b) Infra Red                  | e) Moist Index ( $B8a - B4(B4 + B8)$ ) |
| c) Agriculture (bands 11,8,2) | f) NDWI ( $B3 - B8 / B3 + B8$ )        |

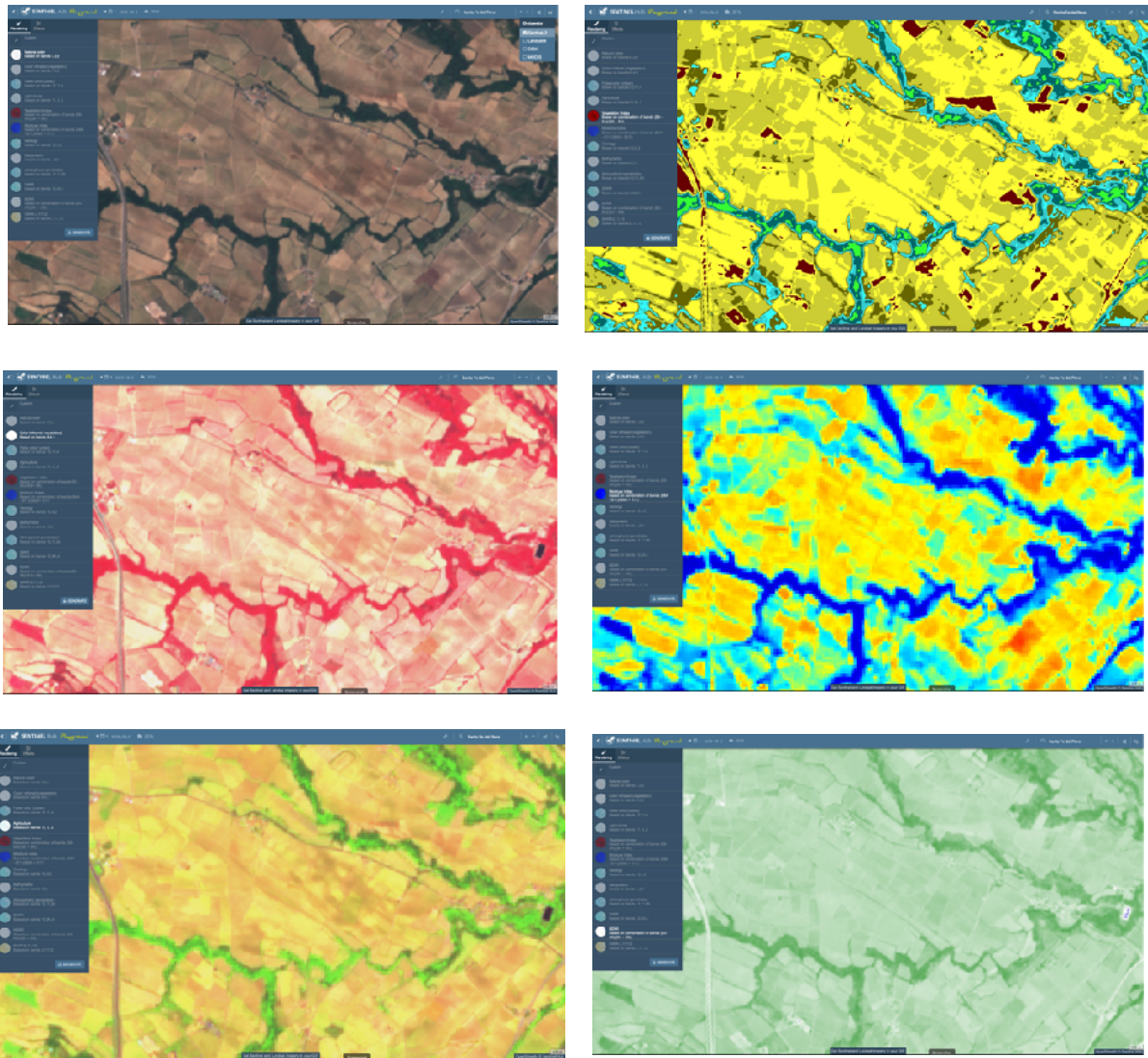


**FIG App III):** Sentinel 2 images for 02 June (clear sky). One week after 25 mm rainfall. Images available at 100 m Resolution from Sentinel Hub EO Browser

- a) Terrain (RGB optical)
- b) Infra Red
- c) Agriculture (bands 11,8,2)
- d) Veg Index ( $B8 - B4 / B8 + B4$ )
- e) Moist Index ( $B8a - B4(B4 + B8)$ )
- f) NDWI ( $B3 - B8 / B3 + B8$ )

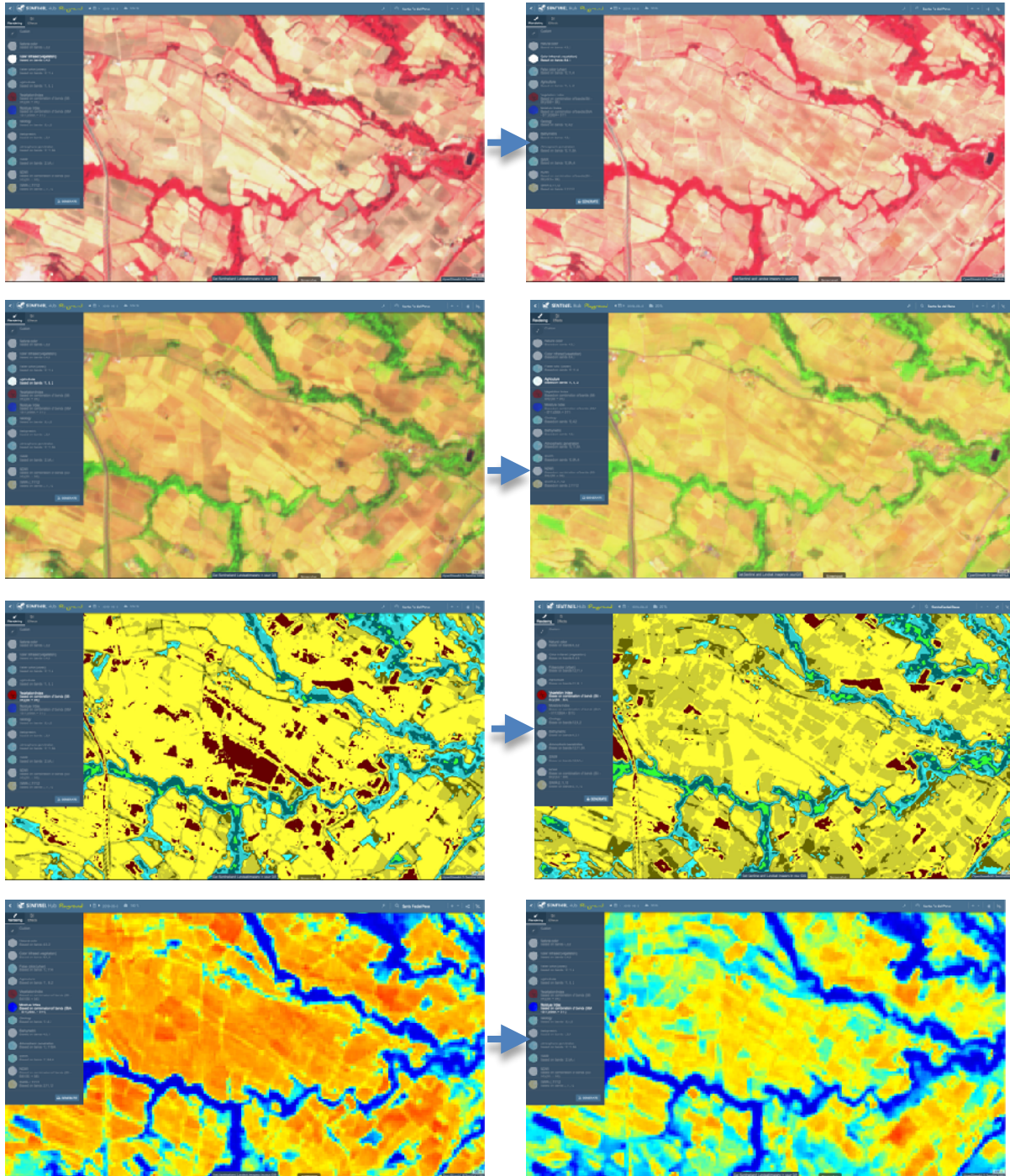
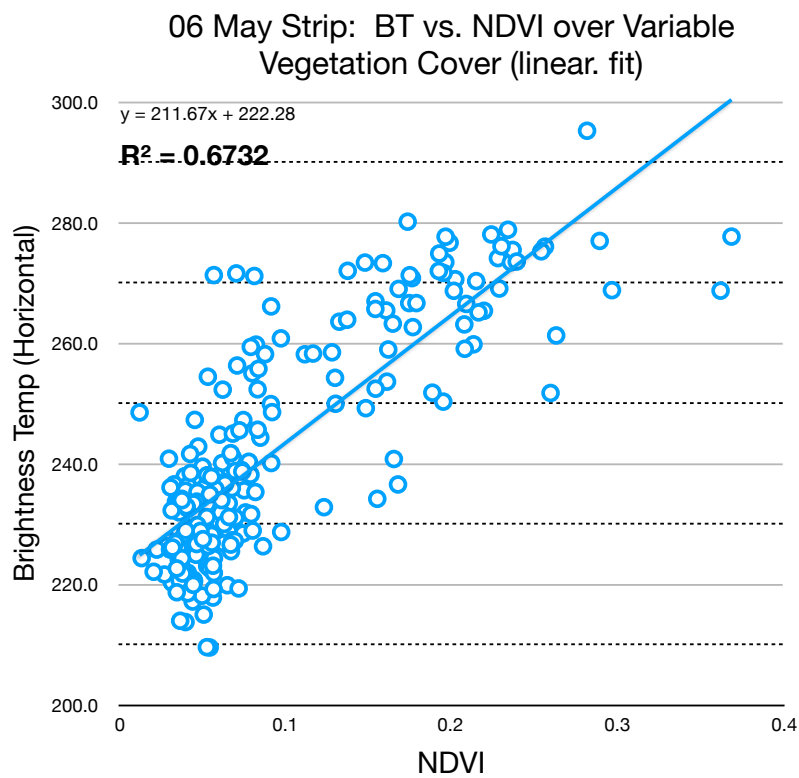
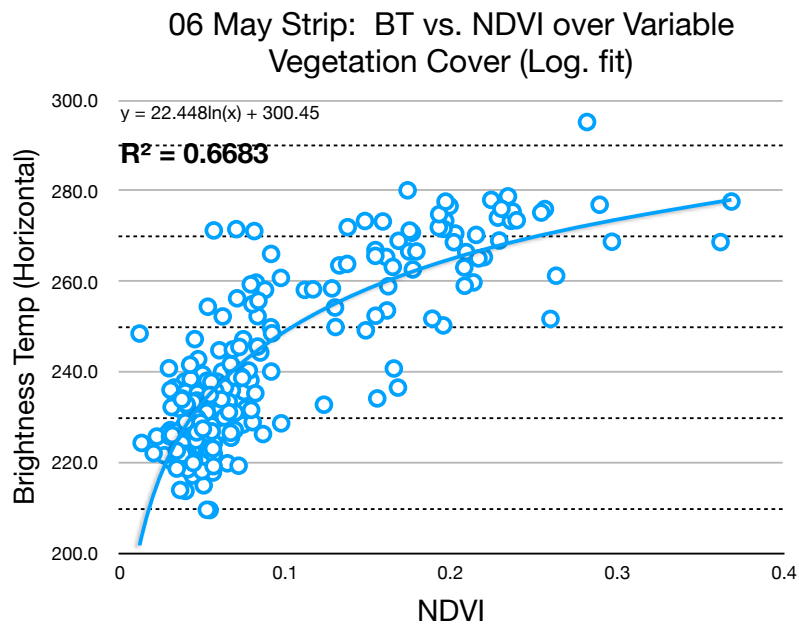


**Fig App IV):** Sentinel 2 images: 01 May (left) and 02 June (right) showing change in conditions conditions due to rainfall. 2nd June is one week after 25 mm rainfall. 100 m Resolution from Sentinel Hub EO Browser. Working from top to bottom:

- a) Infra Red
- b) Agriculture (bands 11,8,2)
- d) Veg Index ( $B8-B4 / B8+B4$ )
- e) Moist Index ( $B8a - B4(B4+B8)$ )

FIG App V) Vegetation Strip Trials (FIGs 20), Brightness Temperature (BT) vs. NDVI: potential correlations were identified but not resolved for mathematical fit in the small data sets. As NDVI approaches zero the effect on BT is reduced, however no correlation was found with above NDVI > 0.1 only





## REFERENCES

- [1] Physical Principles of Passive Microwave Radiometry.  
ESA Earth Observation Summer School, 2012  
Ernesto López Baeza
- [2] Multiscale soil moisture retrievals from microwave remote sensing observations.  
Maria Piles Guillem, Remote Sensing Lab, Universitat Politècnica de Catalunya. Doctoral Thesis, 2010
- [3] Microwave dielectric behaviour of wet soil, Part 1: Empirical Models and experimental observations from 1.4 to 18 GHz.  
M. T. Hallikainen, F. T. Ulaby, M. C. Dobson, M. A. El-Rayes, L. Wu, 1985
- [4] Microwave dielectric behaviour of wet soil, Part 2: Dielectric Mixing Models.  
Myron C. Dobson, Fawwaz T. Ulaby, Martti T. Hallikainen, Mohamed A. El-Rayes, 1985
- [5] Effect of surface roughness on the microwave emission from soils.  
B. J. Choudhury T. J. Schmugge A. Chang R. W. Newton 1979
- [6] A comparison of radiative transfer models for predicting the microwave emission from soil  
Schmugge, T. J., and B. J. Choudhury, 1981
- [7] Sensitivity of L-band NWP forward modelling to soil roughness.  
Sabater, J. M., P. DeRosnay, and G. Balsamo, 2011
- [8] A simple parameterization of the L-band microwave emission from rough agricultural soils.  
Jean-Pierre Wigneron, Laurent Laguerre, Yann H. Kerr, 2001
- [9] Using vegetation indices for soil-moisture retrievals from passive microwave radiometry.  
Eleanor J. Burke, W. James Shuttleworth and Andrew N. French, 2001
- [10] Passive L-Band Microwave Remote Sensing of Organic Soil Surface Layers: A Tower-Based Experiment.  
François Jonard, Simone Bircher, François Demontoux, Lutz Weihermüller, Stephen Razafindratsima, Jean-Pierre Wigneron, Harry Vereecken, 2018
- [11] Use of a soil moisture network for drought monitoring in the Czech Republic  
Martin Mozny & Mirek Trnka & Zdenek Zalud & Petr Hlavinka & Jiri Nekovar & Vera Potop & Michal Virag, 2011
- [12] Field-Scale Spatial Variability of Soil Moisture and L-Band Brightness Temperature from Land Surface Modeling.  
Camille Garnaud, Stéphane Bélair, Marco L. Carrera (Meteorological Research Division, Environment and Climate Change Canada); Heather McNairn, Anna Pacheco (Science and Technology, Agriculture and Agri-Food, Canada), 2016
- [13] Comparative Analysis of High-Resolution Soil Moisture Simulations from the Soil, Vegetation, and Snow (SVS) Land Surface Model Using SAR Imagery Over Bare Soil.  
Mohammed Dabboor, Leqiang Sun, Marco L. Carrera, Matthew Friesen, Amine Merzouki, Heather McNairn, Jarrett Powers, Stéphane Bélair, 2019
- [14] Synthetic Aperture Radar Imaging Using a Small Consumer Drone.  
Chenchen J. Li, Hao Ling, The University of Texas at Austin
- [15] Use of fresh water resources - European Environment Agency, 2018  
Example NGOs: <https://www.waterwise.org.uk>; <https://www.water.org.uk>  
and national organisations <https://www.water.org.uk>; and national ecosystem assessment <http://uknea.unep-wcmc.org>
- [16] NDVI variation according to the time of measurement, sampling size, positioning of sensor and water regime in different soybean cultivars.  
Article in Precision Agriculture, 2017

- [17] Soil and atmosphere influences on the spectra of partial canopies.  
Huete, A.R., and Jackson, R.D., 1988  
Remote Sensing of the Environment.
- [18] Understanding Soil Moisture Sensors: A Fact Sheet for Irrigation Professionals in Virginia.  
David J. Sample, Biological Systems Engineering, Hampton Roads Agricultural Research
- [19] Soil surface roughness: comparing old and new measuring methods and application in a soil erosion model.  
L. M. Thomsen, J. E. M. Baartman, R. J. (Soil Physics and Land Management Group, Wageningen University), Barneveld, T. Starkloff, and J. Stolte (Norwegian Institute for Agricultural and Environmental Research), 2015
- [20] Soil Physical Measurement and Interpretation For Land Evaluation.  
Collingwood, Victoria. McKenzie N, Coughlan K and Cresswell H; CSIRO Publishing, 2002
- [21] Comparative Analysis of High-Resolution Soil Moisture Simulations from the Soil, Vegetation, and Snow (SVS) Land Surface Model Using SAR Imagery Over Bare Soil.  
Mohammed Daboor, , Leqiang Sun, Marco L. Carrera, Matthew Friesen, Amine Merzouki, Heather McNairn, Jarrett Powers and Stéphane Bélair, 2019
- [22] Soil Water Status: content and potential.  
Jim Bilske, Ph.D, Campbell Scientific Inc., 2001
- [23] Impact of soil surface characteristics on soil water content variability in agricultural fields.  
Manns, H. R., A. Berg, and H. McNairn, Paul R Bullock, Heather McNairn, 2014.
- [24] Importance of Soil Organic Carbon on Surface Soil Water Content Variability among Agricultural Fields.  
Hida R. Manns, Aaron Berg, 2014
- [25] Soil organic carbon in soil water content variability; detection and application in agricultural fields.  
Hida Rosemary Manns, 2015 (Thesis presented to The University of Guelph, Canada)
- [26] Soil Moisture Mapping at Regional Scales Using Microwave Radiometry: The Southern Great Plains Hydrology Experiment  
Thomas J. Jackson, David M. Le Vine, Ann Y. Hsu, Anna Oldak, Patrick J. Starks, Calvin T. Swift, John D. Isham, Michael Haken, 1999
- [27] Using SMOS and Sentinel 3 satellite data to obtain high resolution soil moisture maps.  
Cristina González Delgado (Thesis May 21, 2019)
- [28] A New Spectrophotometric Method for Rapid Semiquantitative Determination of Soil Organic Carbon  
Omar R. Harvey, Bruce E. Herbert, J. Pat Harris, Julie-Ann Crenwelge, Eric A. Stiffler, 2009
- [29] Prediction of Topsoil Organic Carbon Using Airborne and Satellite Hyperspectral Imagery  
Juanjo Peón, Carmen Recondo, Susana Fernández, Javier F. Calleja, Eduardo De Miguel, Laura Carretero
- [30] Prediction of Soil Organic Matter by VIS–NIR Spectroscopy Using Normalized Soil Moisture Index as a Proxy of Soil Moisture  
Yongsheng Hong, Lei Yu, Yiyun Chen, Yanfang Liu, Yaolin Liu, Yi Liu, Hang Cheng